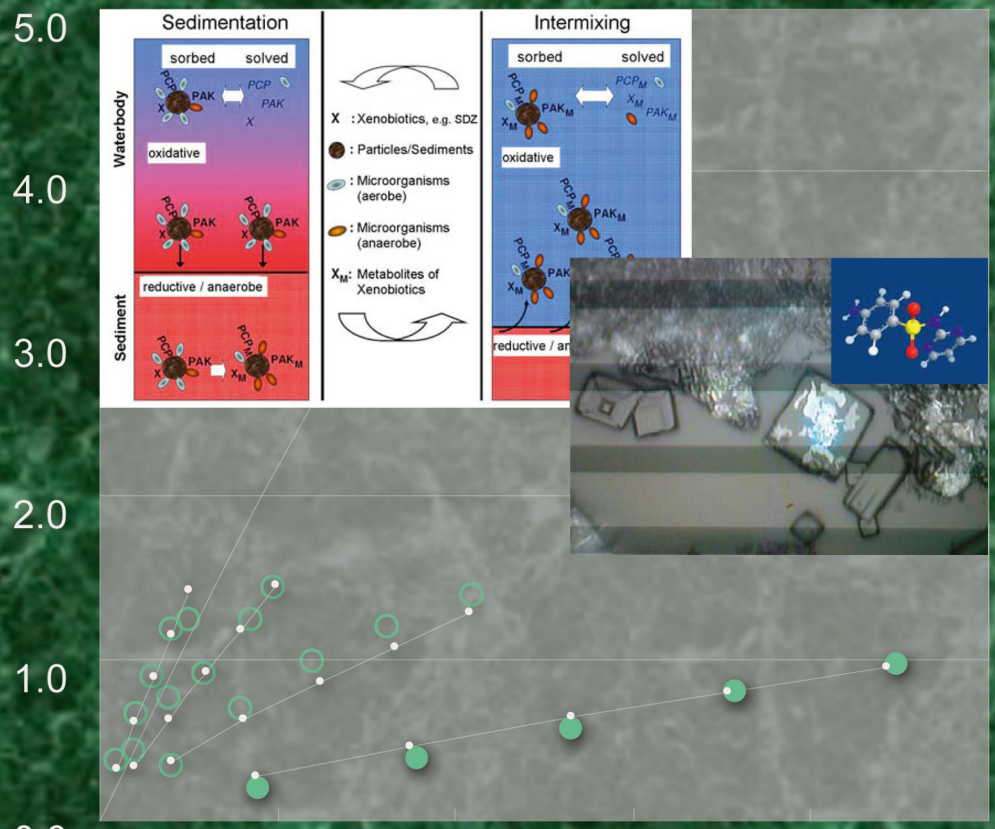

Fate of the Antibiotic Sulfadiazine in Yangtze River Sediments: Transformation, Sorption and Transport

Nan Meng

Mitglied der Helmholtz-Gemeinschaft

JÜLICH
FORSCHUNGSZENTRUM

Schriften des Forschungszentrums Jülich
Reihe Energie & Umwelt / Energy & Environment Band / Volume 120

Forschungszentrum Jülich GmbH
Institute of Bio- and Geosciences (IBG)
Agrosphere (IBG-3)

Fate of the Antibiotic Sulfadiazine in Yangtze River Sediments: Transformation, Sorption and Transport

Nan Meng

Schriften des Forschungszentrums Jülich
Reihe Energie & Umwelt / Energy & Environment Band / Volume 120

ISSN 1866-1793 ISBN 978-3-89336-736-8

Bibliographic information published by the Deutsche Nationalbibliothek.
The Deutsche Nationalbibliothek lists this publication in the Deutsche Nationalbibliografie; detailed bibliographic data are available in the Internet at http://dnb.d-nb.de.

Publisher and Distributor:	Forschungszentrum Jülich GmbH Zentralbibliothek 52425 Jülich Phone +49 (0) 24 61 61-53 68 · Fax +49 (0) 24 61 61-61 03 e-mail: zb-publikation@fz-juelich.de Internet: http://www.fz-juelich.de/zb
Cover Design:	Grafische Medien, Forschungszentrum Jülich GmbH
Printer:	Grafische Medien, Forschungszentrum Jülich GmbH
Copyright:	Forschungszentrum Jülich 2011

Schriften des Forschungszentrums Jülich
Reihe Energie & Umwelt / Energy & Environment Band / Volume 120

D 82 (Diss.,RWTH Aachen University, 2010)

ISSN 1866-1793
ISBN 978-3-89336-736-8

Abstract

Sulfadiazine [4-amino-N-(2-pyrimidinyl) benzene sulfonamide] (SDZ) belongs to the widely used antibiotic veterinary pharmaceuticals. After excretion by animals, these substances and their transformation products are released into agricultural soils and adjacent environmental compartments through the use of manure and sludge as fertilizer. Knowledge of the fate of antibiotics in sediment and soil is crucial for assessing their environmental risk. Especially in China, the behavior of antibiotics in river water and sediment is still poorly known. Therefore, laboratory studies including batch and column experiments were performed to investigate the transformation, sorption and transport behavior of SDZ in Yangtze sediments and their components, such as minerals (goethite, illite, SiO_2, Al_2O_3) and organic matter.

Three abiotic transformation products were only detected in the SDZ-goethite system under the exclusion of light. All these products were found to be SO_2 extrusion from SDZ. One of these products was a new unknown transformation product, and the other two were identified by mass spectrometry as 4-(2-iminopyrimidin-1(2H)-yl)aniline and p-(pyrimidin-2-yl)aminoaniline. A ligand exchange mechanism was assumed for the surface interaction between SDZ and goethite. A possible transformation pathway was proposed on the basis of monodentate inner-sphere complexation and an intramolecular S_N reaction.

Sorption kinetic data were fitted well by first order kinetics. Two days contact time was chosen to avoid degradation of SDZ in sorption experiments. Nearly all the adsorption isotherms determined in this study were nonlinear and could be best described by the Freundlich adsorption isotherm. Surface area and pH were found to be the dominant factors for SDZ sorption on minerals. Additionally, organic matter plays an important role in SDZ sorption on sediments. Reversible sorption was observed for minerals (Al_2O_3 and illite) and desorption hysteresis occurred on most sediments. It was assumed that desorption was started before adsorption had been completed (non-equilibrium conditions) and slow desorption of SDZ from the sorbents. Sorption distribution coefficients (K_d) for SDZ on sediments were low (ranging from 0.3 to 1.1 L kg^{-1}), which indicates that SDZ would be highly mobile in sediments. The rate-limited sorption (RLS) model was successfully used to describe sorption data in this study. The modeling results suggested that the adsorption and desorption rates are the dominant factors for hysteresis of SDZ on sediments. In general, this experimental

procedure combined with the modeling presented here is recommended for adsorption /desorption studies of unstable chemicals like antibiotics in terrestrial systems.

Transport of SDZ was investigated in sediment columns with varying flow rates and input concentrations. Only weak retardation was found, which is in agreement with the low sorption amounts and low K_d values in batch experiments. Column data were modeled successfully by the equilibrium convective dispersion equation (CDE). The retardation factor R obtained from this model was about 50% lower than that calculated from the K_d values of batch experiments. One reason is the loss of active sorption sites due to the release of colloids such as dissolved organic matter and minerals during conditioning of the sediment column. This is an important finding with respect to a new recommendation for transport experiments with sediments.

Table of contents

List of Figures

List of Tables

Abbreviations

^{14}C-SDZ	^{14}C labeled sulfadiazine
2S1R	two-stage one-rate sorption
BTC	breakthrough curve
CBD	citrate-bicarbonate-dithionite
CDE	convective dispersion equation
CEC	cation exchange capacity
DOM	dissolved organic matter
FT-ICR	Fourier transform ion cyclotron resonance
HA	humic acid
HPLC	high performance liquid chromatography
HS	humic substances
ICP-OES	inductively coupled plasma optical emission spectroscopy
iep	isoelectric point
IHSS	international humic substance society
IUPAC	International Union of Pure and Applied Chemistry
LC-MS/MS	liquid chromatography with coupled tandem mass spectrometry
LSC	liquid scintillation counting
M1, 2, 3	transformation product 1, 2, 3
NMR	Nuclear Magnetic Resonance
NOM	natural organic matter
OC	organic carbon
OM	organic matter
POPs	Persistent organic pollutants
pzc	point of zero charge
QTof	Quadrupole time-of-flight
RLS	rate-limited sorption
SDZ	Sulfadiazine
SE	standard error
SOM	sediment/soil organic matter
SSA	specific surface area
SSQ	sum of squares
TGP	Three Gorge Project
TOC	total organic carbon
UV	Ultraviolet

Symbols

A	the concentration of adsorbate in solution in Langmuir isotherm	µg L^{-1}
C	solute concentration in the liquid phase	µg L^{-1}
C_0	input concentration	µg L^{-1}
C_{aq}	total sorptive concentration remaining in the equilibrium solution	µg L^{-1}
C_{eq}	equilibium solute concentration	µg L^{-1}
$C_{initial}$	initial solute concentration in the liquid phase	µg L^{-1}
C_S	solubility in water	µg L^{-1}
D	hydrodynamic dispersion coefficient	cm^2 min^{-1}
f_1	dimensionless fraction of the total soil that exhibits equilibrium sorption	
j_w	water flow density	cm h-1
k_1	first order kinetic rate constant	d^{-1}
K_d	solid-water distribution coefficient	L kg^{-1}
K_f	Freundlich equilibrium constant	$\mu g^{1-1/n} L^{1/n} g^{-1}$
K_l	Langmuir equilibrium constant	
K_{OC}	OC standardized distribution coefficient	L kg^{-1}
K_{SSA}	SSA normalized distribution coefficient	L m^{-2}
m	Freundlich exponent in RLS and 2S1R model	
m/z	mass-charge ratio	
m_{in}	applied mass	mg
$1/n$	Freundlich exponent	
pH	negative decadic logarithm of the hydronium ion concentration	
pK_a	acidity constant	
q	solute concentration in the solid phase	µg g^{-1}
R	retardation factor	
R_{ads}	the rate of adsorption	d^{-1}
R_p	predicted retardation factor	
S_1	local sorbed concentration in first sorption domain	µg g^{-1}
S_2	local sorbed concentration in second sorption domain	µg g^{-1}
t	Time	min
V	Volume	ml
v	flow rate	ml min^{-1}
V_{in}	volume of application solution	L
z	Depth	cm
α	sorption rate coefficient in RLS model	d^{-1}
α_2	sorption rate coefficient in 2S1R model	d^{-1}
Γ	adsorbed amount in Langmuir isotherm	µg g^{-1}
Γ_{max}	maximum adsorbed amount in Langmuir isotherm	µg g^{-1}
Δt_{in}	pulse duration	min
θ	volumetric water content	cm cm^{-1}
ρ	sorbent bulk density	g cm^{-1}

Chapter 1

Introduction and objectives of this thesis

1.1 Sulfonamides (antibiotic pharmaceuticals) in the terrestrial and aquatic environment

Antibiotic pharmaceuticals are widely used for the therapy of infectious diseases of humans and animals. In the EU, of the total of 5000 t of antibiotics used in 1999, 3500 t were used for therapeutic purpose (Kay and Boxall, 2000), while the remaining 1500 t were added to feed in order to promote the growth of farm animals (Alder et al., 2000). In various countries, between 11% and 23% of these antibiotics were sulfonamides (Thiele-Bruhn et al., 2004). Sulfadiazine [4-amino-N-(2-pyrimidinyl) benzene sulfonamide] (SDZ) belongs to the class of potentiated sulfonamides that are frequently applied in livestock husbandry to treat and prevent bacterial diseases (Boxall et al., 2004). After excretion by animals, these substances are released into agricultural soils and adjacent environmental compartments through the use of manure and sludge as fertilizer. Therefore, residual concentrations of pharmaceutical antibiotics are found in surface water, ground water, sediments and soils. Due to surface runoff and leaching, soils can even act as a source of antibiotic contaminants for the aqueous environment (Alder et al., 2001). In Austria, sulfadiazine, sulfadimidine, sulfadoxine, sulfathiazole and sulfamethoxazole were detected in soil in concentrations of 1.0-3.9 $\mu g\ kg^{-1}$ (Martínez-Carballo et al., 2007). Hirsch et al. (1999) reported that in Germany sulfadimidine concentrations were between 0.08 and 0.16 $\mu g\ L^{-1}$ in groundwater below agricultural areas. In soils fertilized with manure in Germany, sulfadimidine was determined in concentrations of 11 $\mu g\ kg^{-1}$ (Höper et al., 2002). Alder et al. (2001) pointed out that sulfadimidine concentrations of up to 0.5 $\mu g\ L^{-1}$ in Swiss river water probably resulted from runoff from agricultural land.

In China, the use of antibiotics in animal feed has been regulated since 1989 and only non-medicated antibiotics are permitted as feed additives (Jin, 1997). However, data on sales or

use of veterinary antibiotics are currently lacking in the public domain (Sarmah et al., 2006). Nevertheless, antibiotics including sulfonamides have been detected in surface waters and sewage treatment plants in China. Their concentration ranged from 5.10 to 7.91 μg L^{-1} (Peng et al., 2006) and from 10 to 1978 ng L^{-1} (Xu et al., 2007) in sewage treatment plants in Guangzhou. Water samples taken from swine feeding plants in Beijing contained 0.62–32.67 μg L^{-1} antibiotics including sulfonamides (Ben et al., 2008). About 0.33 to 0.64 μg L^{-1} sulfonamides were detected in the Small Qing River (Li et al., 2007). In the Pearl River, the concentration of sulfonamides was as much as 0.51 μg L^{-1} in the Guangzhou section (Peng et al., 2008) and ranged from 11 to 460 ng L^{-1} in the Hong Kong section (Xu et al., 2008).

Due to their wide distribution in the environment, sulfonamides may enter the food chain and impact on environment and human health (Sukul and Spiteller, 2006). Thus it is necessary to investigate the fate of sulfonamides in soils, waters and sediments. Degradation (biotic/abiotic) and sorption play an important role in understanding the behavior and fate of sulfonamides in the environment.

Degradation of sulfonamides takes place via microbial, chemical and photoinduced processes in the environment (Kreuzig and Höltge, 2005). Sulfonamides cannot be classified as readily biodegradable (Ingerslev and Halling-Sørensen, 2000). In soil and manure, N_4-acetylsulfadiazine and 4-hydroxysulfadiazine have been identified as major transformation products via biodegradation (Pfeifer et al., 2005; Sukul et al., 2008). The formation of non-extractable residues has also been reported and was assumed to be a chemical reaction with organic matter (Heise et al., 2006; Stoob et al., 2006; Föster et al., 2009). Schmidt et al. (2008) pointed out that non-extractable residues were the main route for the fate of SDZ residues, which appears to be due to covalent binding to soil organic matter (Bialk et al., 2005; Bialk et al., 2007; Bialk and Pederson, 2008).

Photolysis can be another important degradation process for sulfonamides. It was reported that SDZ could be degraded under the influence of light in water (Wolters and Steffens, 2005; Boreen et al., 2005) and in soil manure (Sukul et al., 2008). 4-(2-iminopyrimidin-1(2H)-yl)aniline was identified as the main photoproduct. This compound was also found in soil column transport experiments without photoirradiation (Unold et al., 2009), in which the transformation mechanism remained unclear.

The sorption behavior of sulfonamides has been widely investigated on soil (Boxall et al., 2002; Thiele-Bruhn et al., 2004; Drillia et al., 2005; Sukul et al., 2008b; Yu et al., 2009), soil manure (Sukul et al., 2008b), organic matter (Kahle and Stamm, 2007b; Gao et al., 2010) and clay minerals (Gao et al., 2005; Kahle and Stamm, 2007a). The relevant low K_d values (0.5 - 5 L kg^{-1}) indicate the high mobility and low sorbed amount of sulfonamides in the terrestric and aquatic environment. Lawrence et al. (2000) also reported low K_d values indicating that sulfonamides are very mobile and highly bioavailable in soil. Besides batch studies, column experiments were also performed to obtain a better understanding of the fate of sulfadiazine in the environment (Wehrhan et al., 2007; Unold et al., 2009).

Sulfonamides, like many other pharmaceuticals, are polar compounds, which are ionized as a function of the pH of the matrix. These compounds may adsorb to sediment/soil via ion exchange, cation bridging, surface complexes and hydrogen bonding (Tolls, 2001). Accordingly, sorption of sulfonamides varies between different sediments/soils and is affected by the quantity, composition and structure of sediment/soil colloids (Thiele-Bruhn et al., 2000). It was reported that sorption of sulfonamides increased with decreasing pH values (Bajpai et al., 2000; Gao et al., 2005; Kahle and Stamm, 2007a), with increasing contact time (Kahle and Stamm, 2007a; Stoob et al., 2007) and was affected by ionic strength (Gao et al., 2005). Sorption of sulfonamides on organic matter was also reported in recent studies (Kahle and Stamm, 2007b; Gao et al., 2010). Thiele-Bruhn et al. (2004) pointed out that the chemical composition of the SOM compounds is correlated with sulfonamide sorption indicating that polar regions of complex SOM structures contribute to site-specific binding of sulfonamides.

The possible physicochemical and biological interactions between antibiotic pollutants and other POPs with suspended matter or sediment particles in the water/sediment system are shown in Figure 1.1. Antibiotics such as SDZ in water can be sorbed on suspended particles and accumulated by sedimentation. The sorbed SDZ can also be released by desorption after resuspension of the sediment and in changing aquatic conditions (salinity, pH, redox potential etc.). During these processes, transformation products can arise due to photolysis, hydrolysis, oxidation/reduction and interaction with microorganisms etc. These new substances can act as toxic compounds. As illustrated in Figure 1.1, sediments play an important role as a sink for the pollutants, but, on the other hand, sediments may also be the source of pollutants for surface water by desorption processes. Indeed, there is a need to investigate the fate of antibiotics such as SDZ in the surface water/sediment system.

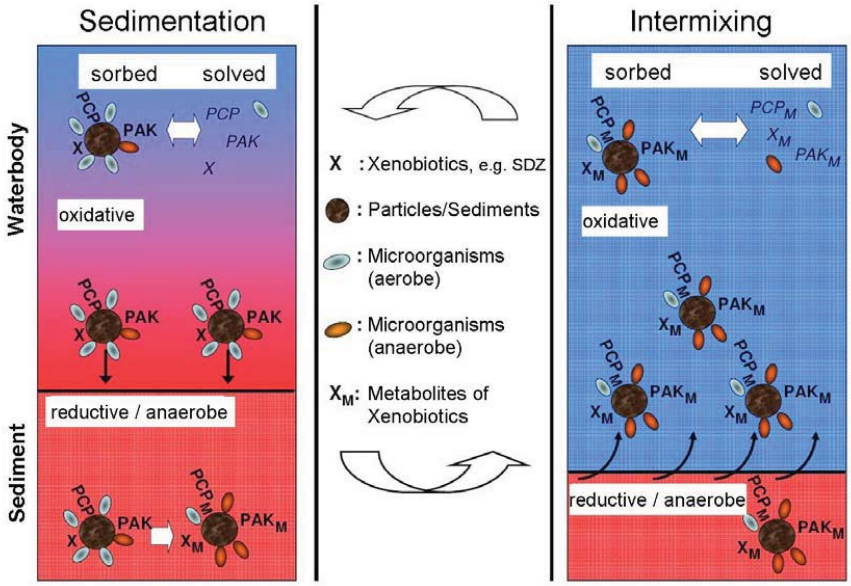

Figure 1.1 Physicochemical and biological interactions in the pollutant/water/sediment system (Thiem et al.)

1.2 An important aquatic environment: Yangtze River and Three Gorges Reservoir

The Three Gorges Project (TGP) located on the Yangtze River is the "largest water conservancy project ever built in China, and hence in the world". The Three Gorges dam is located at the end of Xiling Gorge, near the town of Sandoupin in Yichang city prefecture. The Three Gorges reservoir is used for flood control, power generation and navigation. It is at the widest part of the river, and can store sufficient volumes of water to reduce flooding in the middle Yangtze, where 15 million people are at risk.

The Three Gorges area is at risk because:

1) Millions of tons of solid waste had piled up in the reservoir area which was not cleaned up in time before the dam was closed. The floating garbage therefore accumulated in the surface water of the reservoir.

2) The construction of the Three Gorges Dam alters the river hydrodynamics and results in a

"lake" effect. It causes water flow to slow down, suspended particles to deposit and also leads to nutrient enrichment. The wastewater as an extensive point/non-point source of pollution discharged from industrial processes, agricultural activities, urban and rural areas into the reservoir without appropriate treatment has caused a deterioration in the environment and ecosystem, a crisis of water quality in the reservoir area and its surrounding tributaries.

3) With the raising of the reservoir water level, the pollutants flow back with the water to the upriver tributaries thus making the water quality worse than in the reservoir.

4) Now that the Three Gorges Reservoir is fully operational, there is a land and water interleaving zone, which is called the fluctuation zone. This zone has a vertical fall of 30 m and an area of over 440 km^2. Adsorption and desorption processes of pollutants on sediments play an important role in the fluctuation zone.

5) Sedimentation and soil erosion have occurred both above and below the reservoir. These lead to significant changes in the behavior of inorganic and organic pollutants and their interaction with particulate matter in the water column and in sediments.

In addition to these environmental impacts, knowledge of the fate of antibiotics in the Yangtze River and its drainage area is crucial for assessing the environmental risk of these compounds. To our knowledge, the sorption behavior of SDZ on sediments, especially those of the Yangtze River, have hardly been studied.

1.3 Research objectives and outline of this thesis

The major objective of this thesis is to investigate the physicochemical behavior of sulfadiazine (SDZ), an antibiotic pharmaceutical, in the sediment/water system under laboratory conditions. To better understand the sorption and transport behavior of SDZ on Yangtze sediments, sediment components such as metal oxides, clay minerals and organic materials, were also included in the investigation using batch and column experiments. The experimental data were fitted by different sorption and transport models.

The following major topics were studied:

a) The chemical stability of SDZ in the presence of sediments and their mineral components

The stability experiments were performed with respect to the effect of light, concentration and contact time, as well as aerobic/anaerobic conditions. The transformation products were identified by LC-MS-MS and high-resolution mass spectroscopy (FT-ICR-MS, QTof-MS). A hypothesis for transformation mechanisms was suggested.

b) Adsorption/desorption of SDZ on different sorbents

Batch experiments were conducted to investigate the adsorption/desorption behavior of SDZ with different sorbents including sediment/soil components (Al_2O_3, illite, SiO_2, goethite) and Yangtze sediments. Radioactively labeled SDZ (^{14}C-SDZ) concentrations in solution and solid phase were detected by radio-HPLC, a liquid scintillation counter (LSC) and the oxidizer method. Then the complete mass balance of SDZ can be established. The sorption data were modeled.

c) Transport of SDZ in Yangtze sediments

Column experiments were performed to study the mobility of SDZ in Yangtze sediments. Experimental conditions including flow rate, input concentration and pulse duration were varied to obtain the optimal parameters describing the transport behavior. The modeling was done by the equilibrium convective dispersion equation (CDE) and the non-equilibrium CDE method.

Chapter 2

Theoretical background

2.1 Sulfadiazine as sorptive in aqueous solution

All sulfonamides are N-substituted derivatives of the substance sulfanilamide. The compounds are odorless and white or slightly colored powders that are characterized by moderate solubility in water (C_S = 0.1-5 g L^{-1}) and organic solvents ($\log K_{ow} \approx$ -0.5). Depending on pH, the NH_2 substituent is protonated and the R_1SO_2NHR is deprotonated with acid dissociation constant of pK_{a1} = 2 to 3 and pK_{a2} = 4.9 to 10.4 for the two equilibriums (Ingerslev and Halling-Sørensen, 2000). Therefore, under natural conditions, sulfonamides occur in either neutral form or as anion if pH >> pK_{a2}. In general, the amphoteric sulfonamides behave as weak acid and form salts in strongly acidic or basic solutions which is shown in Figure 2.1.

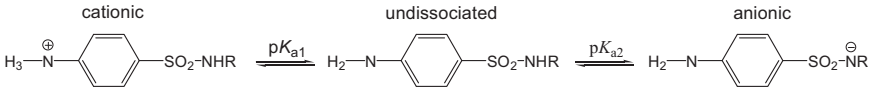

Figure 2.1 Amphoteric properties of sulfonamides (modified after Sakurai, 1979)

Due to the amphoteric properties, SDZ in solution forms as cationic, uncharged and anionic species with different pH. Figure 2.2 gives the fraction of species of sulfadiazine with changing pH and the pH values of some sorbent suspensions studied in this work. Except illite (pH 4.2), pH of all the other sorbents are higher than pK_{a2} (6.4). The species in the solution are mostly in anionic form. Regarding the sorption behavior, SDZ can act as anionic ligand in the metal-SDZ complex which was used as phamaceutical antibiotics. Cook and Turner (1975) proved that the active binding sites of SDZ on silver-SDZ complex are the pyrimidine N atoms, the sulfonamide N and one sulfonic O, giving rise to a polymeric arrangement. As for zinc(II)-SDZ complex, one molecule of SDZ coordinates through the sulfonamide N and the other through one N atom of the pyrimidine ring (Brown et al., 1985). In the case of

cadmium-SDZ complex, the cadmium atom is coordinated to two sulfonamido and amino N atoms from four symmetry-related SDZ anions (Menabue and Saladini, 1993). Ajibade et al. (2006) presented that SDZ behaves as a bidentate anionic ligand in the cobalt-SDZ complexes. The central ion coordinated via the sulfonamide N and pyrimidine N on each of the SDZ anion, with the fifth and sixth coordination sites occupied by two molecules of methanol. These informations are helpful to understand the transformation and sorption behavior of SDZ on different sorbents especially on minerals.

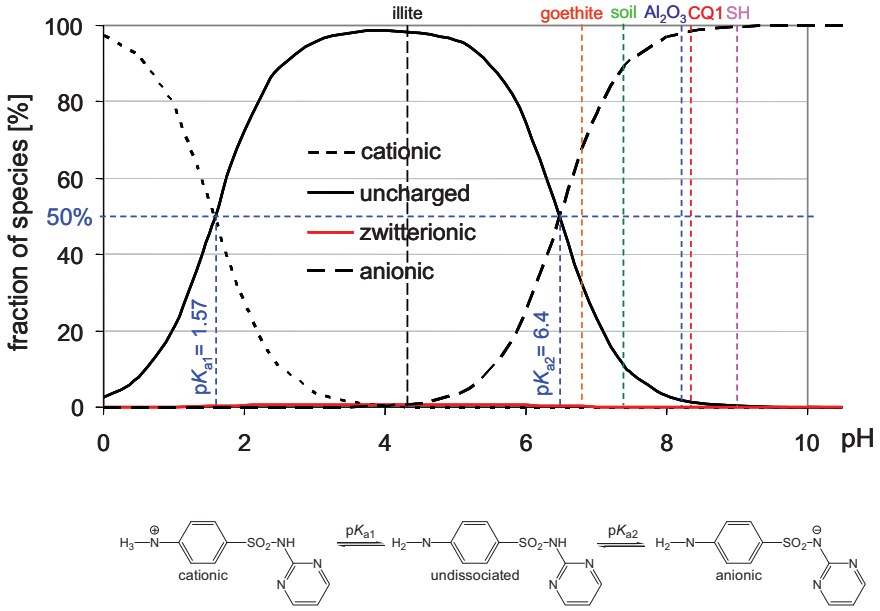

Figure 2.2 Species of sulfadiazine at various pH (suspension pH of different sorbents were also shown)

2.2 Surface properties of goethite

Because the transformation and sorption studies on minerals are a focus of this thesis, a short description of the surface properties of goethite is presented in the following.

The surface areas of both natural and synthetic goethite range from ca. 8 to 200 m^2 g^{-1}. The point of zero charge (pzc) of goethite ranges from 7.5 to 9.5 (Cornell and Schwertmann, 2003). It is important to realize that negative, positive and neutral functional groups can coexist on the oxide surface.

The charge on the oxide surface is established by dissociation (ionization) of the surface hydroxyl groups. The situation corresponds to adsorption or desorption of protons depending on the pH of the solution (Figure 2.3).

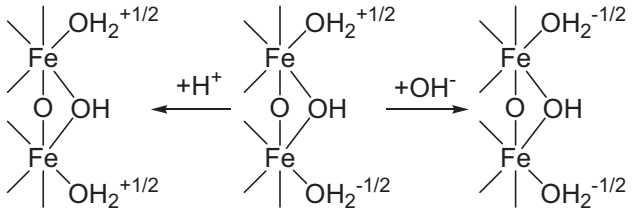

Figure 2.3 pH-dependent charge density at the Fe-oxide/solution interface (after Cornell and Schwertmann, 2003)

Complexing sorptives in the solution (ligands) can interact with the goethite-surface with different consequences. They may accelerate (ligand promoted dissolution), retard, or even block dissolution. In the case of acceleration, a complexing sorptive may promote dissolution by either adsorption or by complexation with Fe^{3+} in solution (Salfity et al., 2000).

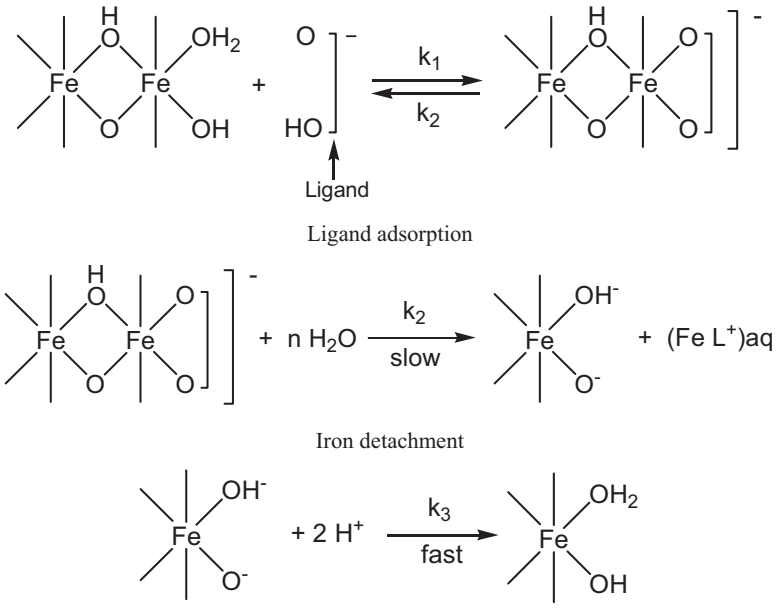

Figure 2.4 The three subsequent reaction steps of the dissolution of an Fe^{III} oxide by an organic ligand: ligand adsorption, iron detachment and proton adsorption (site restoration) (Stumm and Furrer, 1987)

A ligand adsorption on the surface of the Fe oxide weakens the Fe-O bonds to neighbouring atoms and leads to detachment of the Fe^{III} complex. Stumm and Furrer (1987) proposed that dissolution of an M^{III} oxide by an organic ligand through a surface reaction involved three consecutive reactions, namely, ligand adsorption, metal detachment and proton adsorption / surface restoration as shown in Figure 2.4.

Ligands which promote dissolution are thought to form mononuclear (often bidentate) surface complexes, whereas those that inhibit the process form binuclear (or even trinuclear) surface complexes. The former assist detachment of Fe from the surface, whereas the latter are firmly anchored.

2.3 Stability of sulfadiazine in the aquatic and terrestrial environment

After administration to human or animals, the majority of sulfadiazine used is excreted unchanged or as metabolites (Pfeifer et al., 2005) and reaches agricultural soils mainly through the use of manure or directly through grazing livestock (Jørgensen and Halling-Sørensen, 2000). As a consequence, these compounds have been found in waste water (Hartig et al., 1999; Miao et al., 2004) liquid manure (Pfeifer et al., 2002; Haller et al., 2002), soil (Mueller et al., 2003) and surface water and ground water (Hirsch et al., 1998; Lindsey et al., 2001; Kolpin, et al., 2002; Yang et al., 2004).

In general, the possible transformation pathways of SDZ in environment were investigated as biotic processes including excretion from human or animals after medical treatment, bacterial degradation in soil or manured soil and abiotic processes like photodegradation.

The known biotic metabolites of SDZ were isolated and identified as N_4-hydroxysulfadiazine, N_4-acetylsulfadiazine, 4-hydroxysulfadiazine, 5-hydroxysulfadiazine and other sub-metabolites (Vree et al., 1995). N_4-acetylsulfadiazine was also found as corresponding metabolite both from excretion by the animals (Kreuzig and Höltge, 2005) and from the extraction of manured soil (Schmidt et al., 2008). N_4-acetylsulfadiazine and 4-hydroxysulfadiazine were identified as major metabolites in manure (Pfeifer et al., 2005). Lamshöft et al. (2007) investigated the transformation behavior of SDZ after drug administering to pig. They found N-acetylsulfadiazine and 4-hydroxysulfadiazine as the major

metabolites, as well as two minor metabolites identified as N-formylsulfadiazine and N-acetyl-4-hydroxysulfadiazine.

Photodegradation is an abiotic transformation pathway for SDZ. It was reported that SDZ could be degradated under the light of xenon burner in an ozone-controlled environment (Wolters et al., 2005) but without the identification of photodegradation products. Another study of photodegradation of sulfa drugs (Boreen et al., 2005) identified 4-(2-imino-4,6-dimethylpyrimidin-1(2H)-yl)aniline as a photoproduct of sulfamethazine and estimated that 4-(2-iminopyrimidin-1(2H)-yl)aniline could be the photoproduct of SDZ. Then 4-(2-iminopyrimidin-1(2H)-yl)aniline together with N-formyl-SDZ and 4-hydroxyl-SDZ were identified by mass spectrometry and NMR as the main photoproducts of SDZ by photolysis in water and manure (Sukul et al., 2008). Elimination of SO_2 was found to be the main degradation process during irradiation. This photoproduct and 4-hydroxysulfadiazine was also found as transformation products in soil column transport experiments without photo-irradiation (Unold et al., 2009).

2.4 Theory of sorption

2.4.1 Adsorption isotherm

Adsorption processes are discussed primarily in terms of intermolecular interactions between solute and solid phases. It includes: 1) covalent binding (e.g. surface complexation); 2) electrostatic interaction (e.g. Coulomb interaction); 3) H-bridges; 4) van der Waals interaction; 5) expulsion of hydrophobic substances (“hydrophobic interactions”).

Adsorption is often described in terms of isotherm, which shows the relationship between the bulk aqueous phase activity of sorptive and the amount adsorbed at constant temperature at equilibrium. The shape of this isotherm line suggests information about the adsorbate-adsorbent interaction. Giles et al. (1974) proposed a general modeling of sorption isotherms, in which 4 particular cases are now used as the 4 main shapes of isotherm commonly observed (Figure 2.5).

(1) The S-type isotherm suggests “cooperative adsorption”, which operates if adsorbate-

adsorbate interaction is stronger than the adsorbate-adsorbent interaction. This condition favors the "clustering" of adsorbate molecules at the surface because they bond more strongly with one another than with the surface. (2) The L-type (Langmuir) isotherm reflects a relatively high affinity between the adsorbate and adsorbent, and is usually indicative of chemisorption. (3) The H-type isotherm, indicative of very strong adsorbate-adsorbent interaction (i.e., chemisorption), is really an extreme case of the L-type. This isotherm is not often encountered with organic molecules because only few of them form strong ionic or covalent bonds with soil colloids but it is typical for the polyelectrolyte adsorption (polyacrylic acid, PAA) on the minerals. (4) The C-type (constant-partitioning) isotherm, which suggests a constant relative affinity of the adsorbate molecules for the adsorbent, is usually observed only at the low concentration range of adsorption. Deviation from the linear isotherm is likely at high adsorption levels. Nevertheless, because many nonlinear sorbing organic compounds of interest in sediment/soils are adsorbed at quite low concentrations, the linear C-type isotherm is often a reasonable description of adsorption behavior.

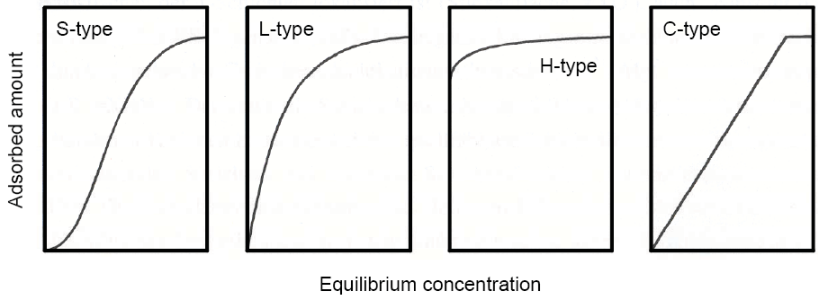

Figure 2.5 Classification of adsorption isotherms (Giles et al., 1974)

This work will focus on the C- and L-type (Langmuir and Freundlich adsorption isotherm).

The typical C-type isotherm (Henry-isotherm) could be described by the distribution coefficient K_d (L kg^{-1}) of the substances on adsorbents, which is calculated as (equation 2.1):

$$K_d = \frac{C_S}{C_{aq}} \qquad [2.1]$$

where C_S (μmol kg^{-1}) is the total sorbate concentration associated with the sorbent, C_{aq} (μmol L^{-1}) is the total sorptive concentration remaining in the equilibrium solution.

K_d coefficients can be normalized to the specific surface area (SSA, $m^2\ g^{-1}$) to compare the effect of SSA on sorption (Kahle and Stamm, 2007a) (equation 2.2):

$$K_{SSA} = \frac{K_d}{SSA} \qquad [2.2]$$

where K_{SSA} ($L\ m^{-2}$) is the SSA normalized distribution coefficient.

K_d coefficients can also be standardized to the organic carbon (OC) fraction of the solid (%) (equation 2.3):

$$K_{OC} = \frac{K_d}{OC}100 \qquad [2.3]$$

K_{OC} values can also be semi-empirical calculated from physicochemical properties of the adsorbate. For example, the K_{OC} value could be obtained from the pH-corrected octanol-water partition coefficient D_{ow} using a modified equation from Gerstl (1990) (equation 2.4):

$$\log K_{OC} = -0.41 \log D_{OW} + 0.97 \qquad [2.4]$$

This equation was originally developed to estimate the sorption of carbamates, a group of pesticides with log K_{ow} values of approximately 2, but it's not suited to sufficiently estimate the K_{OC} of sulfonamides from molecular properties. Experimental and calculated K_{OC} values were not correlated ($r^2 = 0.07$). This result indicates that the log linear K_{OC} model (equation 2.4) is in general not valid for sulfonamides (Thiele-Bruhn et al., 2004).

The typical L-type isotherm is Langmuir and Freundlich isotherm. The equation of the Langmuir isotherm could be stated as (Stumm, 1992) (equation 2.5):

$$\Gamma = \Gamma_{\max} \frac{K_l[A]}{1 + K_l[A]} \qquad [2.5]$$

Γ is adsorbed amount; Γ_{max} is maximum adsorbed amount as A increases; K_l is the Langmuir equilibrium constant; A is the concentration of sorptive in solution.

The assumptions of Langmuir isotherm (Langmuir, 1916) make it unfit for many cases such as organic sorption on sediment/soil.

The Freundlich Isotherm is an equilibrium isotherm that is used most often in "real world" examples. The Freundlich equation can be stated as:

$$C_s = K_f C_{aq}^{1/n} \quad [2.6]$$

K_f is the Freundlich equilibrium constant ($\mu mol^{1-1/n} L^{1/n} kg$) and the exponent, *1/n*, measure of nonlinearity. In the simplest case, $n = 1$ then K_f is equivalent to K_d, irrespective of the magnitude of C_{eq}. In that case, C-type sorption is treated in analogy to Henry equation. For many organic chemicals in low concentration range, the "Henry partition" approach has been successful (Chiou, 1989). To better describe the nonlinear adsorption isotherms, the logarithmic-transformed Freundlich isotherm was fitted to the transformed adsorption data (equation 2.7):

$$\log C_S = \frac{1}{n} \log C_{aq} + \log K_f \quad [2.7]$$

The Freundlich equation leads to a better fit to the adsorption data of sulfonamides than does the Langmuir isotherm (Thiele-Bruhn, 2000). For selected cases, the nonlinearized Freundlich isotherm was additionally fitted to the adsorption data.

2.4.2 Sorption kinetics

For sorption processes, the rate of adsorption, R_{ads}, of a molecule onto a surface can be expressed in the same manner as chemical kinetic processes (Roger, 1997). For example, the adsorption of SDZ on sediments could be described as:

$$A(SDZ) + B(sed) \rightarrow C(sed - SDZ) \quad [2.8]$$

where A represents for SDZ, B for sediment and C for sorbed SDZ. So the adsorption rate, R_{ads}, could be calculated as:

$$R_{ads} = \frac{d[C]}{dt} = k[A][B] \quad [2.9]$$

But as the sorbents, the amount of sediment is in a great excess and therefore constant, so [*B*] gives together with the rate constant *k* the new constant *k´* in this equation:

$$R_{ads} \approx k'[A] \quad [2.10]$$

So the adsorption process appears to be first-order.

First-order kinetics is easier to apply to transport and degradation models because they do not require knowledge about particle geometry (Pignatello and Xing, 1996). In this study, the first-order kinetics was used to calculate the transformation rate and sorption rate of SDZ on different adsorbents.

2.4.3 Sorption of sulfonamides

Sorption is one of the key processes controlling the fate of sulfonamides in environment. Table 2.1 shows some literature about the sorption studies of sulfonamides in recent years.

As shown in this table, the values of sorption partition coefficient K_d range from 0.1 to 40 L kg^{-1} depending on different sorption conditions (different sorptives and sorbents, pH, contact time etc.). But in most cases, K_d values are in the range of 0.1-5 L kg^{-1}. This result indicates the high mobility and low sorbed amount of sulfonamide in the terrestric and aquatic environment. The much higher K_{OC} values (20 – 4700 L kg^{-1}) indicate the strong interaction between OM and SDZ. The Freundlich equilibrium constant, K_f values range from 0.2 to 36.2, which could be referent values for this study.

Several factors such as concentration of sulfonamides, pH value, temperature, ionic strength, organic matter content and physicochemical properties of the adsorbents influence the adsorption.

Table 2.1 Sorption of sulfonamides – a literature review

sorptives	adsorbents	shaking time	pH	K_d (L kg^{-1})	K_{oc} (L kg^{-1})	K_f (μmol$^{1-1/n}$ L$^{1/n}$ kg)	Literature
sulfadiazine	KAL Ap (soil)	48 h	5.7			6.14	Kasteel et al., 2010
	KAL Bw		6.1			1.58	
	MRZ Ap		7.0			5.0	
	MRZ Bw		7.4			1.27	
sulfadimethoxine	sand	48 h	6.97	0.4	-	3.1	Sanders et al., 2008
	soil 1		5.03	10.4	1195.4	2.1	
	soil 2		4.66	25.8	2148.9	14.5	
sulfadiazine	soil I-V	50 h		0.1-24.3	18.9-837.9		Sukul et al., 2008b
	soil with manure			6.9-40.2	1301.9-4698.4		
sulfamethoxazole	Burgen sediment	24 h		0.2	25.1	0.2±1.5	Stein et al., 2008
	Dausenau sediment			0.9	20	2.5±1.4	
sulfathiazole	compost	1, 14 d	3-9		232-654		Kahle and Stamm, 2007a
	pig manure				159-1078		
	HA				352-1142		
Sulfamethazine	soil (WA)	14 h	7.5			6.75	Accinelli et al., 2007
	soil (PR)		7.2			4.21	
sulfachloropyridine	soil (WA)		7.5			6.11	
	soil (PR)		7.2			3.97	
sulfachloropyridazine	clay loam	2 d	6.8	16.6		2.5	Ter Laak et al., 2006a
	loamy sand		6.6	8.1		1.5	
sulfachloropyridazine	11 soils	2 d		0.9-34.8			Ter Laak et al., 2006b
^{14}C-Sulfadiazine	manured soil	24 h		2.1			Kreuzig and Höltge, 2005
sulfamethazine	montmorillonite kaolinite	2.5 h dark		2.3-22.2		11.1-15.6	Gao et al., 2005
sulfamethoxazole				2.9			
sulfapyridine				4.0			
sulfamethoxazole	soil 1	24 h	6.8	37.6	530	36.2	Drillia et al., 2005
	soil 7		4.3	0.23	62.2	0.28	
sulfanilamide	soil pig slurry	16 h, dark	7.5	0.57	35.4		Thiele-Bruhn and Aust, 2004
sulfadiazine			4.8	2	124		
sulfadimidine				0.79	49.1		
sulfadimethoxine				0.73	45.3		
sulfapyridine				1.02	63.4		
sulfapyridine	whole soil	16 h	7	3.47			Thiele-Bruhn et la., 2004
	clay		6.9	3.53			
	fine silt		6.4	3.44			
	medium silt		6.1	1.4			
	coarse silt		6.4	0.45			
	sand		7.4	0.83			
sulfapyridine	silt loam	16 h	7	3.5	217		Thiele-Bruhn et al., 2002
sulfadiazine			7	2	124		
sulfanilamide			7	2.4	149		
sulfadimidine			7	1.7	106		
sulfadimethoxine			7	2.3	143		
sulfachloropyridazine	soil	48 h	6.8	0.9			Boxall et al., 2002
	soil/slurry		6.5	1.8			
L-methionine-sulphoximine	HA (from soil)	14 h	6.0				Gelsomino et al., 2000
	kaolinite						
	montmorillonite						

sulfapyridine	fertilized soil	16 h dark		4.6	308	5.5	Thiele-Bruhn et al., 2000
4-ABA	unfertilized soil			4.1	101	2.2	
sulfathiazole	loamy sand		5.2	4.9	200		Langhammer,1989
sulfamethazine			5.8	1.2	173.9		

pH value and ionic strength

Sorption of hydrophilic compounds like sulfonamides is strongly affected by the surface charges. In low pH range, the sorption of sulfonamides tends to decrease with increasing ionic strength. Because the sulfonamides appear to be cationic species at low pH, the high ionic strength solution will provide much more cations on the surface of sorbents, which will block the sorption of sulfonamides. Gao et al. (2005) investigated the ionic strength effect on the sorption of sulfamethazine (SMZ) on clay minerals. They found out that K_d values were significantly lower at high ionic strength (310 mM) than those at 10 mM below pH 5.5 by the experiments of SMZ adsorption on Na-SWy-2 clay (a kind of montmorillonite). But in the high pH range, when sulfonamides are mostly in anionic form, the repulsion of both negative charges of sorbent surface and sulfonamides will strongly decrease the sorption. In this case, with increasing ionic strength, the negative charges are screened by the cations from electrolyte. The screening effect is expected to increase the sorption of sulfonamides. In the same work of Gao et al. (2005), they found that at pH values > 8.3, no SMZ sorption to Na-Swy-2 clay was apparent at 10 mM ionic strength, while some sorption occurred at higher ionic strength. As for sulfadiazine, Bajpai A.K. (2000) pointed out the adsorption on alumina increases with rise in concentration of the added inorganic salts at pH 7.7. So the influence of ionic strength on the adsorption depends on pH value and properties of the adsorbents.

The change of pH results in the change in charge profile of the sorptive and sorbent which consequently influences the interactions between the sorptive and adsorbent. To evaluate possible effects of pH on sulfonamide sorption to sediment/soil, portions of dissociated species (α_a), of the sulfonamides were calculated from the acid dissociation constants with the equation (Schwarzenbach et al. 1993) (equation 2.11):

$$\alpha_a = \frac{1}{1+10^{(pH-pK_a)}} \qquad [2.11]$$

This equation could be used for the calculation of adsorption coefficients of the cationic, uncharged and anionic species. Gao et al. (2005) investigated the pH effect on the sorption of three different sulfonamides on clay minerals. The results showed that the sorption amount

decreased with increasing pH values. The same effect was found in the sorption of sulfathiazole to clay minerals (Kahle and Stamm, 2007a) and organic materials (Kahle and Stamm, 2007b). The pH effect indicated the surface charge of adsorbents and the dissociation of SDZ may play an important role on the sorption.

Organic matter

Langhammer and Büning-Pfaue (1989) described a higher adsorption of sulfonamides in soils with higher organic matter content. Kahle and Stamm (2007b) investigated the influence factors of sulfathiazole sorption to organic materials such as composition of sorbent, solute chemistry and contact time. They demonstrated the sorption is most strongly affected by pH and contact time. Thiele-Bruhn et al. (2004) pointed out that the chemical composition of the SOM compounds correlate with the sulfonamide sorption indicating that polar regions of complex SOM structures contribute to site-specific binding of sulfonamides.

Sorption on sediment/soil fractions: empirical model

To investigate the influence of soil and sulfonamides physicochemical properties on adsorption, Thiele-Bruhn et al. (2004) developed a regression model to calculate adsorption coefficients (K_d) using physicochemical properties of sulfonamides together with properties of soils and soil fractions by multiple linear regression (equation 2.12):

$$K_d = 0.14(OC)k' + 0.32CF_a + 0.94 \qquad [2.12]$$

k' is the chromatographic capacity factor of sulfonamides determined by reversed-phase HPLC, and CF_a is the nondissociated species concentration. This model indicates that the contribution of SOM, determined as OC, to the adsorption of sulfonamides nonlinearly increases with the antibiotics' polarity. Further more, adsorption varies with the fraction of nondissociated sulfonamides species, which depends on the soil pH. In contrast, parameters like the cation exchange capacity and specific surface area did not significantly contribute to the model. The test result of this model by using the data from literature indicated acceptable estimates of K_d values for the sulfonamides.

The results of sulfonamide adsorption on the pig slurry (Thiele-Bruhn and Aust, 2004) showed low sorption coefficients which indicate high mobility and availability of the sulfonamides in manured soil and correspond with their water solubility (comparing with

hydrophobic chemicals) and low logK_{ow}. Lawrence et al. (2000) also reported that the low K_d values indicate that sulfonamides are very mobile and highly bioavailable in soil with no bioaccumulation. It also been reported that the linear isotherms are not suited to properly describe the soil sorption of polar compounds such as the sulfonamides.

2.4.4 Desorption Hysteresis

Desorption hysteresis refers to the apparent asymmetry of sorption/desorption equilibrium and kinetics. There are several different causes leading to observed hysteresis phenomenon which are summarized in Figure 2.6 (Wang, 2008).

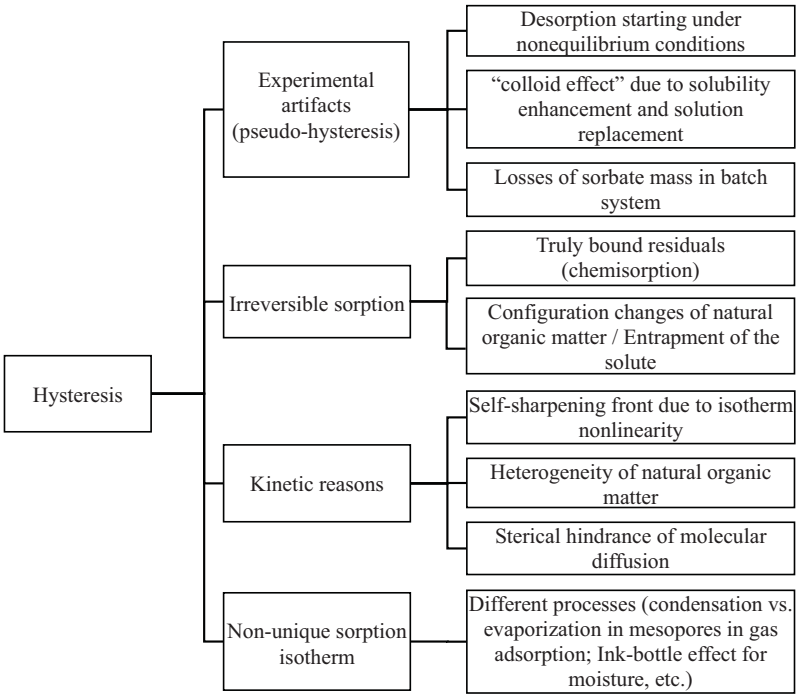

Figure 2.6 Process and manifestations of hysteresis (Wang, 2008)

From all of these causes, "Pseudo-hysteresis", which is due to experimental artifacts in the traditional batch sorption/desorption method, is mostly discussed. It can be classified into three categories: 1) desorption starting under nonequilibrium conditions (Pignatello, 2000); 2) sorbate losses from the batch system; 3) the "colloid effect" in the conventional batch vial decant-and-refill method (association of solute with dissolved or suspended matter in the batch system results in apparent solubility enhancement, thus less sorption; dilution of the

aqueous phase in the batch by solution replacement to initiate desorption then clearly results in artificial hysteresis). Huang et al. (1998) performed three different batch experimental protocols to study sorption of phenanthrene on five EPA reference soils and sediments. They found that hysteresis occurs in different types of artifacts and different degrees due to the different experimental setups. The most common experimental artifacts result from nonattainment of sorption/desorption equilibrium since the true equilibrium requires very long time. Pignatello and Xing (1996) pointed out that sorption of organic chemicals may in fact require weeks to months to reach equilibrium. So it should be seriously taken into consideration that the slow adsorption causes the desorption hysteresis.

2.5 Ad/desorption modeling

2.5.1 Rate-limited sorption (RLS)

If the equilibrium distribution of a substance is not reached instantaneously, a rate-limited solute uptake by the sorbent needs to be considered. This is described by the following equation:

$$\frac{dS}{dt} = \alpha(K_f C^m - S) \qquad [2.13]$$

where α is the sorption rate coefficient (d^{-1}), K_f is the Freundlich equilibrium constant, m is dimensionless Freundlich exponent, C and S are solute concentration in the liquid ($\mu g\ L^{-1}$) and solid phase ($\mu g\ g^{-1}$). The sorption isotherm for the equilibrium distribution is given by Equation 2.6. The change of solute concentration in the liquid phase with time is expressed as:

$$\theta \frac{dC}{dt} = \alpha(C_t - \theta C - \rho K_f C^m) \qquad [2.14]$$

where θ is the volumetric water content ($cm^3\ cm^{-3}$) and ρ is the sorbent bulk density ($g\ L^{-1}$).

2.5.2 Two-stage one-rate sorption (2S1R)

The two-stage one-rate approach (2S1R) assumes nonlinear (Freundlich) sorption with instantaneous equilibrium between the aqueous solution and one sorption domain with local concentration S_1, whereas the other sorption domain with local concentration S_2 takes up the solute rate-limited from the instantaneous region (Streck et al., 1995). In Domain 1, sorption is fast compared with the duration of the experiment so that equilibrium can be assumed:

$$S_1 = K_f C^m \qquad [2.15]$$

In contrast, sorption in Domain 2 is rate-limited:

$$(1 - f_1)\frac{dS_2}{dt} = \alpha_2 (K_f C^m - S_2) \qquad [2.16]$$

The total sorption is described by:

$$S = f_1 S_1 + (1 - f_1) S_2 \qquad [2.17]$$

where f_1 is the dimensionless fraction of the total sediment/soil that exhibits equilibrium sorption, and α_2 is the sorption rate coefficient (d^{-1}). The parameter K_f denotes the Freundlich equilibrium constant ($mg^{1-m}L^m kg^{-1}$), m is the Freundlich exponent. There are also models for more sorption sites and rates, like two sites two rates (2S2R), three sites two rates (3S2R) etc. But in this study, the first two models were used for data modeling.

2.6 Transport modeling

The transport of non-degradable dissolved substances in homogeneous sediment/soil with a constant water content and steady state flow conditions is typically described by the convection-dispersion equation (CDE) (Hillel, 1998):

$$\frac{\partial C_t}{\partial t} = D\theta \frac{\partial^2 C}{\partial z^2} - j_w \frac{\partial C}{\partial z} \qquad [2.18]$$

Where t is time (min), z is depth (cm), D is the hydrodynamic dispersion coefficient (cm^2 min^{-1}), θ is the volumetric water content (cm^3 cm^{-3}), j_w is the water flow density (cm min^{-1}), C is the solute concentration in the liquid phase (μg L^{-1}) and C_t is the total mass of solute per unit volume of sediment/soil (μg L^{-1}). For non-volatile compounds C_t is given as the sum of concentration in the dissolved and sorbed phase:

$$C_t = \theta C + \rho S \qquad [2.19]$$

where ρ is the soil bulk density (g cm^{-3}) and S is the sorbed solute concentration (μg g^{-1}).

To account for flow related effects on solute transport, the transport of reactive substance is usually compared to a simultaneously applied conservative tracer. The difference in the transport behavior (i.e. retardation and tailing) of the two tracers is then assigned to sorption of the reactive tracer (Wehrhan, 2007).

Various sorption concepts are available to describe the interaction of dissolved substances with the sediment/soil material. These sorption models differ with respect to the type of sorption isotherm (linear or non-linear), the assumptions made concerning the time-dependency (instantaneous or rate-limited) and reversibility of the sorption process (reversible and irreversible). In this study, two models including Equilibrium CDE and Nonequilibrium CDE were used to simulate the fate and transport behavior of SDZ in Yangtze sediments.

2.6.1 Deterministic Equilibrium CDE

The convection dispersion equation (CDE) for one-dimensional transport of reactive solutes, subject to adsorption, first-order degradation and zero-production, in a homogeneous sediment or soil, is written as

$$\frac{\partial}{\partial t}(\theta C_r + \rho_b S) = \frac{\partial}{\partial x}(\theta D \frac{\partial C_r}{\partial x} - j_w c) - \theta \mu_l C_r - \rho_b \mu_s s + \theta \gamma_l(x) + \rho_b \gamma_s(x) \qquad [2.20]$$

where C_r is the volume-averaged or resident concentration of the liquid phase (μg L^{-1}), s is the concentration of the adsorbed phase (μg g^{-1}), D is the dispersion coefficient (cm^2 min^{-1}), θ is

the volumetric water content ($cm^3\ cm^{-3}$), j_w is the volumetric water flux density (cm min^{-1}), ρ_b is the soil bulk density (g cm^{-3}), μ_l and μ_s are first-order decay coefficients for degradation of the solute in the liquid and adsorbed phases, respectively (min^{-1}) and can not be negative; γ_l (μg cm^{-1} min^{-1}) and γ_s (μg g^{-1} min^{-1}) are zero-order production terms for the liquid and adsorbed phases, respectively; x is distance (cm) and t is time (min).

Solute adsorption by the solid phase is described with a linear isotherm as

$$s = K_d C_r \qquad [2.21]$$

where K_d is an empirical distribution constant (L kg^{-1}). Using [2.21] and assuming steady-state flow in a homogeneous sediment or soil, [2.20] could be rewritten as

$$R\frac{\partial C_r}{\partial t} = D\frac{\partial^2 C_r}{\partial x^2} - v\frac{\partial C_r}{\partial x} - \mu C_r + \gamma(x) \qquad [2.22]$$

where v (= $J_w\,\theta^{-1}$) is the average pore-water velocity, R is the retardation factor give by

$$R = 1 + \frac{\rho_b K_d}{\theta} \qquad [2.23]$$

So K_d value of the reactive solute in column could be calculated from equation [2.23] if R is known from the modeling.

Table 2.2 Dimensionless parameters for the Equilibrium CDE

Parameters	T	Z	P	R	C	μ^E	γ^E
Expressions	$\frac{vt}{L}$	$\frac{x}{L}$	$\frac{vL}{D}$	$1+\frac{\rho_b K_d}{\theta}$	$\frac{C}{C_0}$	$\frac{L(\theta\mu_l + \rho_b K_d \mu_s)}{\theta v}$	$\frac{L(\theta\gamma_l + \rho_b \gamma_s)}{\theta v c_0}$

Table 2.2 lists the dimensionless parameters that allow [2.22] to be written in reduced form as

$$R\frac{\partial C_r}{\partial T} = \frac{1}{P}\frac{\partial^2 C_r}{\partial Z^2} - \frac{\partial C_r}{\partial Z} - \mu^E C_r + \gamma^E(Z) \qquad [2.24]$$

where C_r is the volume-averaged solute concentration, P is the Peclet number, μ^E is a first-

order decay coefficient, γ^E is a zero-order production coefficient for equilibrium transport, Z and T are the dimensionless space and time variables, respectively.

2.6.2 Deterministic nonequilibrium CDE

Solute transport in the subsurface is affected by a variety of chemical and physical nonequilibrium processes (Nielsen et al., 1986; Aharoni and Sparks, 1991). Chemical nonequilibrium may occur as a result of kinetic adsorption while physical nonequilibrium is caused by a heterogeneous flow regime.

Although the chemical and physical Nonequilibrium CDE are based on different concepts, they can be put into the same dimensionless form for conditions of linear adsorption and steady-state water flow (Nkedi-Kizza et al., 1984; van Genuchten and Wagenet, 1989).

The two-site and two-region models can be defined as dimensionless form (Nkedi-Kizza et al., 1984):

$$\beta R\frac{\partial C_1}{\partial T}=\frac{1}{P}\frac{\partial^2 C_1}{\partial Z^2}-\frac{\partial C_1}{\partial Z}-\omega(C_1-C_2)-\mu_1 C_1+\gamma_1(Z) \qquad [2.25]$$

$$(1-\beta)R\frac{\partial C_2}{\partial T}=\omega(C_1-C_2)-\mu_2 C_2+\gamma_2(Z) \qquad [2.26]$$

where β is a partitioning coefficient, ω is a dimensionless mass transfer coefficient.

Table 2.3 Dimensionless parameters for the nonequilibrium CDE

Parameter	One-Site	Two-Site	Two-Region
R	$1+\frac{\rho_b K_d}{\theta}$	$1+\frac{\rho_b K_d}{\theta}$	$1+\frac{\rho_b K_d}{\theta}$
β	$\frac{1}{R}$	$\frac{\theta+f\rho_b K_d}{\theta+\rho_b K_d}$	$\frac{\theta_m+f\rho_b K_d}{\theta+\rho_b K_d}$
ω	$\frac{\alpha(R-1)L}{v}$	$\frac{\alpha(1-\beta)RL}{v}$	$\frac{\alpha L}{\theta v}$

β is a partitioning coefficient, ω is a dimensionless mass transfer coefficient

Table 2.3 defines the various dimensionless parameters for the one-site (f = 0) and two-site as

well as two-region adsorption models.

The modeling was done by the software Stanmod (version 2.07) with CXTFIT code. The program CXTFIT 2.1 may be used to estimate parameters in several models for transport during steady one-dimensional flow by fitting the parameters to observed laboratory or field data obtained from solute transport experiments (Simunek et al., 1999). For the equilibrium CDE, the program may be used to estimate the pore water velocity (v), the dispersion coefficient (D), the retardation factor (R), the first-order degradation coefficient (μ) and/or the zero-order production coefficient (γ) from observed concentration distributions versus time and/or distance. As for Nonequilibrium CDE, the coefficient of partitioning between the equilibrium and nonequilibrium phases (β) and the mass transfer coefficient (ω) for transfer between the two phases can also be fitted well. From the definition of R, β and ω (Table 2.2 and Table 2.3), the empirical distribution constant K_d could be calculated for both Equilibrium and Nonequilibrium CDE models and compared with batch experiments and modeling.

Chapter 3

Materials and methods

3.1 Chemicals and Adsorbents

3.1.1 Chemicals

Sulfadiazine (99%) was purchased from Sigma-Aldrich. ^{14}C-labeled sulfadiazine (99%) was provided by Bayer HealthCare AG (Wuppertal, Germany). The labeling position is at pyrimidine ring (Table 3.1). The ^{14}C-SDZ used in this study is a mixture of unlabeled and labeled (95.3%:4.7%) with specific radioactivity of 0.43 MBq mg^{-1}. Stock solution (40.0 mg L^{-1}) was prepared with Millipore water (Milli-Q Plus 185 with QPAK2, Millipore, Germany) with 0.01 M NaCl solution.

Table 3.1 Structure and physicochemical properties of SDZ

Structure of SDZ	Properties of SDZ
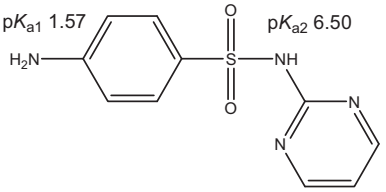	Molecular formula: $C_{10}H_{10}N_4O_2S$ Molar weight: 250.3 g mol^{-1} Water solubility: strong pH dependence pK_{a1} = 1.57, pK_{a2} = 6.50 logK_{ow} = -0.09

$FeCl_3$, $NaNO_3$ and NaCl were obtained from Merck (Darmstadt, Germany) with purity of 99%. Acetonitrile and methanol for HPLC are economy grade (99%), purchased from LGC-Promochem, Wesel, Germany. Liquid scintillation cocktail for LSC and oxidizer are Instant Scint-Gel Plus (Canberra Packard GmbH, Dreieich, Germany) and Oxysolve C-400 (Zinsser Analytics, Germany) respectively. Phosphoric acid (25%) was obtained from Grussing Diagnostika, Filsum, Germany.

3.1.2 Sediment/soil components

Goethite (α-FeOOH) was purchased from Merck (99%). To eliminate the impurities, the goethite powder was washed with distilled water several times until the conductivity keeps constant and dried by frozen-drying.

Aluminium Oxide C (δ-Al_2O_3) was obtained from Degussa. The chemical purity is > 99.6% and the density is 2.9 g cm^{-3}. Aluminium oxide C is produced by flame hydrolysis of anhydrous aluminium chloride ($AlCl_3$) and Debye-Scherrer X-ray diffraction patterns reveal that it has primarily a gamma structure. It contains chlorine contamination originating from the production procedure. In order to eliminate chlorine contamination, the powder sample was heated for 6 h at 1000 °C (Tombácz et al, 2001).

Illite purchased from KFT (99%) is cleaned by fractionation method to get the homogeneous particles: 100 g of illite and 200 ml Millipore water were added into a 1 L glass bottle for 6 hours shaking on a horizontal shaker at 150 rpm. Then 600 ml water was added in and shaking shortly to homogenize. After 6 min precipitation, the big particles more than 20 μm were deposited. The supernatant (up to 700 ml) was removed by 100 ml pipette into 250 ml centrifugation bottles and centrifuged for 90 min with 8000 rpm at 20 °C. The solid phase was deepfreezed and dry-freezed. The dry illite was crashed into fine powder for the following experiments.

SiO_2 was obtained from Merck with purity 99%.

The properties of these minerals are listed in Table 3.2.

Table 3.2 Properties of mineral adsorbents

	SSA (m^2 g^{-1})	pH (0.01 M NaCl)	Point of zero charge
goethite	12.6	6.8	7.5-9.5[b]
Al_2O_3	85[a]	8.2	8.1[c]
illite	36.5	4.0	3.5[d]

[a] Khalaf (2003); [b] Cornell and Schwertmann (2003); [c] Tombácz et al. (2001); [d] Lan et al. (2007)

Humic acid (Elliott soil Humic Acid standard, 1S102H) used in this study was purchased from International Humic Substance Society (IHSS).

3.1.3 Sediments and Soil

The soil (orthic luvisol) used in this study was taken from the field of Merzenhausen (Germany). The air dried soil was crashed and sieved by 2 mm sieve (see also in thesis of Unold, 2009).

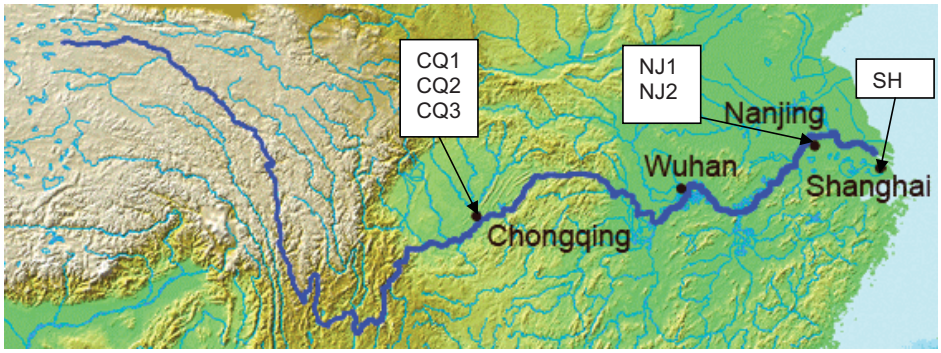

Figure 3.1 Sampling locations of Yangtze sediments

The sediment samples were obtained from Yangtze River, China. The three sampling sites located at three big cities along the Yangtze River: Chongqing, Nanjing and Shanghai. The surface sediment samples (up to 10 cm) were collected from the river bank in Shanghai (December 2006), Nanjing (May 2007) and Chongqing (June 2007). The sediment samples were air-dried, then crashed and sieved by 2 mm sieve. The information about sampling sites is shown in Figure 3.1 and GPS position and some physicochemical properties of sediments are listed in Table 3.3.

Table 3.3 Sampling sites and properties of Yangtze sediments

Number	Name	location	SSA m^2 g^{-1}	TOC %	pH (NaCl)
1	SH	Shanghai (N 31°37'05", E 121°23'71")	7.01	0.58	8.8
2	CQ1	Chongqing (water treatment plant)	32.5	3.34	8.2
3	CQ2	Chongqing, Beibei, Jialing river (N 29°50'24", E 106°25'38")	6.3	1.50	9.1
4	CQ3	Chongqing, Wanzhou (N 30°41'54", E 108°23'32")	10	1.07	8.9
5	NJ1	Nanjing (N 32°07' 02", E 118°49' 00")	12.7	0.60	9.5
6	NJ2	Nanjing (N 32°27' 01", E 118°43' 59")	17	0.94	9.1

Elemental analysis

The elemental analysis of Yangtze sediments and illite was done by Inductively Coupled Plasma Optical Emission Spectroscopy (ICP-OES) method. The results are shown in Table 3.4.

Table 3.4 Elemental analysis of Yangtze sediments and illite

	Al	Ca	Fe	K	Na	Si	Mg	Mn
				%				
SH	6	3.1	3	2.5	1.7	32.3	1.3	0.064
CQ1	9	3.9	3.5	2.2	0.86	20.3	1	0.13
CQ2	6.1	5.5	3.6	2.5	0.72	32	0.96	0.088
CQ3	7.4	3.4	4.1	2.7	0.85	31.7	1.1	0.069
NJ1	6.9	3.4	4.1	2.8	0.92	32.8	1.4	0.078
NJ2	8.1	3.5	4.9	3.2	0.7	30.3	1.6	0.11
illite	15.2	0.081	0.2	9.7	0.049	26	1.2	<0.005

Particle size fractions of Yangtze Sediments

The sediments were analyzed by sedimentation after dispersion with Na-pyrophosphate (humus and carbonate were not destroyed) and the results are listed in Table 3.5.

Table 3.5 Particle size fractions of Yangtze sediments*

Name	SH	CQ1	CQ2	CQ3	NJ1	NJ2	Soil
Sand %	11.75	44.75	30.25	7.75	21.5	4.5	6.4
Silt %	84.65	46.13	63.88	76.13	68.65	79.03	78.2
Clay %	3.6	9.13	5.88	16.13	9.85	16.48	15.4

* Measured by INRES, University Bonn

Clay mineral composition of Yangtze sediments

The clay mineral composition of Yangtze sediments was determined by X-ray diffraction (XRD). The results are shown in Table 3.6. Illite is the dominant clay mineral in Yangtze sediments and ranges from 60% to 80%.

Table 3.6 Components of clay minerals*

Name	SH	CQ1	CQ2	CQ3	NJ1	NJ2
Smectite %	20	5	10	10	10	15

Chlorite %	10	5	10	20	10	15
Illite %	60	80	70	60	70	60
Kaolinite %	10	10	10	10	10	10

* Measured by INRES, University Bonn

Surface area and pore volume of Yangtze sediments

Specific surface area, total pore volume and micropore volume were measured using the N_2 BET-method (see Chapter 3.3). The values are listed in Table 3.7.

Table 3.7 Surface characterization of sorbents

sorbents	specific surface area ($m^2 g^{-1}$)	total pore volume * ($cm^3 g^{-1}$)	Micropore volume ** ($cm^3 g^{-1}$)
		Model sorbents	
illite	36.6	0.165	0.015
		Pristine sediments	
SH	7.01	0.024	0.002
NJ1	12.65	0.044	0.004
CQ2	6.28	0.041	0.002
CQ1	32.48	0.101	0.010
		Fe, Al, Si extracted sediments	
SH	1.99	0.015	0.001
NJ1	3.40	0.028	0.001
CQ2	3.71	0.038	0.001
CQ1	30.29	0.089	0.008

* total pore volume was measured at *ca.* $P/P_0 = 0.995$

** micropore volume was calculated by Dubinin-Radushkevich (DR) method

3.2 Experimental procedures

3.2.1 Stability of SDZ in the investigated systems (minerals, sediments and soil)

Stability of SDZ solutions (light/dark)

To investigate the stability of SDZ solution in light and dark, two SDZ stock solutions (10 mg L^{-1}) were prepared in 20 ml airtight glass tubes. One was exposed under normal lab condition with natural light, the other one was covered by aluminium foil and stored in dark. 1 ml sample was taken after 6 and 65 days, respectively, and analyzed by HPLC-UV.

Stability of SDZ in the presence of different sorbents

^{14}C-SDZ stock solution with 0.01 M NaCl was diluted to 0.5 mg L^{-1}, 10 ml solution was added into each tube. All the adsorbents were weighted in the amounts according to batch experiments (Al_2O_3 0.1 g, illite 0.5 g, goethite 0.2 g, soil and sediments 1 g). The tubes were shaken in dark for 7 days with 150 rpm. After centrifugation (5000 rpm, 30 min), 1 ml supernatant was taken out for Radio-HPLC measurement. All the samples were done in duplicate and with blanks.

Influence of goethite concentration

The same procedure was conducted to prepare stock solution and samples as described above, 0.002 g, 0.02 g, 0.2 g and 0.4 g goethite was weighted into each tube. All the samples were prepared in duplicate together with blanks and shaken for 24 hours with 150 rpm. Then 1 ml of supernatant was taken out for Radio-HPLC measurement after centrifugation.

Influence of contact time

The samples were prepared as described before, 10 ml ^{14}C-SDZ solution (0.5 mg L^{-1}) and 0.2 g goethite were mixed in the centrifuge tubes. The tubes were shaken in dark with 150 rpm. Samples were taken every 24 hours from the supernatant after centrifugation and analyzed by Radio-HPLC. All the samples run with blank and the experiment took 7 days.

Influence of redox condition

The ^{14}C-SDZ stock solution was separated into 2 vials, one was saturated with O_2 and another was aerated by argon before mixed with goethite powder. The duplicate samples were shaken with 150 rpm in dark for 24 hours and then analyzed by Radio-HPLC after centrifugation.

Influence of SDZ concentration on Fe-solubility in a goethite suspension

The goethite amounts of all the samples used in this experiment were 0.2 g. Unlabelled SDZ stock solution were diluted to 0.1, 0.5, 1.0, 2.5 and 5.0 mg L^{-1}. The sample mixture of 10 ml SDZ solution with goethite was shaken in dark for 24 hours. After centrifugation (5000 rpm, 30 min), 5 ml of supernatant was carefully moved out and filtered by 0.45 μm filter to eliminate the possible small goethite particles in suspension. The first 2-3 ml solution was used to saturate the filter and the last 2 ml was removed into Teflon tubes. The Fe-ion concentration was measured by ICP-OES.

Stability of SDZ in Fe^{3+}_{aq} solution

To investigate the stability of SDZ in presence of Fe^{3+}_{aq}, the experiment was performed with 1.8 g L^{-1} $FeCl_3 \cdot 6H_2O$ solution (nearly the same Fe content as in the goethite/SDZ system) and 0.5 mg L^{-1} ^{14}C-SDZ. After shaking 2 days in dark, the solution was measured by radio-HPLC.

Identification of SDZ transformation products on goethite

Two aqueous 10 mg L^{-1} solutions of SDZ (with and without 10 mM NaCl) were shaken with suspended goethite (20 g L^{-1}) at RT in the dark for 48 h. After centrifugation with 3000 rpm for 30 min, the supernatants were taken out. Firstly, the samples were injected in HPLC-UV to determine whether the transformation products exist. Then the samples were analyzed by LC-MS-MS, APCI-FTICR-MS and QTof-MS for identification of the transformation product structure. The conditions of chromatography are given in Chapter 3.3.

Photolysis of SDZ solution

The photolysis effect of SDZ was investigated to compare the transformation product with goethite/SDZ system. The experimental procedure followed with Sukul et al. (2008a).

3.2.2 Sorption batch experiments

Sorption kinetics

To investigate the equilibrium time of adsorption, kinetics study was conducted for each sorbent. 0.1 g Al_2O_3, 0.5 g illite, 0.2 g goethite, 1.0 g soil and sediments were weighted into plastic tubes for each sample. 10 ml diluted ^{14}C-SDZ stock solution (0.2 mg/L) with 0.01 M NaCl electrolyte solution was added into each tube. All the samples were shaken with speed of 150 rpm under room temperature in dark. Samples were taken every 24 hour and centrifuged for 30 min at 3000 rpm. 5 ml supernatant was taken out and mixed with 10 ml scintillating liquid, then the radioactivity was measured by LSC.

Adsorption Isotherms

To investigate the adsorption behavior and distribution coefficients (K_d) of sulfadiazine on different adsorbents, batch experiments according to OECD recommendation (OECD, 2000) were conducted. Unlabelled SDZ was used for high concentration range (1.0–10 mg L^{-1}) and ^{14}C-SDZ was used for low concentration range (< 1.5 mg L^{-1}). For low concentration isotherm, 0.1 g of Al_2O_3, 0.5 g of illite, 0.2 g goethite, 1.0 g soil and 1.0 g sediment, respectively, were

weighted into 10 ml plastic centrifuge tubes. ^{14}C-SDZ stock solution was diluted into different concentrations (50 µg L^{-1} - 2.0 mg L^{-1}) with 0.01 M NaCl electrolyte and then 10 ml solutions were added into tubes with caps. Considering the adsorption effect on plastic tubes, blanks (without adsorbents) were also prepared for each concentration. All samples were prepared in triplicate and left in the shaker with speed of 150 rpm under room temperature for 48 h in dark. From the preliminary experiments, any transformation of the SDZ during this time was considered to be negligible. Samples were subsequently centrifuged for 30 min at 3000 rpm. 5 ml supernatant of each sample was mixed with 10 ml scintillating liquid and counted 15 min in Liquid Scintillation Counter. For the high concentration range, the procedure was nearly same. The stock solution of SDZ was 10.0 mg L^{-1}. Then the samples were measured by HPLC-UV. The amount of sorbed solute was calculated from the difference in concentrations between initial and equilibrium concentration.

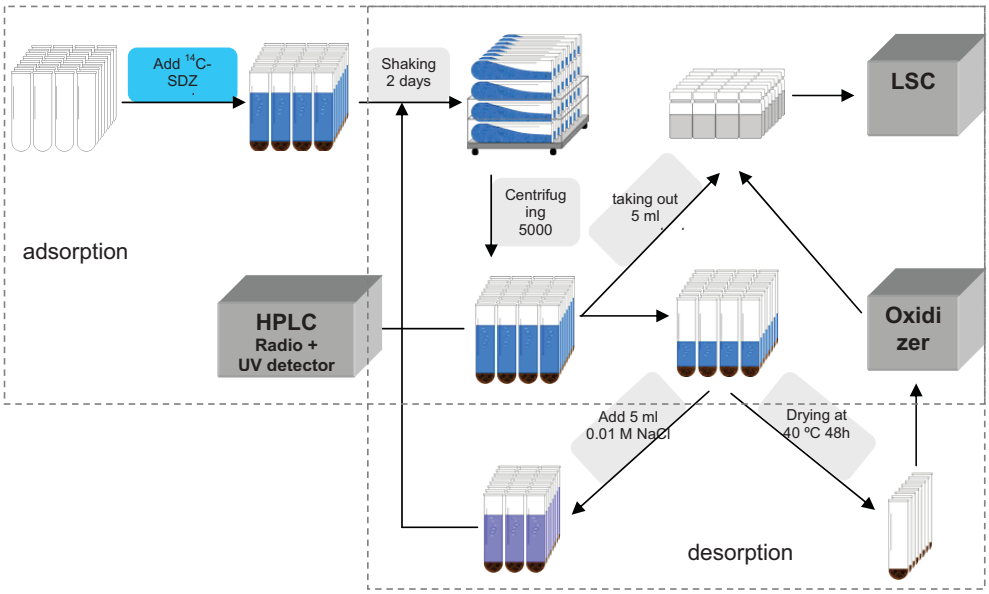

Figure 3.2 Ad/desorption procedure

Desorption Isotherms

The experimental conditions for desorption follow the OECD guidelines (OECD, 1999). All the experiments were done with ^{14}C-SDZ and the desorption amounts were determined by the oxidizer method and measuring the radioactivity in the solid residual. So for each SDZ concentration, 12 parallel samples were prepared for one adsorption step and 3 desorption steps as well triplicate samples for each step. The adsorption step is the same as in adsorption

isotherm experiments described above. After adsorption and centrifugation, 5 ml supernatant was taken out for mass balance by LSC analysis. 3 from the 12 same samples were dried in the oven for 48 hours at 40 °C and the residues were combusted by Oxidizer to measure the radioactivity, then the sorbed amounts could be calculated. It should be considered that the measured concentration in the solid phase is the sum of sorbed SDZ and solved SDZ in solution on wet solid sample. So the SDZ amount in solution could be calculated by the solid water content and SDZ concentration in solution. For the rest of 9 samples, another 5 ml 0.01 M NaCl solution without SDZ was added into each tube to maintain the total amount of solution to 10 ml. The residue was suspended again by shaking. The tubes were then shaked with a speed of 150 rpm under room temperature for 48 h in dark again. This step was repeated 3 times to get the desorption isotherms. The procedure of sorption batch experiments is shown in Figure 3.2.

Mass balance

For the unlabeled SDZ, the adsorbed amount (C_s) is determined by the difference of the total mass input in the system (batch or column) and the measured equilibrium concentration in the water phase. The errors could be caused by: 1) Mass losses in the system, e.g. diffusion into the caps and/or diffusive losses from the vial (wall adsorption). To avoid it, every experiment would performed with blank samples which only contain solution without sorbent. 2) Biodegradation could be ruled out from the preliminary experiments. 3) Measurement errors of the concentration in the water phase, especially for column experiments, if the concentrations were near the detection limit of HPLC-UV.

For ^{14}C-labeled SDZ, the solid surface concentration could be measured directly by the oxidizer method. It is easily to obtain the total recovery of the experiments. But care should be taken for this method that, after drying, the solved SDZ in pore water on the wet solid residuals was also counted. Thus the real sorbed amount should be calculated and corrected with concentration of water phase. The ad/desorption isotherms in low concentration range were all obtained by this method. The totally recovery of adsorption experiments ranged between 95-105%.

3.2.3 Transport experiments

The transport experiments were conducted in packed Yangtze sediment columns near water

saturation to assess the mobility of SDZ in the sediment.

The column was made of stainless steel with 3 cm inner diameter and 10 cm height. It was mounted on a porous ceramic plate (high flow, air-entry point > 1 bar). An HPLC-pump supplied a constant irrigation from a reservoir. The outflow was collected by a fraction-sampler.

Dry sediment was packed in the column in small increments with water and vacuum pump to ensure the column filling is homogenous. The column was weighted before and after filling to control the sediment mass and water content in the column and to get the pore volume.

The sediment columns were irrigated with electrolyte (0.01 M NaCl) at a constant velocity of approximately 0.2 cm min^{-1} for 2 days to establish steady state flow conditions. Although the flow rate was regulated by the HPLC-pump, it was additionally controlled by weighting the reservoir per unit time as well as the leached volume in the single fractions.

The breakthrough curve of NO_3^- as a non-reactive tracer was determined for each packed sediment column to characterize the flow behavior. The NO_3^- (0.01 M $NaNO_3$) was applied as the same pulse duration as SDZ with approximately 3 pore volume (500 min). The concentration of NO_3^- in the leachate was determined by HPLC-UV.

All the transport experiments were performed by using unlabeled SDZ. The application solution of SDZ (40 – 775 µg L^{-1}) was prepared with 0.01 M $NaNO_3$. The pulse duration of SDZ was 500 min for each column and the concentration of SDZ was determined by HPLC-UV. The data analysis and modeling of breakthrough curves (BTCs) are described in theory part (Chapter 2.6).

Table 3.8 Experimental conditions of column experiments

column	C_0	V_{in}	Δt_{in}	m_{in}	v	j_w
	µg L^{-1}	L	min	µg	ml min^{-1}	cm h^{-1}
SH-Q	100	0.105	500	10.5	0.21	1.68
CQ1-Q	100	0.105	500	10.5	0.21	1.68
CQ2-Q	100	0.105	500	10.5	0.21	1.68
NJ1-Q	100	0.105	500	10.5	0.21	1.68
SH-a	775	0.105	500	81.4	0.21	1.68
SH-b	40	0.105	500	4.2	0.21	1.68

SH-c	49	0.105	2000	5.1	0.048	0.41

C_0 is the SDZ concentration in the application solution, V_{in} is volume of application solution, Δt_{in} is the pulse duration, m_{in} is the applied mass, v is the flow rate, j_w is irrigation rate

Three column experiments on SH sediment with different input scenarios (SH-a, SH-b, SH-c) were performed in order to investigate the effect of concentration and flow rate on SDZ-transport.

3.3 Analytical methods

HPLC-UV

In this work, High Performance Liquid Chromatography (HPLC) with UV detector was used for the measurement of concentrations of the unlabelled SDZ solutions. The Gynkotek HPLC system was equipped with a reversed-phase column (Phenomenex Synergi Fusion RP 80, 250 mm×4.6 mm ID 4µm) and a Gynkotek High Precision pump (Model 480) with GINA 50 Autosampler (DIONEX). The injection volume was 150 µL for each sample. The column was eluted with a mixture of methanol and 0.1% phosphoric acid in water with 1.0 ml min^{-1} flow rate by gradient operation. The gradient started with water (with 0.1% phosphoric acid) for 3 min, the methanol fraction increased linearly to 57% till minute 23, then increased to 100% till minute 32. After 5 min, it changed to water till 100% in next 3 min and then kept 10 min. The samples were detected by Gynkotek UVD3405 (variable wavelength monitor) detector at wavelength 267 nm and the results were analyzed by Chromeleon V6.40 of DIONEX software. The detection limit of the HPLC-UV for SDZ is about 50 µg L^{-1}.

Radio-HPLC

^{14}C-SDZ and the transformation products were separated and detected by radio-HPLC. The HPLC system with a reversed-phase column (Phenomenex Synergi Fusion RP 80, 250 mm×4.6 mm, ID 4µm) was eluted with a mixture of water and methanol (49:1) and buffered with 0.5 ml of a 25% phosphoric acid solution. The injection volume was 250 µL for each sample. A gradient with an increased amount of methanol was used for peak separation, starting with 100% water for 6 min, the methanol fraction increased linearly to 27% till minute 23, then to 37% in the next 3 min and to 47% in the following 2 min. The methanol part reached its maximum with 57% after 30 min. The detection limit of Radio-HPLC is about 40 Bq ml^{-1}, which correspond to about 93 µg L^{-1} SDZ due to the ^{14}C-SDZ used in this study

was mixture (about 5% ^{14}C-SDZ).

LSC

Liquid Scintillation Counting (LSC, 2500TR, Packard Bioscience GmbH, Dreieich, Germany) was used to measure the ^{14}C radioactivity in the liquid samples. The detection limit of the LSC-method is 0.25 Bq per sample, which corresponds to 1.2 µg L^{-1} SDZ for 5 ml sample in this study. Normally the measured volume was chosen according to the specific radioactivity of the sample and 5 ml was taken for all the samples in this study. The sample was mixed with 10 ml scintillation cocktail (Instant Scint-Gel Plus) gel, then measured in triplicate and corrected for the background radiation. The corresponding specific radioactivity was calculated from the measured radioactivity. The SDZ concentration in solution was determined after division by the specific radioactivity of the applied SDZ, assuming that ^{14}C-radioactivity is linearly related to the SDZ concentration. But this method is only valid for the total radioactivity of ^{14}C and could not distinguish the SDZ as well as its transformation products.

Oxidizer

The SDZ concentration in solid adsorbents (minerals and soil/sediments) was determined by measuring the ^{14}C-radioactivity after total combustion of the solid samples with oxidizer (Robox 192, Zinsser Analytik GmbH, Frankfurt, Germany). After combustion, the evolving gas was washed into a scintillation cocktail (Oxysolve) in which the labeled CO_2 was trapped. This cocktail was measured with LSC. The performance of the method was checked in each measuring series. Blanks were run before and after the samples to check for background contamination and cross contamination during the measurement. The efficiency of the combustion process (> 96%) was ascertained by combusting samples spiked with a known amount of the model compound ^{14}C-anilazine prior and after the samples of the experiment. The total concentration of SDZ in the adsorbents was calculated from the mass of the adsorbents, the specific radioactivity of the applied SDZ and the measured radioactivity corrected for the corresponding recovery. As discussed above, the measured radioactivity is the sum of both SDZ and transformation products.

LC-MS/MS (Biospec)

HPLC: Agilent, (1100 series Santa Clara, CA, USA)

MS: TSQ Quantum (Thermo Fisher, Waltham, MA, USA)

Column: Phenomenex Synergi 4µ Fusion-RP 80 A (150 x 2 mm) (Torrance, CA, USA)

Gradient: A: 1 mM NH_4Ac + 0.1 % formic acid

B: Acetonitrile + 0.1 % formic acid

Program: 100 % A isocratic for 5 min, linear gradient to 60 % A during 10 min, and to 100 % B during next 2 min. 100 % B isocratic for 6 min, return to initial condition (100 % A) within 1 min, holding for 7 min.

Flow rate: 0.3 ml/min

Injection: 20 µl

Flow switch: 0 – 1.5 min towards waste, 1.5 – 13.5 min towards APCI source, 13.5 – 30 min towards waste (only used in case of SDZ/goethite solutions in order to avoid contamination of the MS by high SDZ concentrations)

Column Temperature: 20°C

Ionization: APCI (+):

Discharge Current:	4.0 µA
Sheath Gas:	25 psi
Aux Gas:	5 units
APCI Vap. Temp.:	450°C
Capillary Temp.:	200°C
Collision Gas:	1.5 mTorr

BET

The specific surface area (SSA) of adsorbents was determined with Micromeritics Gemini 2360 Analyzer (Micromeritics, Norcross, GA, USA) using N_2 gas sorption at 77K. Before gas sorption analysis, the samples were degassed on a Micromeritics FlowPrep 060 Degasser for one hour at 200 °C with N_2 as carrier gas. A multi-point BET surface area determination was performed at partial pressures < 0.3. All the measurements were done in triplicate.

Chapter 4

Results and discussion

4.1 Transformation of SDZ on minerals and sediments: stability, structure, mechanisms

The transformation of SDZ occurs via biotic and abiotic processes. The biotic processes including excretion from human or animals and bacterial degradation in manured soil were studied in some recent papers. The biotic metabolites of SDZ detected from monkey urine were isolated and identified as N_4-hydroxysulfadiazine, N_4-acetylsulfadiazine, 4-hydroxysulfadiazine, 5-hydroxysulfadiazine and other sub-metabolites (Vree et al., 1995). N_4-acetylsulfadiazine was also found as metabolite both from excretion by animals (Kreuzig and Höltge, 2005) and in manured soil (Schmidt et al., 2008). Another metabolite, 4-(2-iminopyrimidin-1(2H)-yl)aniline, together with 4-hydroxysulfadiazine were detected in transport experiments with soil (Unold et al., 2009). For abiotic processes, the study by Sukul et al. (2008) shows that photolysis of SDZ leads to 4-(2-iminopyrimidin-1(2H)-yl)aniline and other five metabolites. Another possibility of abiotic transformation is the chemical reaction between SDZ and sediment/soil components. But it has been poorly studied until now.

All these studies show that SDZ is not a stable compound in the natural environment. To interpret the behavior of SDZ in ad/desorption batch experiments and transport experiments, decomposition must be considered. Al_2O_3, goethite, illite and SiO_2 were chosen as model adsorbents to investigate the transformation of SDZ under different conditions. Al_2O_3 is a model sorbent for metal oxide, goethite is the most important transition metal oxide in sediments, SiO_2 is the most abundant mineral phase on earth and illite is a typical clay mineral in Yangtze sediments (see Chapter 3.1.3, Table 3.6).

Additionally, the possible transformation products are also potential environmental toxic substances.

4.1.1 Stability of SDZ solutions (in natural light and in dark)

To test the stability in light ("photolysis"), a SDZ solution in glass tubes was exposed under normal laboratory condition with natural light for about 2 months. Figure 4.1 shows the HPLC chromatogram results after 6 days and 65 days exposure.

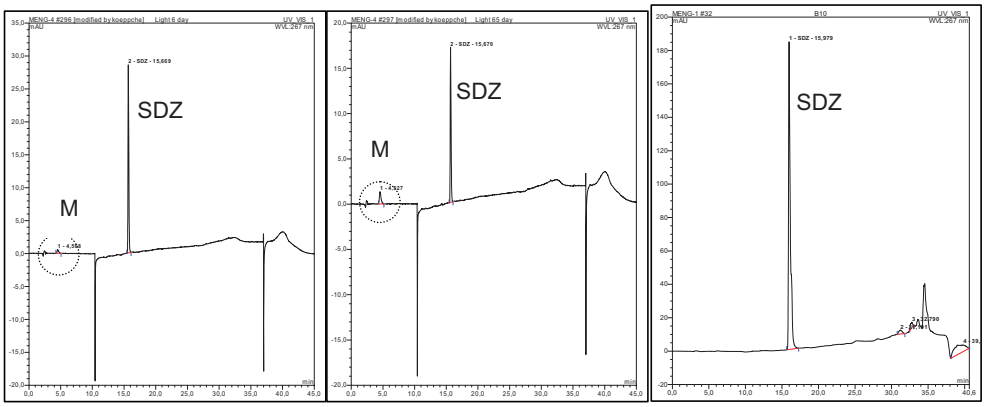

Figure 4.1 HPLC chromatogram with UV-detection of SDZ solution under light after 6 days (A), 65 days (B) and in dark after 65 days (C) (C_{SDZ} = 0.7 mg L^{-1}, in light: natural light under laboratory condition)

After 6 days, a transformation product M with retention time 4.5 min appeared. After 65 days, the M peak area increased from 3.3% to 13.5% and the concentration of SDZ decreased from 0.68 mg L^{-1} to 0.41 mg L^{-1}. In contrast, Figure 4.1 (C) indicates that transformation (abiotic and/or biotic) can be totally avoided in dark. To avoid the photolysis/biodegradation effect in this work, the batch experiments were performed in dark.

4.1.2 Stability of SDZ in the presence of different sorbents

Beside the photolysis, a chemical transformation of SDZ at the surface of the different sorbents may occur. In order to prove this hypothesis the following experiments were performed under the same conditions as in batch experiments (see Chapter 3.2.2) with the minerals used in this study. The samples were shaken 7 days and the possible transformation products were determined with Radio-HPLC. The results are shown in Figure 4.2.

There is no transformation product found in samples of Al_2O_3 and SiO_2, less than 5% (peak area) transformation product M was found in the illite suspension. But nearly 60% of the total

radioactivity was found as M in the goethite suspension which indicates that this Fe-oxide appears to play a role as catalyst or chemical reaction medium in the transformation of SDZ.

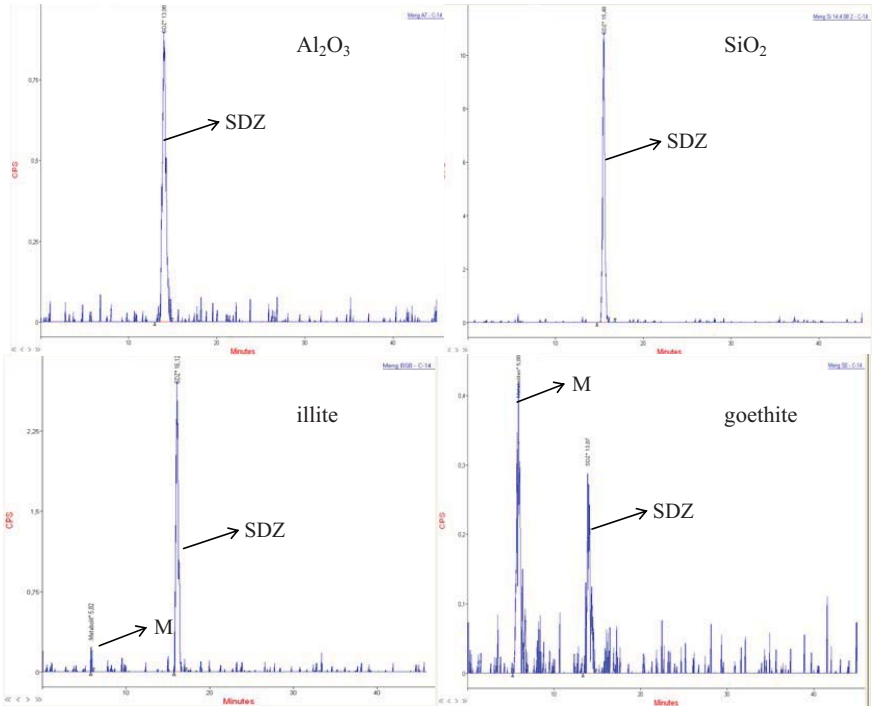

Figure 4.2 Radio-HPLC chromatograms of the supernatant of ^{14}C-SDZ sorption on Al_2O_3, SiO_2, illite and goethite after 7 days shaking in dark ($C_{SDZ_{initial}}$ = 0.5 mg L^{-1}, $C_{Al_2O_3}$ = 10 g L^{-1}, C_{illite} = 50 g L^{-1}, $C_{goethite}$ = 20 g L^{-1}, C_{SiO_2} = 100 g L^{-1})

Additionally to the minerals, Yangtze sediments and a soil from Merzenhausen were shaken with SDZ-solution for 7 days to determine possible transformation products. No detectable amounts of transformation products were found. Therefore biodegradation can also be ruled out.

From the results by now, the transformation product M is only detected in considerable amounts in the goethite suspension, thus the further experiments will focus on the interaction between SDZ and goethite. Assuming that the SDZ-transformation on goethite is a surface chemical reaction, a clear dependence from typical chemical parameters should be found (goethite- and SDZ-concentration, contact time and redox condition).

4.1.3 Influence of goethite concentration

Assuming that transformation products arise from the chemical transformation of SDZ on the surface of goethite, the concentration of goethite in the suspension and the surface area respectively should have an influence on the amount of transformation products.

In Figure 4.3 the peak areas of SDZ and the transformation product M versus goethite concentration are shown.

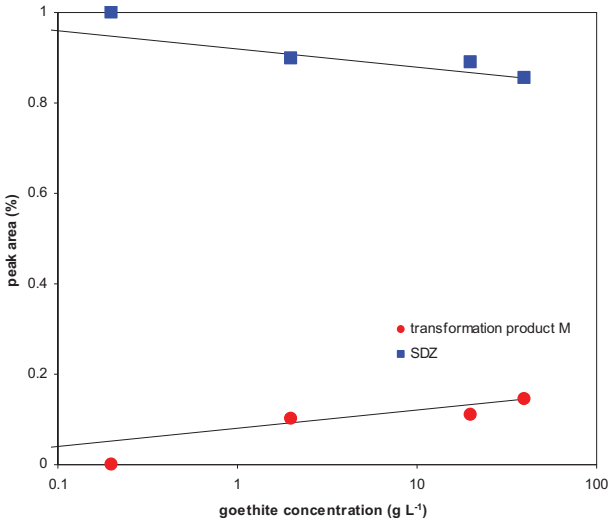

Figure 4.3 Peak area (Radio-HPLC) of ^{14}C-SDZ and transformation product M vs. goethite concentration (^{14}C-SDZ: 0.5 mg L^{-1}, 24 h shaking in dark)

For 0.2 g L^{-1} goethite concentration, there was no transformation product detected. If the goethite concentration was 10 times higher (2 g L^{-1}), the peak area of the transformation product was about 10.3% and it increased only a little in the 20 g L^{-1} goethite suspension. At 40 g L^{-1}, the transformation product increased to 14.4%. A significant dependence between the formation of the transformation product M and the goethite concentration in the suspension was found. It can be assumed that more goethite provide more reactive sites to SDZ for chemical transformation.

4.1.4 Influence of contact time

The peak areas of SDZ and the transformation product M versus contact times are shown in Figure 4.4.

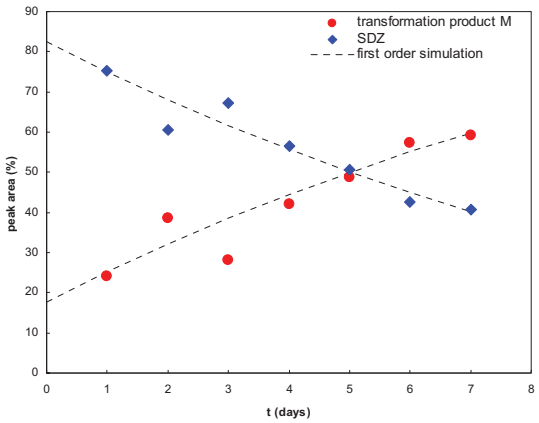

Figure 4.4 Peak area of transformation product M and SDZ (Radio-HPLC) versus contact time (^{14}C-SDZ: 0.5 mg L^{-1}, goethite: 20 g L^{-1}, in dark)

After 1 day the peak area (percentage) of transformation product M was 24.0% and increased to 59.3% after 7 days. Correspondingly the concentration of SDZ in solution decreased.

Based on equation 2.9 and 2.10 in Chapter 2.4.2, the rate constant k_1 = 0.075 d^{-1} and the half-life value $t_{1/2}$ = 9.7 d (r^2 = 0.97) were calculated. Except biodegradation and photolysis, which can be excluded in this work as mentioned before, the most probable mechanism is a chemical reaction on goethite surface. In the study of Torrents and Stone (1991), the goethite surface catalyzed the hydrolysis of phenyl-picolinate and it was also first-order kinetics with a rate constant k_1 about 0.0283 d^{-1}. Dannenberg and Pehkonen (1998) investigated the goethite catalyzed hydrolysis of the pesticide diazinon and the kinetics could be described by first-order rate law. The rate constant k_1 was 0.0268 d^{-1} at pH 5.7 and 0.0302 d^{-1} at pH 8.5 respectively. In another paper from the same group (Hong and Pehkonen, 1998), the hydrolysis of pesticide phorate by different iron oxides including goethite was investigated. The hydrolysis reaction was treated as pseudo-first-order reaction and the rate constant k_1 for goethite was 0.24 d^{-1} at pH 5.7 and 0.34 d^{-1} at pH 8.5. Chun et al. (2005) reported a study about the degradation of chlorinated disinfection byproducts (BDPs) by Fe(II) in the presence of goethite and magnetite. The overall hydrolysis and reductive kinetics of trichloro-

acetaldehyde hydrate (TCAh) were described by a pseudo-first-order model and the overall rate constant k_1 for goethite was 0.043 d^{-1}. The similarity of the rate constant in this work with literature data indicates a chemical reaction between SDZ and goethite surface. The reaction mechanism is discussed in Chapter 4.1.9.

On the other hand, the degradation via photolysis of SDZ in soil and manured soil were also investigated (Sukul et al., 2008b) and could be compared with the SDZ/goethite system. For example, the SDZ photolysis in manure shows a half-life time about 6.6 d (Sukul et al., 2008) which is in the same order of magnitude as the transformation in the goethite system ($t_{1/2}$ = 9.7 d). In contrast, the photolysis in water in the presence of photo sensitizers, that means a system without solids, is rapid with $t_{1/2}$ between 3.8 h – 32 h (Boreen et al., 2005).

4.1.5 Influence of redox condition

Assuming that the transformation is a redox reaction with iron oxides, an influence of oxic/anoxic conditions could be expected. Thus experiments were performed under O_2 and Ar atmosphere, respectively.

After 24 hours shaking of the SDZ/goethite suspension under O_2 and Ar, the peak area of the transformation product was 55.2% (O_2) and 54.8% (Ar), respectively. There was no significant difference between both chromatograms. It can be assumed that the oxic/anoxic conditions have no influence on the formation of the transformation product in this experimental design. It is to note here that O_2 (air) diffusion inside the system during shaking could not be excluded. Even thus, the O_2 content in Ar system was definitely much lower than that in the O_2 system.

4.1.6 Influence of SDZ concentration on Fe-solubility in a goethite suspension

The factors influencing the solubility of iron oxide are pH, complexation, redox reactions, ionic strength and solid properties like particle size (Cornell and Schwertmann, 2003). Assuming that there is a chemical reaction between goethite and SDZ, following processes can be considered to influence the dissolution:

1) complexation of Fe-ions in the solution with SDZ as ligand. This leads to an increasing total Fe-concentration in the solution via shift of the dissolution equilibrium.

2) complexation of Fe-ions with SDZ at the goethite-surface. This weakens the Fe-O bonds and causes the detachment of Fe-ions into the solution (see Chapter 2.2).

To confirm this mechanism, sorption experiments with the same goethite amount but different SDZ concentrations were performed and the total Fe-concentration in the supernatant was measured (Figure 4.5).

The Fe-ion concentration in a goethite suspension without SDZ is undetectable with ICP-OES (< 0.03 mg L^{-1}), which is in agreement with literature data. Goethite is one of the least soluble iron oxides (Cornell and Schwertmann, 2003). In the pH range 4-10 and in the absence of complexing or reducing agents Fe_T is < 10^{-6} M (< 0.056 mg L^{-1}). After addition of 0.1 mg L^{-1} SDZ, the Fe-ion content in solution was 0.032 mg L^{-1}, and it increases to 0.76 mg L^{-1} up to 5 mg L^{-1} SDZ.

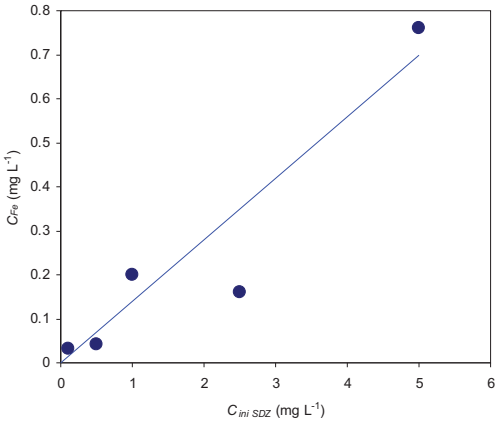

Figure 4.5 Influence of initial SDZ concentrations on Fe content in the supernatant of a goethite-suspension (24 h shaking in dark, 0.01 M NaCl, $C_{goethite}$ = 20 g L^{-1}, data measured by ICP-OES after filtration)

The complexation between SDZ and goethite could be the key factor leading to this result. SDZ acts as a ligand and the following reaction can be assumed,

$$FeOOH + H_2O + SDZ^- \rightleftharpoons Fe\text{-}SDZ^{2+} + 3OH^-$$

The higher concentration of SDZ provides more SDZ^- ligand, consequently increases the soluble iron content. The experimental results appeared to confirm this hypothesis.

4.1.7 Influence of Fe^{3+}_{aq} on the transformation of SDZ

The Lewis acid properties of metals such as Cu^{2+}, Fe^{3+} and Al^{3+} appear to be important to mineral-catalyzed hydrolysis of organic compounds (McBride, 1994). To confirm whether the Fe^{3+} ion in solution could catalyze the formation of M from SDZ, the experiment was performed by shaking the mixture of $FeCl_3$ and ^{14}C-SDZ solution in dark for 24 hours. Comparing with the SDZ/goethite system, the total amount of Fe^{3+} should be the same. Thus, the concentration of $FeCl_3 \cdot 6H_2O$ in solution was calculated to be about 60 g L^{-1}. Then the solution was investigated by Radio-HPLC. There was no transformation product found in this experiment which indicates that only Fe^{3+} ions in solution do not cause such transformation effect. This could be an indication that the reaction of Fe ions with SDZ to form M can only take place on the surface of the iron oxide.

4.1.8 Identification of SDZ transformation products: investigations with mass-spectrometry

In order to identify the transformation product M, the supernatant of goethite suspension was investigated by LC-MS using full scan mode to separate and determine all possible transformation products. Only the masses of protonated ions *m/z* 187 could be detected (not shown). Thus, further investigations were focused on all *m/z* 187 products in photolysis solution (for comparison) and goethite suspension with LC-MS-MS. The MRM chromatograms are shown in Figure 4.6.

Figure 4.6-A is the chromatogram of SDZ-standard solution for the mass *m/z* 251 ($SDZ+H^+$) as a control. From the MRM chromatogram of *m/z* 187 in SDZ-photolysis solution (Figure 4.6-B), not only one peak but three peaks were detected and named as M1, M2, M3 with sequential retention time 3.7, 5.7 and 11.1 min, respectively. All these three peaks can be found in SDZ-goethite suspension but with different concentration ratio (Figure 4.6-C). The relative peak areas of M2 and M3 are much lower than that from SDZ-photolysis solution.

The mass difference (Δm = 64) between SDZ (*m/z* 251) and three transformation products M1, M2 and M3 (*m/z* 187) fits well with the mass of the SO_2 group which indicates that these transformation products result from the elimination of SO_2 from SDZ. The loss of SO_2 from sulfonamides including SDZ is well described in literature via photolysis process. Boreen et al.

(2005) investigated triplet-sensitized photodegradation of sulfamethazine and 4-(2-imino-4,6-dimethylpyrimidin-1(2H)-yl)aniline was identified as a main photoproduct. They estimated that 4-(2-iminopyrimidin-1(2H)-yl)aniline could be the photoproduct for SDZ. Sukul et al. (2008) confirmed this hypothesis in their work, 4-(2-iminopyrimidin-1(2H)-yl)aniline together with N-formyl-SDZ and 4-hydroxyl-SDZ were identified by mass spectrometry and NMR as the main photoproducts of SDZ by photolysis in water and manure. Elimination of SO_2 was found to be the main degradation process during irradiation.

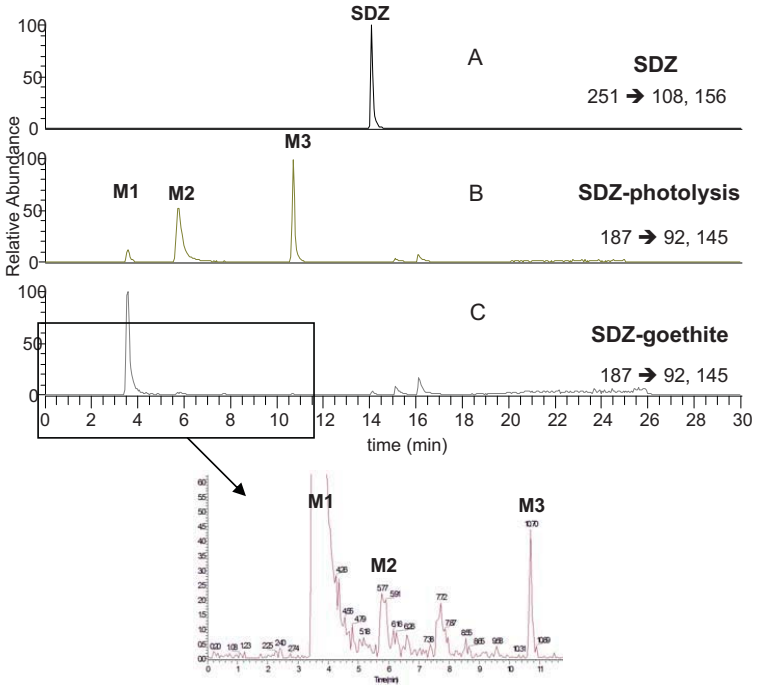

Figure 4.6 MRM chromatograms of SDZ solution (a), SDZ-photolysis solution (b) and SDZ-goethite suspension (C) after separation by Polar-RP column (150 x 3mm) and MS-detection in MRM-Mode (LC-MS-MS). The numbers on the right are *m/z* ions of Q1 (protonated precursor ion) and Q3 (product ions)

Thus the transformation products M1, M2 and M3 can be described with same sum formula $C_{10}H_{10}N_4$ as shown in Figure 4.7. The retention time of M2 under the same chromatographic conditions is very close (5.7 min) to that in Sukul's work (5.4 min) (Sukul et al., 2008a). Thus it can be assumed that M2 is 4-(2-iminopyrimidin-1(2H)-yl)aniline (photoproduct A). M1and M3 are isomers of M2.

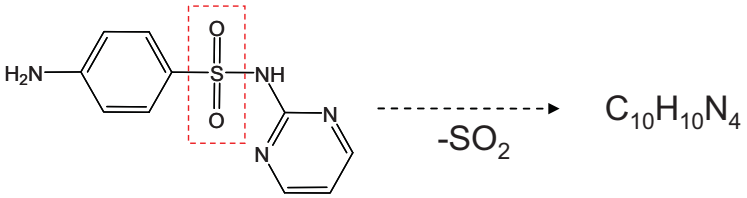

Figure 4.7 Transformation break down of SDZ by photolysis and in goethite suspension

The fragmentation of the three transformation products was performed by collision induced dissociation with Argon atoms in the collision cell of the LC-MS-MS which gives characteristic product ion spectra of M1, M2 and M3, respectively.

4.1.8.1 Transformation product M1

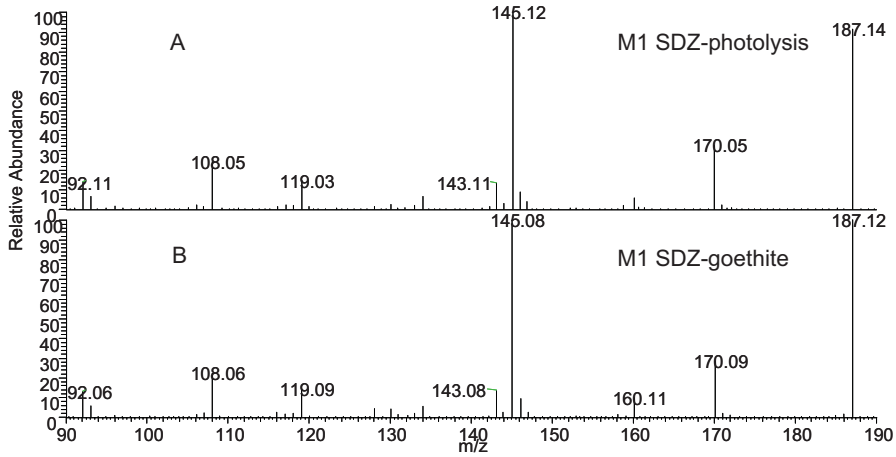

Figure 4.8 APCI-MS product ion spectrum of SDZ transformation product M1 (MS^2 of precursor ion *m/z* 187) obtained from SDZ-photolysis (A) and SDZ-goethite suspension (B)

Figure 4.8 shows the product ion spectra of transformation product M1 in SDZ-photolysis (Figure 4.8-A) and SDZ-goethite suspension (Figure 4.8-B). Both product ion spectra reveal same daughter ion masses *m/z* 170, 145, 108, 92 with nearly the same intensities. Thus the transformation product M1 from goethite suspension and from photolysis is identical. But the structure is still unclear.

4.1.8.2 Transformation product M2

The product ion spectrum of M2 in the photolysis solution gives the same product ions m/z: 170, 145, 108 and 92 as shown in Fig 4.8. The concentration of M2 in SDZ-goethite

suspension was not sufficient for the complete product ion spectrum analysis. But from the same retention time as mentioned before it can be concluded that both M2 peaks revealed the same substance and the structure is very similar to M1.

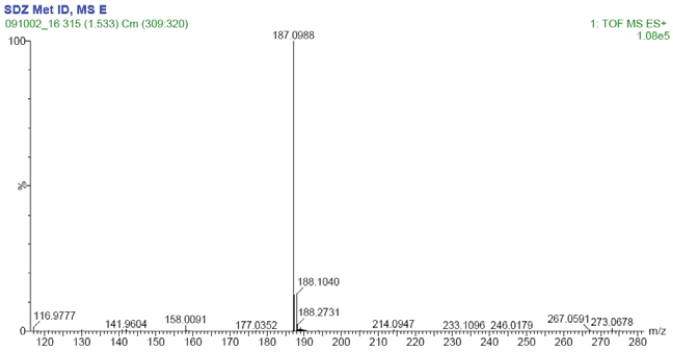

Figure 4.9 QTof-MS spectrum of an aqueous SDZ solution after photolysis (Waters GmbH)

The structure of M2 in SDZ-photolysis solution was elucidated by QTof-MS measurement. Figure 4.9 shows the accurate mass *m/z* 187.0988 for M2 in a UV irradiated SDZ-photolysis solution. This measured mass fits within a mass error of 2.1 ppm with a calculated mass of 187.0984 which belongs to the formula $C_{10}H_{11}N_4$ (see Table 4.1) and confirms our hypothesis.

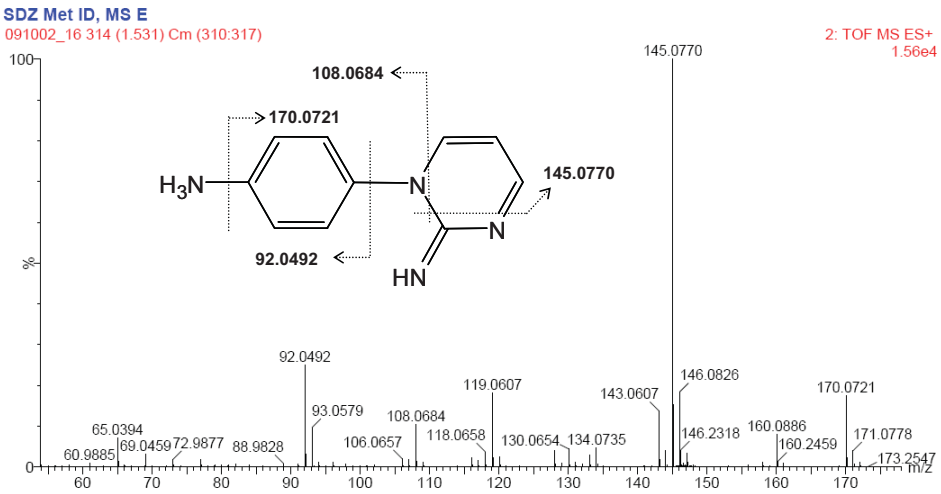

Figure 4.10 QTof-MS product ion spectrum of the precursor ion *m/z* 187 at t_R = 1.53 min

Additionally, the fragmentation of M2 (assumed as 4-(2-iminopyrimidin-1(2H)-yl)aniline) gives the product ion spectrum in Figure 4.10 with accurate masses of all daughter ions. The

main daughter ions are listed in Table 4.1.

Table 4.1 Results of accurate mass determination of M2 and fragments from SDZ photolysis

MS	RT	Measured Mass	Calc. Mass	Mass Error		Formula
	min	Da	Da	mDa	ppm	
MS^E	1.53	187.0988	187.0984	0.4	2.1	$C_{10}H_{11}N_4$
MS^E	1.53	145.0770	145.0766	0.4	2.8	$C_9H_9N_2$
MS^E	1.53	108.0684	108.0687	-0.3	-2.8	$C_6H_8N_2$
MS^E	1.53	92.0492	92.0500	-0.3	-8.7	C_6H_6N

At least with the help of the formula of the product ions in Table 4.1, it is possible to explain the fragmentation of 4-(2-iminopyrimidin-1(2H)-yl)aniline as follows:

formula	possible product
$C_{10}H_8N_3$	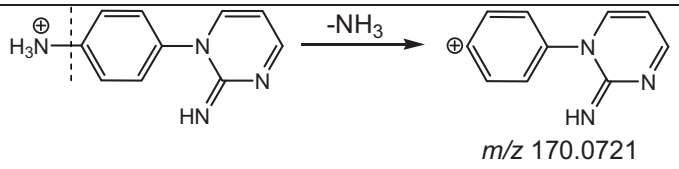
$C_9H_9N_2$	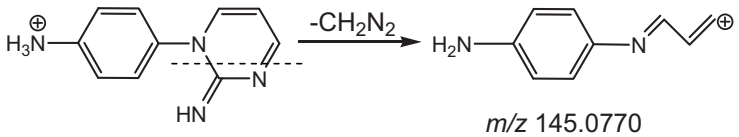
$C_6H_8N_2$	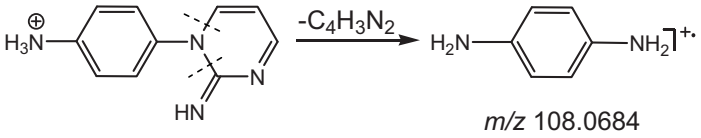
C_6H_6N	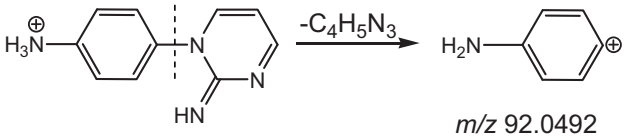

The ion at *m/z* 170 is due to the cleavage of the N-C bond on aniline part. Loss of CH_2N_2 from pyrimidine ring leads to the ion at *m/z* 145. The ion at *m/z* 108 is supposed to be benzene-1,4-diamine by the sum of formula $C_6H_8N_2$. The fragment at *m/z* 92 represents aniline group as supposed in literature (Klagkou et al., 2003; Sukul et al., 2008). The results of QTof-MS for M2 in SDZ-photolysis solution proved that the transformation product M2 in photolysis solution and in goethite suspension is 4-(2-iminopyrimidin-1(2H)-yl)aniline (photoproduct A) which is in agreement with the conclusion of Sukul et al. (2008).

4.1.8.3 Transformation product M3

As is shown in Figure 4.11, the product ion spectra of M3 in both SDZ-photolysis and SDZ-goethite system are identical. Significant difference is found between the fragmentation of M1 and M3 in intensities of *m/z* 145 (lower) and *m/z* 108 (higher) (Figure 4.8).

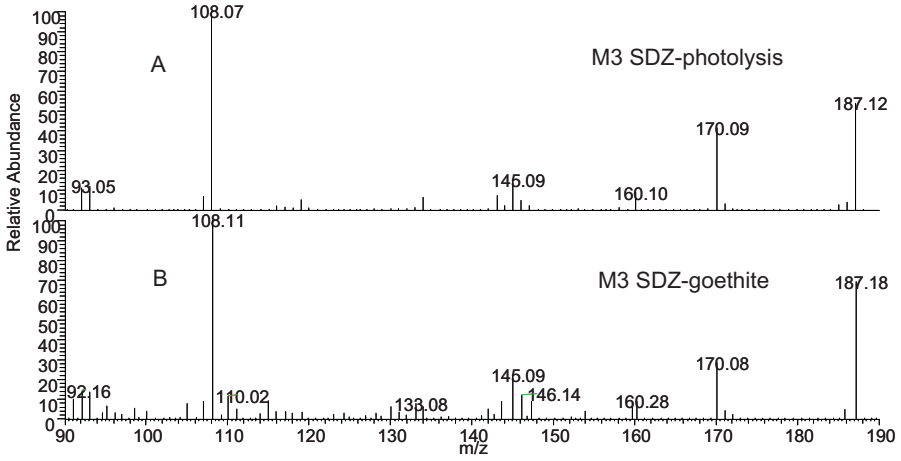

Figure 4.11 APCI-MS product ion spectrum of SDZ transformation product M3 (MS^2 of precursor ion *m/z* 187) obtained from SDZ-photolysis (A) and SDZ-goethite suspension (B).

As discussed above, the ion at *m/z* 92 supposed to be aniline group, the ion at *m/z* 170 was the elimination of NH_2 group and *m/z* 108 suggested to be 1,4-diaminobenzene. All these results indicate the structure of transformation products M1, M2 and M3 are the combination of aniline group and 2-amino-pyrimidine group. The difference can be the bond position of both groups. As elucidated above, M2 is 4-(2-iminopyrimidin-1(2H)-yl)aniline in which the pyrimidine N atom bonds to the para-C atom of aniline. For M1 and M3, it can be assumed that the amino group N of 2-amino-pyrimidine bonds to aniline instead of pyrimidine N. Thus the substance p-(pyrimidin-2-yl)aminoaniline (see Figure 4.12) was synthesized by University Budapest with purity > 99% and characterized by FT-IR and NMR (spectra not shown) as a reference substance.

Figure 4.12 shows the accurate mass spectrum of p-(pyrimidin-2-yl)aminoaniline as well as the assignment of structural fragments of three daughter ions *m/z* 170, 160 and 145.

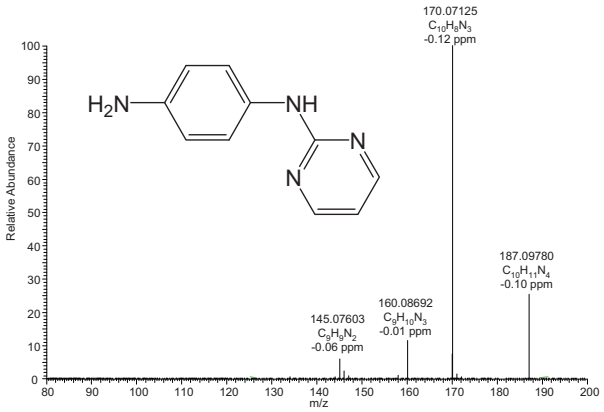

Figure 4.12 Accurate mass: APCI-FTICR-MS product ion spectrum of p-(pyrimidin-2-yl)aminoaniline (MS^2 of precursor ion *m/z* 187). The empirical formulas are calculated on the basis of the high resolved masses, the deviations from the theoretical masses are expressed in ppm

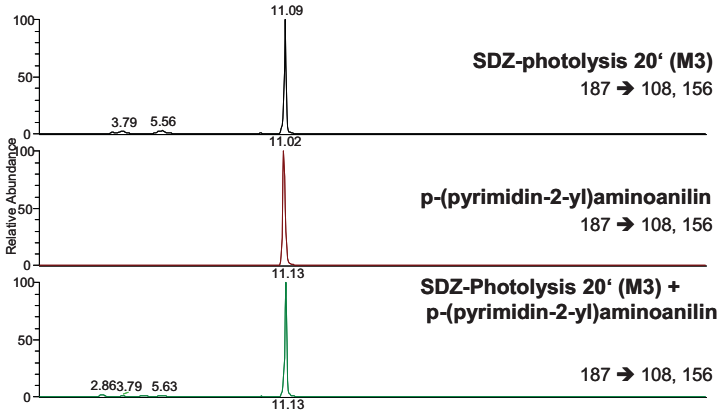

Figure 4.13 Ion chromatograms for SDZ-photolysis product M3, p-(pyrimidin-2-yl)aminoaniline and mixture of both with different ratio after separation by Polar-RP column (150 x 3mm) and MS-Detection in MRM-Mode

This substance was spiked in the SDZ-photolysis system with different concentrations and the ion chromatograms are shown in Figure 4.13.

As shown in Figure 4.13, the retention time of p-(pyrimidin-2-yl)aminoaniline is 11.02 min which is nearly the same with M3 (t_R=11.09 min). The mixture of both with different ratio exhibits only one peak at t_R=11.13 min. Complete peak overlap of p-(pyrimidin-2-yl)aminoaniline and M3 indicates that both are the same substance.

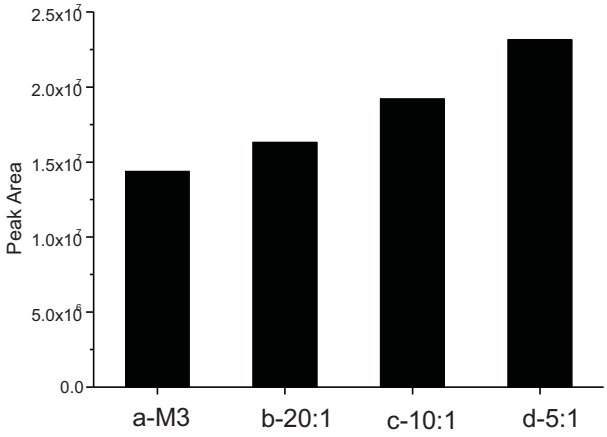

Figure 4.14 Peak area of M3 in SDZ photolysis samples spiked with p-(pyrimidin-2-yl)aminoaniline (a-M3, b-mixture with ratio 20:1, c- mixture with ratio 10:1, d- mixture with ratio 5:1)

Figure 4.14 shows the peak area of M3 in SDZ-photolysis solution spiked with p-(pyrimidin-2-yl)aminoaniline at retention time 11.13 min. The peak area increases with concentrations of p-(pyrimidin-2-yl)aminoaniline which also proved the conclusion above.

The transformation products M1, M2 and M3 were proven to be the same in both SDZ-photolysis solution and SDZ-goethite suspension, respectively. The structure of M2 was identified as 4-(2-iminopyrimidin-1(2H)-yl)aniline, the same with photo product A (Sukul et al., 2008) and M3 was p-(pyrimidin-2-yl)aminoaniline. In SDZ-goethite system, M1 is the main product, but the structure is still not identified directly due to the insufficient amount for accurate MS analysis. Nevertheless, comparing the mass spectra of all three transformation products, M1 and M2 are nearly identical with similar peaks and intensities for all main daughter ions at *m/z* 170, 145, 108 and 92. But for M3, the intensities of ions at *m/z* 145 and 108 are different. This result indicates that the structure of M1 and M2 are more similar than M3. On the other hand, the close retention time from chromatograms of M1 (3.7 min) and M2 (5.7 min) comparing with M3 (11.1 min) also supports this conclusion.

As discussed above, M1 was supposed to be bond of pyrimidine N to aniline C on different position comparing with M2 and the supposed structure of M1 together with M2 and M3 is shown in Figure 4.15.

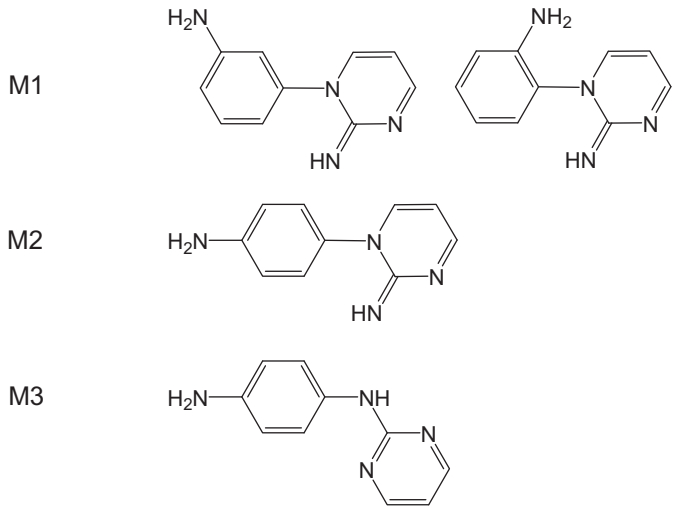

Figure 4.15 Possible structures of M1 and structure of M2 and M3

4.1.9 Proposed pathways for the reaction between SDZ and goethite

4.1.9.1 Surface complexation of SDZ on goethite

Surface complexation as well as chemical transformation of SDZ at the goethite surface can take place according to the proposed general reaction scheme in Figure 4.16:

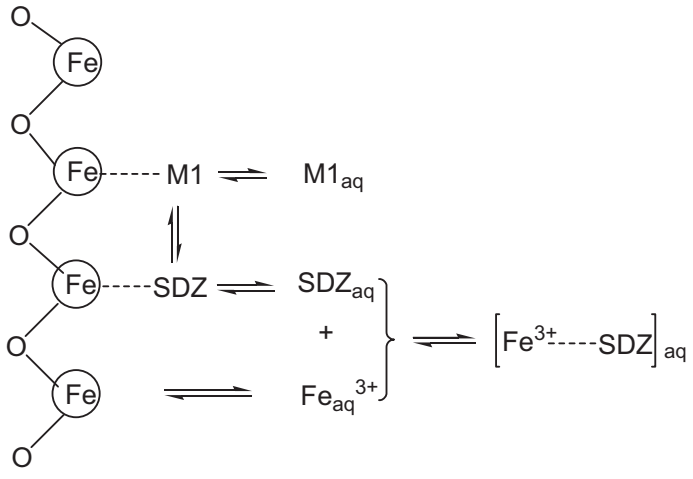

Figure 4.16 Scheme of possible SDZ reaction on the goethite surface

There are two proposed major processes in the SDZ-goethite suspension: i) solved SDZ may

adsorb to the goethite surface and forms a mono/bidentate complex; ii) chemical reaction can occur via the complex and leads to the transformation products M1, M2 and M3 (M1 as an example in Figure 4.16). These products may adsorb on the surface or release to the solution. Goethite plays a key role as sorbents, catalyst or even as reactant during these processes. Sheals et al. (2002) used a combination of adsorption measurements, X-ray photoelectron spectroscopy (XPS) and Fourier-transform infrared spectroscopy (FTIR) to investigate the adsorption of glyphosate (PMG) on goethite and confirmed that the surface complex is formed through one oxygen of PMG's phosphonate group. In our study, Raman and FTIR spectroscopic methods were attempted to investigate the surface complex of SDZ-goethite, but a direct observation of the SDZ surface complexation was not possible because of the low adsorbed amount of SDZ (μg g^{-1} range).

Due to the amphoteric properties, SDZ in solution forms cationic, uncharged and anionic species at different pH. In the SDZ-goethite suspension with pH 6.8, about 70% of SDZ is in anionic form (see Figure 2.2) with deprotonated sulfonamide-group (Figure 4.17-B). Then the SDZ ligand can be written in the mesomeric forms as shown in Figure 4.17-C and D.

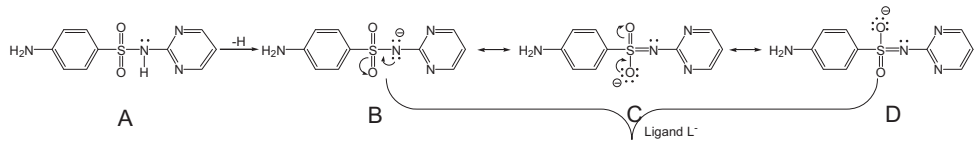

Figure 4.17 Ligand formation of SDZ (A: SDZ; B, C and D: deprotonated SDZ and its mesomeric structures)

The anionic SDZ ligand may adsorb on the goethite surface via the O and/or N of the sulfonamide group and form inner sphere complexes with Fe. As shown in Figure 4.18, SDZ-goethite surface complex may be formed by the substitution of OH^- group from goethite with SDZ ligands ("ligand exchange mechanism"). Additionally, a ligand adsorption on the surface of the iron oxide weakens the Fe-O bonds to neighbouring atoms and leads to detachment of the Fe^{III} and Fe^{III}-SDZ complex, respectively (see also Chapter 4.1.6).

The type of complex formed with the goethite surface is important because it dictates the number of surface iron atoms involved in sorption and therefore the stoichiometry of the surface complexation reactions used to provide model fits to sorption data (Evanko and Dzombak, 1999). In fact, it's not possible to determine the SDZ-goethite complex form without the spectroscopic evidence. But this mechanism can be assumed on the basis of the

studies of structure-similar complexation from literature.

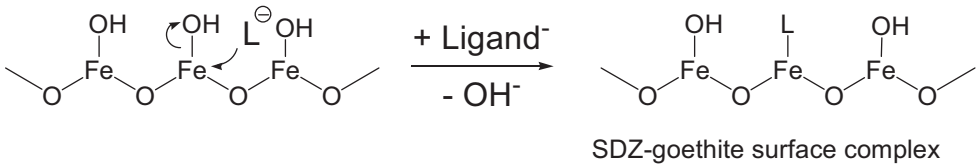

Figure 4.18 Formation of SDZ-goethite surface complex

Surface complexation on goethite was described as mono/bidentate, mono/binuclear and/or inner-/outer-sphere forms with different sorbates like salicylate (Yost et al., 1990), benzoate and phthalate (Tejedor-Tejedor et al., 1990), carbonate (Villalobos and Leckie, 2001), small weak organic acid (Filius et al., 1997) and glyphosate (Sheals et al, 2003). It was reported that adsorption of EDTA onto goethite showed ligand-like adsorption behavior and formed mononuclear complex at high pH (Nowack and Sigg, 1996). Geelhoed et al. (1997) concluded that the adsorption behavior of sulfate on goethite can be described well using only one inner-sphere surface complex. Jonsson et al. (2008) investigated the adsorption of glyphosate (PMG) on goethite and supposed two major surface species, both are inner-sphere complexes where glyphosate is bound in a monodentate fashion to a surface iron through one of the phosphonate oxygens. The amine group of adsorbed PMG is not coordinated to iron at the surface. The SDZ-goethite complex can also be assumed as an inner-sphere form in a monodentate fashion through one oxygen of the sulfonyl group.

Besides monodentate inner-sphere complexation, other mechanisms also can not be ruled out. Peak et al. (1999) investigated the mechanism of sulfate adsorption on goethite via *in situ* ATR-FTIR spectroscopy and supposed the formation of monodentate bisulfate surface complexes with and without hydrogen bond. They also found at pH values greater than 6, that sulfate adsorbs on goethite only as an outer-sphere complex. With a combination of Raman and ATR-FTIR spectroscopy, Wijna and Schulthess (2000) showed that on goethite, sulfate forms a monodentate surface complex which is inner-sphere at pH 3-6, but outer-sphere at higher pH. With the charge distribution multisite complexation (CD-MUSIC) model, sulfate adsorption on goethite at pH 3-8 could be described by inner-sphere, monodentate complex (Rietra et al., 1999). For organic compounds like oxalate, the hydrogen-bonded complexes and electrostatically bonded complexes were proposed to dominate the surface speciation of oxalate at the goethite/water interface (Boily et al., 2007). A further work suggested in this

topic is to find spectroscopic evidence of surface complexation and interpret the transformation mechanism.

4.1.9.2 Transformation pathways of SDZ to M1 and M2 on the goethite surface

On the basis of the structure of M2 (photoproduct A) and complexation assumption above, the transformation pathway of M2 in SDZ-goethite suspension has been proposed and is shown in Figure 4.19.

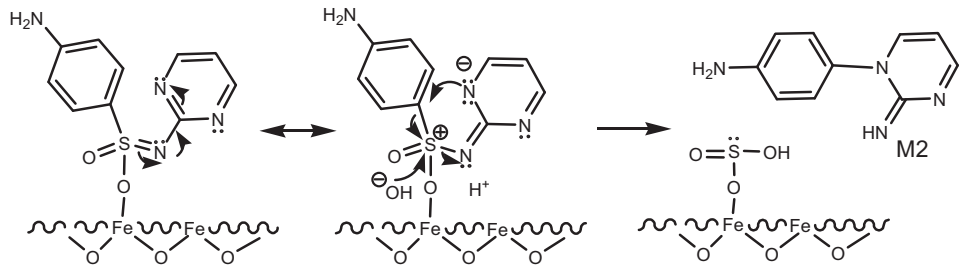

Figure 4.19 Proposed transformation pathway of SDZ to M2 in SDZ-goethite suspension

The complex via sulfonyl oxygen weakens the electron density of sulfonyl group leading to a significant increase of negative charge at the pyrimidine N atom. Then the negative pyrimidine-N attacks the positively polarized C-atom in para-position of aniline ring (S_N reaction at the aromatic ring). Simultaneously, OH^- group also involves in the complexation via direct nucleophilic attack on the S atom. Due to the similar structure of M1 and M2, the similar pathway has been supposed also for M1.

4.1.9.3 Transformation pathway of SDZ to M3 on the goethite surface

The reaction scheme which leads to transformation product M3 is in accordance with the so called “Ramberg-Bäcklund reaction”, which is well known as desulfonation reaction in organic chemistry (Ramberg and Bäcklund, 1940).

The suggested reaction mechanism is based on the assumption that the SDZ-goethite complex weakens the binding strength of the R-SO_2-R bond. Simultaneously an S_N-mechanism occurs via the negatively charged N (sulfonamide-N) on the positive polarized para-C in the aniline

ring. This positive charge is caused by the electronegative SO_2 group. Then following the Ramberg-Bäcklund reaction, the SO_2 group is eliminated and the transformation product M3 is released.

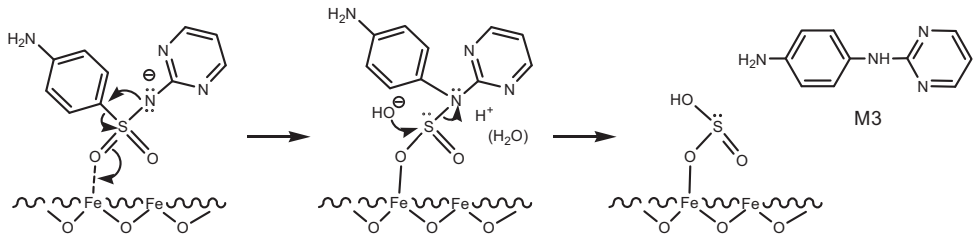

Figure 4.20 Proposed transformation pathway of SDZ to M3 in SDZ-goethite suspension

Finally depending on the redox conditions the sorbed $S^{IV}O_2$-species may undergo further reaction, e.g. reduction to S^{2-} or oxidation to SO_4^{2-} with corresponding oxidation/reduction in the system Fe^{2+}/Fe^{3+}-oxide. In contrast to Al_2O_3, SiO_2 and illite, goethite (FeOOH) may act as a redox catalyst.

4.2 Sorption of SDZ to minerals and organic matter (OM)

The sorption and transport of SDZ in sediments largely depend on its interaction with the inorganic and organic sediment components. The properties of the inorganic matrix and especially its charges in relation to the charge of SDZ are important parameters for the sorption process (Thiele-Bruhn, 2003). The sorption behavior of sulfonamides on soil, manured soil (Thiele-Bruhn, 2004; Sukul et al., 2008) and clay minerals (Gao et al., 2005) has been reported. But to our knowledge adsorption and desorption of SDZ on sediment inorganic components like metal oxide (e.g. Al_2O_3 and goethite), clay mineral (illite) in comparison with sediments have not been reported. Additionally, the contribution of organic substances to the overall process should be elucidated.

4.2.1 Adsorption kinetics on Al_2O_3 and illite

Kinetic experiments were performed to obtain the kinetic parameters as input for modeling and to establish the equilibrium time of SDZ sorption on different adsorbents. Sorption kinetics for minerals are shown in Figure 4.21. The SDZ-kinetics on organic matter (OM) is discussed later in Chapter 4.2.4.

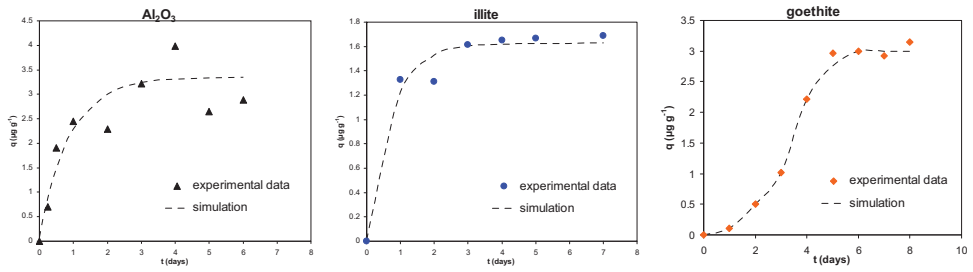

Figure 4.21 ^{14}C-SDZ sorption kinetics on Al_2O_3 and illite (dashed lines-fitted curves by first order kinetics); on goethite, the "kinetic curve" cannot be evaluated because of the simultaneous transformation process ($C_{SDZ_{initial}}$ = 0.5 mg L^{-1}, $C_{Al_2O_3}$ = 10 g L^{-1}, C_{illite} = 50 g L^{-1}, $C_{goethite}$ = 20 g L^{-1})

The kinetic curve of SDZ sorption on Al_2O_3 shows that the sorption sharply increases in the first 2 days and a plateau can be observed after 3 days, which can be assumed as the equilibrium time under this experimental condition. The kinetic curve of illite shows a similar result. In contrast, on goethite, the "kinetic curve" is of S-shape. It must be emphasized that

because of the transformation of SDZ to M1, M2 and M3, this data obtained by measuring the total ^{14}C radioactivity can not be interpreted. As discussed in Chapter 4.1, SDZ and its transformation products in the SDZ-goethite suspension cannot be distinguished using LSC, thus the measured "kinetic curve" is the result of the overall process.

Considering the instability of SDZ, 2 days contact time of the adsorption experiment was chosen. That's the frequently used contact time for sulfonamide sorption in the literature (see Table 2.1, Chapter 2.4.3).

Sorption kinetics on Al_2O_3 and illite could be described by a first order kinetics and the fitted parameters are listed in Table 4.2. Both materials have a similar rate constant k_1 (1.12 d^{-1} and 1.39 d^{-1}) and half-life time $t_{1/2}$ (0.61 d and 0.50 d).

Table 4.2 Kinetic parameters for the sorption of SDZ on Al_2O_3 and illite

	Al_2O_3	illite
k_1 (d^{-1})	1.12	1.39
$t_{1/2}$ (d)	0.61	0.50
r^2	0.926	0.985

4.2.2 Adsorption isotherms on Al_2O_3, SiO_2 and illite

Adsorption isotherm is an efficient tool to compare the sorption behavior on different sorbents. Al_2O_3, SiO_2 and illite were chosen as model sorbents representing typical sediment/soil components. As mentioned in the experimental part (Chapter 3.2.2), adsorption data obtained from labeled and non-labeled SDZ matched well in overlap concentration range, so the combination of both data sets was used for the isotherms.

SDZ adsorption isotherms on Al_2O_3 and illite in low and high concentration range and on SiO_2 in low concentration range are shown in Figure 4.22. Due to the transformation of SDZ sorbed on goethite, the "sorption isotherm" on goethite was only determined at the low concentration range for comparison with other sorbents.

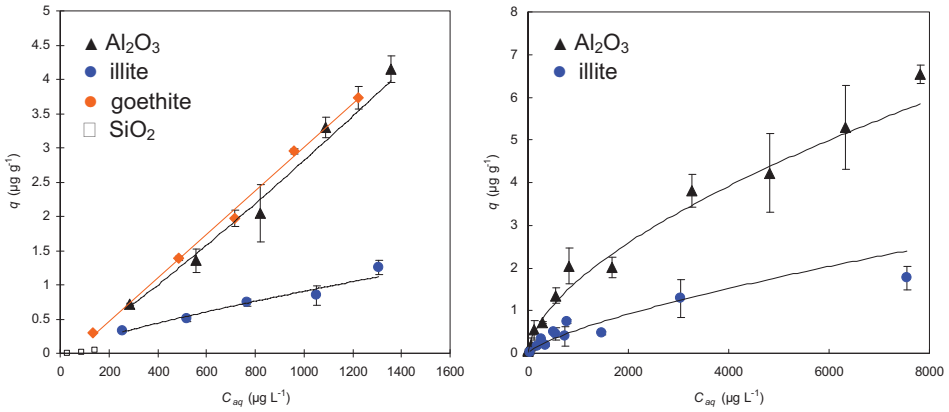

Figure 4.22 SDZ adsorption isotherms on Al_2O_3, illite, SiO_2 and goethite (on goethite, the "adsorption isotherm" cannot be evaluated because of the simultaneous transformation process) in low concentration range (left-curves fitted by linear regression) and in high concentration range for Al_2O_3 and illite (right-curves fitted by Freundlich model) ($C_{Al_2O_3}$ = 10 g L^{-1}, pH 8.2, C_{illite} = 50 g L^{-1}, pH 4.2, $C_{goethite}$ = 20 g L^{-1}, pH 6.8, C_{SiO_2} = 100 g L^{-1})

In the low concentration range, linear isotherms (Henry-behavior) were observed (K_d values see Table 4.3) for all three minerals. The SDZ adsorption affinity for Al_2O_3 is significant higher than for illite. The sorption on SiO_2 is quite low and negligible.

The adsorption isotherms in the high concentration range fitted the Freundlich adsorption equation well with values of $r^2 > 0.92$. The Freundlich equilibrium constant K_f is 1.74 for Al_2O_3 and 0.59 for illite respectively. The Freundlich exponent *1/n* varied between 0.56 and 0.62, indicating strong sorption nonlinearity. The strong nonlinearity was often observed for the sorption of polar solutes in soils, and was related to specific interactional groups of SOM (Chiou et al., 2000) and limited number of specific sorption sites in humic substances for sorption (Thiele-Bruhn et al., 2004). For oxides and clay minerals, it can also be assumed that sorption sites are not sufficient for higher concentration of SDZ which leads to sorption nonlinearity.

4.2.2.1 Role of surface area

Surface area (see Chapter 3.1.2, Table 3.2) can be a main factor for sorption. After normalization of sorption isotherms by the specific surface area, the role of surface area for different sorbents can be assessed.

Figure 4.23 shows the SDZ adsorption isotherms on Al_2O_3 and illite in low and high concentration range and additionally goethite in low concentration range normalized by surface area.

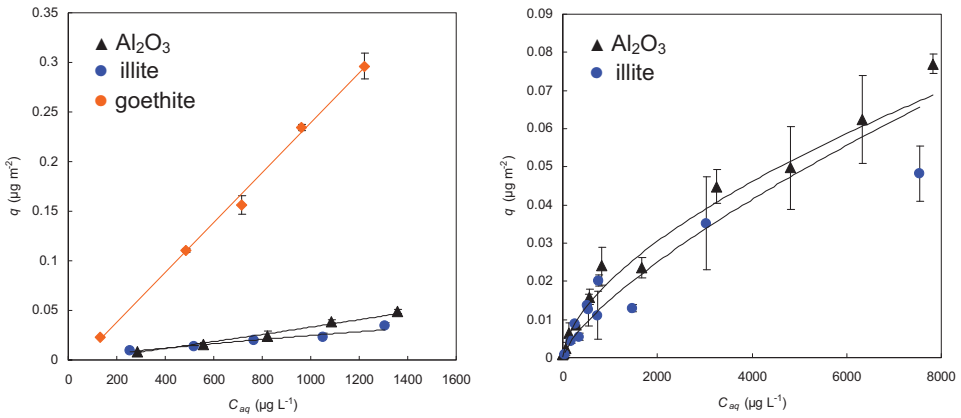

Figure 4.23 SDZ adsorption isotherms on Al_2O_3, illite and goethite (on goethite, the "adsorption isotherm" cannot be evaluated because of the simultaneous transformation process) in low concentration range (left-curves fitted by linear regression) and in high concentration range for Al_2O_3 and illite (right-curves fitted by Freundlich model) normalized by surface area ($C_{Al_2O_3}$ = 10 g L^{-1}, pH 8.2, C_{illite} = 50 g L^{-1}, pH 4.2, $C_{goethite}$ = 20 g L^{-1}, pH 6.8)

It's obvious that after normalization by surface area, both isotherms of Al_2O_3 and illite are similar over the whole concentration range. That means the higher adsorbed amount on Al_2O_3 is due to its higher surface area. These results are indicative of a weak physical sorption mechanism on both minerals. In Figure 4.23 (left) the "adsorption isotherm" on goethite is also shown to demonstrate the enhanced uptake of the mixture of SDZ and its transformation products. The strong increase is indicative of the surface area independent "strong binding" of SDZ as well as its transformation products on goethite.

Based on a space requirement of 150 $Å^2$ for SDZ, the estimated surface coverage on Al_2O_3 amounts to 0.01%. Assuming M free goethite/SDZ system only 0.1% of the surface of goethite is covered by SDZ molecules. So due to the very low surface coverage it's difficult to investigate the sorption mechanism by spectroscopic methods such as Raman or IR.

4.2.2.2 Effect of pH

Due to the amphoteric property of sulfonamides and the varying charge of minerals (see Chapter 2), pH is one of the dominant factors for the sorption. Sorption of sulfonamides on minerals decreases with increasing pH values (Kahle et al., 2007a; Gao et al., 2005). Natural pH values of Al_2O_3 and sediments suspensions are all above 8, for illite and goethite they are 4.2 and 6.8, respectively. To compare the sorption behavior on sediments at the same pH, the pH values of goethite and illite suspensions were adjusted to 8.0 by Tris buffer.

Figure 4.24 shows the SDZ adsorption isotherms on illite and the SDZ/M transformation product adsorption isotherms on goethite in low concentration range with pH adjustment:

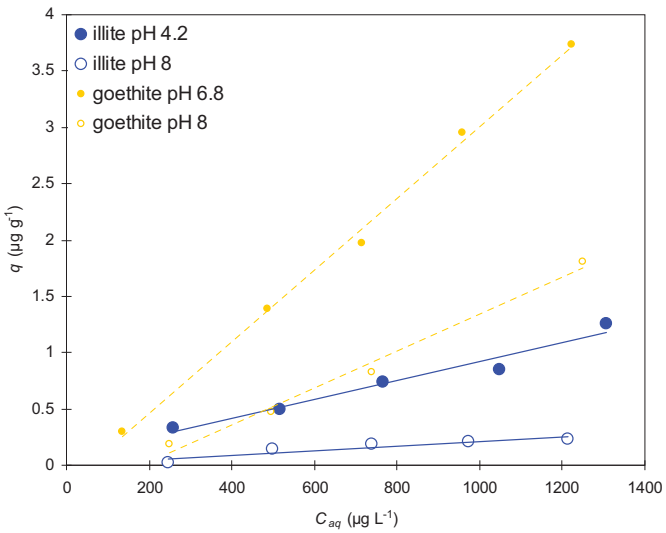

Figure 4.24 ^{14}C-SDZ adsorption isotherms on illite and goethite with pH adjustment (on goethite, the "adsorption isotherm" cannot be evaluated because of the simultaneous transformation process; pH was adjusted by Tris buffer)

Additionally, for the low environmental relevant concentration range, K_d-values of SDZ sorption on minerals at different pH are given in Table 4.3. Normalized K_d value by surface area, K_{SSA} values, are also listed in this table. (K_d was determined by the slope of linear isotherms at low concentration)

Table 4.3 K_d values of ^{14}C-SDZ adsorption on minerals at different pH

adsorbents	pH	K_d (L kg^{-1})	K_{SSA} (L m^{-2})
Al_2O_3	8.2	2.81	$3.31 \cdot 10^{-5}$
illite	4.2	0.91	$2.49 \cdot 10^{-5}$
illite *	8.0	0.21	$0.57 \cdot 10^{-5}$

* pH adjusted by Tris buffer

All the sorption isotherms in low SDZ concentration range with different pH value are linear. For goethite, the adsorbed amount is the result of the adsorption of both SDZ and transformation products. Therefore, a quantitative evaluation can not be discussed.

As shown in Figure 4.24, adsorbed amounts on illite decrease with increasing pH suggesting that electrostatic interactions play a role. The point of zero charge (pzc) of illite is 3.5 (Lan et al., 2007), so illite is negatively charged at pH 8. At the same pH, more than 90% SDZ species are negatively charged, thus the adsorbed amount decreases with increasing pH value because of the electrostatic repulsion between SDZ^- anion and the overall negative charge of the illite surface. The same conclusion can be found in literature (Boxall et al., 2002; Gao et al., 2005; Kahle and Stamm, 2007a).

To examine the contributions of individual sulfadiazine species to overall sorption, the adsorption coefficient K_d at a given pH value can be represented as the sum of the contributions of the individual species (Schwarzenbach, 2003):

$$K_d = K_d^+ \alpha^+ + K_d^n \alpha^n + K_d^- \alpha^- \qquad [4.1]$$

where K_d (L kg^{-1}) is the overall equilibrium adsorption coefficient, K_d^+, K_d^n and K_d^- are the adsorption coefficients of the cationic, uncharged and anionic species, respectively. α^+, α^n and α^- represent the mass fraction of these species in bulk solution. The minor zwitterionic species was neglected because the model fit is not improved by inclusion of a zwitterion term (Gao et al., 2005).

From the acid dissociation constants of sulfadiazine (pK_{a1}, pK_{a2}) and the batch solution pH (pH 4.2 and pH 8.0 for illite), species fractions were calculated:

$$\alpha^- = \alpha^n 10^{(pH - pK_{a2})} \qquad [4.2]$$

$$\alpha^{+} = \alpha^{n} 10^{(pK_{a1} - pH)} \quad [4.3]$$

$$\alpha^{+} + \alpha^{n} + \alpha^{-} = 1 \quad [4.4]$$

From the equations above, the calculated K_d^+, K_d^n and K_d^- values of SDZ sorption on illite are listed in Table 4.4.

Table 4.4 K_d values for the sorption of sulfadiazine species to illite

	K_d^+ (L kg^{-1})	K_d^n (L kg^{-1})	K_d^- (L kg^{-1})
illite	-	0.91	0.19

Considering the pH range in these experiments (4.2 to 8), the cationic species of SDZ was excluded. The K_d^n value for illite is much higher than K_d^- value. Kahle and Stamm (2007a) investigated the pH-dependent sorption of sulfathiazole on illite. They presented a similar K_d^n value (1.01 L kg^{-1}) after 14 days sorption and K_d^- value was negligible due to the quite low sorption at high pH values. It confirms the conclusion above, the anionic surface of the minerals obstructs SDZ anion sorption on the surfaces. Gao et al. (2005) proposed water bridging as a possible sorption mechanism between neutral sulfamethazine and montmorillonite surfaces as well as complexation of exchangeable cations through a pyrimidine N and/or the SO_2 group. The same mechanism can be assumed for SDZ sorption on illite.

4.2.3 Desorption isotherms on Al_2O_3 and illite

Desorption investigation is an effective tool to obtain additional information about the sorption mechanism, mobility and bioavailability of the sorptive.

Desorption isotherms of ^{14}C-SDZ sorbed on different adsorbents in low concentration range (0.25 mg L^{-1} -1.25 mg L^{-1}) are shown in Figure 4.25. The experiments were performed at five different initial concentrations, followed by three desorption steps. The solid residuals were dried and burned by Oxidizer, and the radioactivity of $^{14}CO_2$ was determined by LSC (see Chapter 3.3). SDZ adsorbed amounts were obtained directly from this procedure resulting in more reliable and accurate data compared with traditional calculation method using batch

technique.

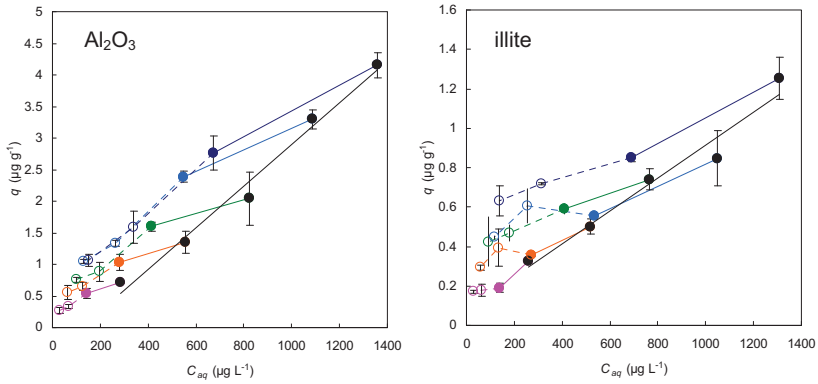

Figure 4.25 Desorption isotherms of ^{14}C-SDZ on Al_2O_3 and illite (● – adsorption, black solid line – fitted adsorption isotherm, colored point – first desorption step, colored open points – second and third desorption steps)

The first desorption step of Al_2O_3 (colored points connected to adsorption point by solid line) shows slight hysteresis. But the second and third desorption steps are almost totally reversible. Considering the kinetic curve of Al_2O_3 shown in Figure 4.21, the equilibrium time of SDZ sorption on Al_2O_3 is about 3 days. So after 2 days, the adsorption continued simultaneously with desorption which leads to such slight hysteresis effect. So it can be assumed that SDZ sorption on Al_2O_3 is nearly reversible.

For illite, the first desorption step is already nearly reversible. The data obtained from the second and third desorption is not reliable enough for fitting and modeling because of the scattering of the analytical data according to the quite low sorbed amount (less than 5%). But the conclusion still can be drawn that the SDZ sorption on illite is reversible.

Desorption hysteresis can be quantified by several hysteresis indices like H-index (Huang et al., 1998), exponent of the Freundlich equation (Ma et al., 1993; Swanson and Dutt, 1973), the distribution coefficient (K_d) (Laird et al., 1994) etc. Sander et al. (2005) pointed out the limitations of these indices and developed a thermodynamically based method to quantify true sorption hysteresis. But in this work, hysteresis was almost a kinetic phenomenon (see Chapter 4.3 and 4.4) when desorption experiment was started before reaching adsorption equilibrium. That means an adsorption step has even not been completed (Drillia et al., 2005).

The desorption isotherms were described by Freundlich model for each initial concentration (Barriuso et al., 1994; Pusino et al., 2004) without calculation of hysteresis index. Desorption results can be quantified by modeling. These modeling results are discussed in the Chapter 4.4.

Freundlich equilibrium constants (K_f) and the exponents ($1/n$) of different initial concentrations were determined by nonlinear regression for Al_2O_3 and illite, respectively (Table 4.5). The Freundlich model fits the desorption data on Al_2O_3 well ($r^2 > 0.96$) for all the initial SDZ concentrations. The K_f values increase with initial SDZ concentrations. The similar values of desorption Freundlich exponent ($1/n$) compared with adsorption (0.62**,** see Chapter 4.2.2) indicate the reversible sorption which is consistent with the conclusions above. Similar results were found for illite, but the correlation coefficient was not satisfying (about 0.7) because of the data scattering in the low concentration range as discussed above.

Table 4.5 Freundlich isotherm parameter values for SDZ desorption on Al_2O_3 and illite

adsorbent	C_i* (mg L^{-1})	K_f** ($\mu g^{1-1/n} L^{1/n} g^{-1}$)	$1/n$[b]	r^2
Al_2O_3	0.25	1.32 (±0.10)	0.48 (±0.04)	0.989
	0.50	1.75 (±0.24)	0.44 (±0.04)	0.988
	0.75	2.30 (±0.16)	0.51 (±0.07)	0.966
	1.00	3.18 (±0.13)	0.57 (±0.06)	0.985
	1.25	3.43 (±0.08)	0.64 (±0.04)	0.995
illite	0.25	0.47 (±0.14)	0.34 (±0.15)	0.740
	0.50	0.55 (±0.08)	0.22 (±0.09)	0.772
	0.75	0.78 (±0.03)	0.28 (±0.03)	0.978
	1.00	0.79 (±0.08)	0.27 (±0.10)	0.789
	1.25	1.08 (±0.07)	0.33 (±0.08)	0.904

*C_i is initial concentration of solution

**value in parentheses is the 95% confidence interval

4.2.4 SDZ sorption on organic matter (OM)

The sediment/soil organic matter (SOM) is a very active sorbent for sulfonamides (Thiele-Bruhn et al., 2004; Kahle and Stamm, 2007b). So it is necessary to investigate the sorption behavior of SDZ on SOM to better understand the fate and transport of SDZ in sediment and soil. As a model for SOM, a Luvisol humic acid purchased by International Humic Substance Society (IHSS-HA) was used.

Figure 4.26 shows the uptake curve of SDZ on IHSS-HA. The contact time for the uptake curve was 30 days. The free SDZ was determined by HPLC and then the bound SDZ on HA could be calculated by mass balance. Under the used experimental conditions, slow sorption kinetics can be observed from this figure, nearly after 15 days the sorption equilibrium is reached. After dialysis the total bound amount of SDZ on HA are approx 0.5% (wt) that corresponds to approx. 5 mg SDZ / g HA.

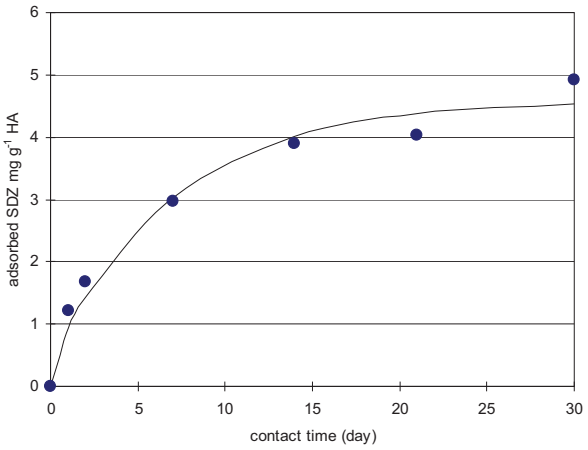

Figure 4.26 Sorption kinetic uptake curve of SDZ on IHSS-HA, curve was fitted by first order kinetics (C_{HA} = 1500 mg L^{-1}, $C_{SDZ_{initial}}$ = 60 mg L^{-1}, pH = 6)

The sorption kinetic uptake curve can be described by first-order kinetics with r^2 = 0.979 and the parameters $t_{1/2}$ = 4.86 d and k = 0.14 d^{-1}. Sorption on OM is slower than on minerals (see Table 4.2).

Table 4.6 Calculated K_d values of SDZ on Al_2O_3, illite and IHSS-HA (2 days contact time and C_{eq} = 60 mg L^{-1})

adsorbents	K_d (L kg^{-1})	K_{OC} (L kg^{-1})
Al_2O_3	0.37*	-
illite	0.10*	-
IHSS-HA	24.5**	42.2**

* calculated from adsorption isotherm, see Figure 4.22

** calculated at 2 d from Figure 4.26

To compare OM and mineral at the same experimental conditions (temperature, contact time

and SDZ initial concentration), a contact time t = 2 days and an initial concentration C_0 = 60 mg SDZ L^{-1} for both systems were chosen and the sorption distribution coefficients K_d and K_{OC} of SDZ on HA were calculated. The values of sorption distribution coefficient K_d for Al_2O_3 and illite were calculated from adsorption isotherm at C_{eq} = 60 mg L^{-1} in Figure 4.22 and the results are presented in Table 4.6.

The K_d value of HA at 2 d from the uptake curve is 24.5 L kg^{-1} at C_{aq}=60 mg L^{-1}. Comparing with the K_d values of Al_2O_3 (0.37 L kg^{-1}) and illite (0.10 L kg^{-1}) at the same equilibrium concentration, the sorption affinity of HA is 60-250 times higher than those of the minerals. The organic carbon content (OC) of IHSS-HA is about 58.1%, so the K_{OC} value is about 42.2 L kg^{-1}. This value is in the same order of magnitude with literature data (Thiele-Bruhn et al., 2004; Stein et al., 2008; Sukul et al., 2008b).

In sediments/soil, HA could form a coating with minerals (e.g. organo-clay complexes), which can reduce sorption capacity of HA to SDZ. The reason is the conformational change between free OM in solution and adsorbed OM on mineral surfaces which influence the sorption behavior. Free OM in the solution forms a more expanded or coil-like structure, which exhibits more available binding sites (hydrophobic parts; hydrophilic polar groups).

This estimation indicates that the sediments/soil organic matter play an important role in the SDZ sorption. However, in deeper sediment layers, the OC content is low and the sorption of SDZ occurs on minerals.

4.3 Sorption of SDZ to Yangtze sediments

There are some recently published studies on the fate of antibiotic pharmaceuticals in soil or clay minerals (Thiele-Bruhn et al., 2004; Gao et al., 2005; Sukul et al., 2008), but the fate of these compounds in the aquatic environment, particularly in river and stream sediments, remains poorly understood. Especially in Yangtze river, no information is yet available on the sorption of these pollutants to sediments. This chapter will focus on the ad/desorption behavior of sulfadiazine on Yangtze sediments.

4.3.1 Adsorption kinetics

The sorption kinetic experiment was performed i) to determine the contact time for isotherms, and ii) to describe the kinetics by an appropriate time law, rate constants and half life times, respectively.

Kinetics of SDZ adsorption on Yangtze sediments and Merzenhausen soil (for comparison) are shown in Figure 4.27. The time required for SDZ to reach “quasi equilibrium” state in the test sediments were 2 to 4 days (about more than 5 days for soil, 4 days for CQ2, 3 days for CQ3 and NJ2, 2 days for the others). Sukul et al. (2008) reported the equilibrium time for SDZ sorption to soil and soil manure was about 50 h. Stein et al. (2008) determined the kinetics of sulfamethoxazole sorption to sediments and took 24 h as equilibrium time. In most studies on the sorption of sulfonamides (e.g. Thiele-Bruhn et al., 2002; Thiele-Bruhn et al., 2004; Drillia et al., 2005; Ter Laak et al., 2006a, Ter Laak et al., 2006b; Sanders et al., 2008), the equilibrium time was chosen within 48 h. But all these results can be regarded as quasi equilibrium, because the sorption process of organic compounds to soil appears to include a fast and a slow kinetic step, respectively (Altfelder et al., 2000). The “true equilibrium” may need months (Pignatello and Xing, 1996) due to the slow kinetic step which can however lead to (bio)degradation and decomposition of the SDZ (Schmidt et al., 2008). To avoid this effect and for the comparison with sediment components like Al_2O_3, iron oxide and illite, 2 days sorption contact time were chosen for all the sorbents. This experimental condition has a significant influence on the ad/desorption isotherms and their interpretation are discussed in the Chapter 4.3.2.

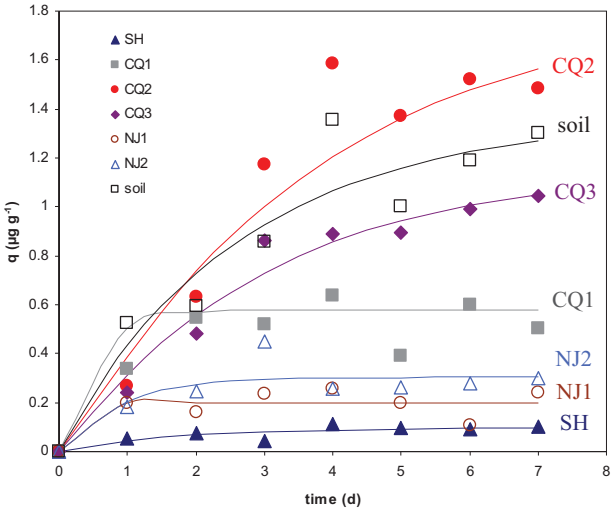

Figure 4.27 ^{14}C-SDZ sorption kinetics on Yangtze sediments and Merzenhausen soil in 7 days; curves are fits by first order kinetics ($C_{SDZ_{initial}}$ = 0.5 mg L^{-1}, $C_{sediment,\ soil}$ = 100 g L^{-1})

The kinetic curves from Figure 4.27 were fitted by first order kinetics and the parameters are listed in Table 4.7.

Table 4.7 Kinetic parameters of SDZ sorption on sediments and soil

	SH	CQ1	CQ2	CQ3	NJ1	NJ2	soil
k_1 (d^{-1})	0.57	2.00	0.27	0.34	4.75	1.13	0.37
$t_{1/2}$ (d)	1.21	0.35	2.52	2.02	0.15	0.61	1.86
r^2	0.882	0.910	0.985	0.984	0.825	0.854	0.951

The first order kinetic rate constant k_1 ranged from 0.27 d^{-1} to 4.75 d^{-1} in the order CQ2 < CQ3 < soil < SH < NJ2 < CQ1 < NJ1. The great difference of the rate constants can be related to the different properties of the sediments such as clay content, OM content, surface area and porosity. Nevertheless, because of multiple-effects, no significant correlation between the kinetic behavior and the sediment properties could be found.

4.3.2 Adsorption isotherms

Because of the environmental relevance, the adsorption isotherms were determined only in the low SDZ concentration range (< 1500 µg L^{-1}) and based on the discussion of kinetic

experiments, 2 days were chosen as contact time.

Adsorption isotherms of ^{14}C-SDZ on Yangtze sediments (together with Merzenhausen soil) are presented in Figure 4.28. For all the systems investigated, mass balances at the sorption points were statistically indistinguishable from 100% (i.e. within 95%-105%). The increase in error at higher concentration is an unavoidable consequence of using the batch method on a poorly sorbing material (MacIntyre et al., 1991).

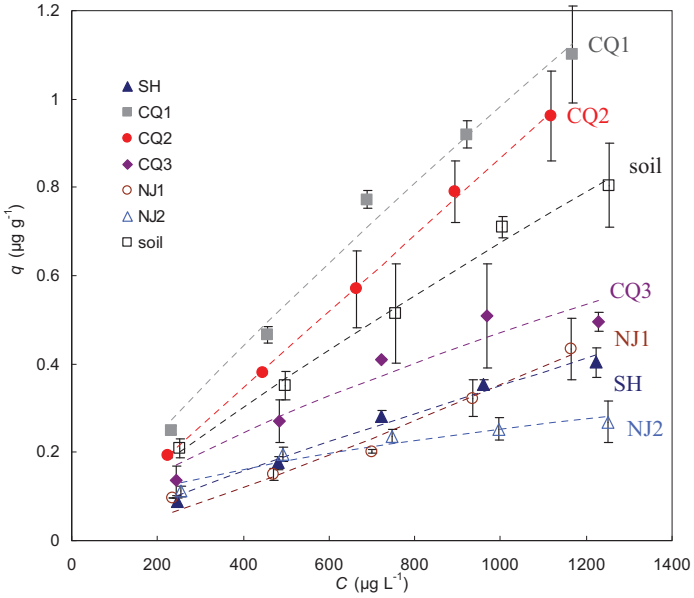

Figure 4.28 ^{14}C-SDZ adsorption isotherms on Yangtze sediments and Merzenhausen soil in low concentration range (dashed lines - fitted curves by Freundlich model; $C_{sediment,\ soil}$ = 100 g L^{-1}, contact time = 2 days)

Figure 4.28 illustrates the different sorption affinities of sediments. Data were fitted with Freundlich model and the Freundlich parameters are listed in Table 4.8. Sorption of SDZ on CQ2 and NJ1 are nearly linear with Freundlich exponent *1/n* near to unity. All the other isotherms showed pronounced nonlinearity with Freundlich exponent smaller than unity (i.e. *1/n*=0.48-0.88). Nonlinear isotherms can be attributed to adsorption site heterogeneity (Brownawell et al., 1990), the limited number of specific sorption sites e.g. in humic substances (Thiele-Bruhn et al., 2004) or even sorptives “adsorb” to high affinity internal microvoids (i.e. holes) within the matrix of NOM (Xing and Pignatello, 1997). Chiou et al. (2000) pointed out that specific interactions with the active groups of soil organic matter are

responsible for the generally higher nonlinearity sorption of the polar solutes.

Table 4.8 Freundlich parameters, K_d and K_{SSA} values of ^{14}C-SDZ adsorption on Yangtze sediments and Merzenhausen soil

adsorbents	pH	K_f ($\mu g^{1-1/n} L^{1/n} g^{-1}$)	*1/n*	R^2	K_d (L kg^{-1})*	K_{SSA} (L m^{-2})
SH	8.8	0.35±0.010	0.88±0.08	0.985	0.38	$5.43 \cdot 10^{-5}$
CQ1	8.2	0.98±0.027	0.88±0.07	0.987	1.07	$3.29 \cdot 10^{-5}$
CQ2	9.1	0.87±0.008	1.0±0.03	0.999	0.86	$1.37 \cdot 10^{-4}$
CQ3	8.9	0.47±0.028	0.71±0.15	0.925	0.57	$5.74 \cdot 10^{-5}$
NJ1	9.5	0.35±0.016	1.17±0.15	0.972	0.31	$2.46 \cdot 10^{-5}$
NJ2	9.1	0.25±0.010	0.48±0.08	0.935	0.36	$2.14 \cdot 10^{-5}$
Soil	7.4	0.67±0.013	0.88±0.06	0.992	0.73	$7.3 \cdot 10^{-5}$

*K_d = 'apparent' distribution coefficient determined at C_w = 0.5 mg L^{-1}

From the sorption data, the 'apparent' distribution coefficient K_d (L kg^{-1}) of SDZ to sediments was calculated by equation 2.1 (Chapter 2.4.1). In case of nonlinear isotherms K_d is concentration dependent and the comparison of K_d under different solution conditions can lead to biased results. Thus the corresponding K_d values as well as K_{OC} and K_{SSA} values were calculated at constant aqueous concentration C_w=0.5 mg L^{-1} and the results are also listed in Table 4.8. The values of K_d range from 0.31 to 1.07 L kg^{-1} and decrease in the following order: CQ1 > CQ2 > soil > CQ3 > SH > NJ2 > NJ1. These values are in good agreement with published data (see Table 2.1). The low K_d values indicate the high mobility of SDZ in sediment and/or soil. In general, SDZ adsorbed amounts for all the sediments are quite low, only about 1-10% of the SDZ molecules in the system are adsorbed. Because sulfadiazine is amphoteric and tends to ionize depending on the pH of the medium, electrostatic interactions are important for SDZ sorption mechanism (Holten Lützhøft et al., 2000). The species of SDZ at different pH values are shown in Figure 2.2 (Chapter 2.1). Since pH values for all the sediments are higher than 8.2 (Table 4.8), the anionic form of SDZ is mainly present. Anionic species usually have low sorption coefficients, because they are often repulsed by the generally negatively charged mineral surfaces of soil (ter Laak et al., 2006).

The different sorption affinity can also be attributed to the properties of water/sediment systems including clay content, surface area and OM. The comparison of K_{SSA} values from pure minerals and from sediments gives some ideas on the importance of mineral phases for

the SDZ sorption. After normalization by surface area, the K_{SSA} values for sediments range from $2.14 \cdot 10^{-5}$ to $1.37 \cdot 10^{-4}$ L m^{-2}, that's nearly the same range which was found for Al_2O_3 and illite. This result indicates the importance of mineral phases in sediments for SDZ sorption.

The distribution coefficients (see Table 4.8) were normalized to the OC content of the sediments resulting in the K_{OC} coefficients. The comparison of K_d and K_{OC} values is shown in Figure 4.29. The K_{OC} values are much more similar for all the sediments as well as soil than the respective K_d values ($32 \leq K_{OC} \leq 66$ L kg^{-1}) which is in good agreement with literature (e.g. Thiele-Bruhn et al., 2004; Drillia et al., 2005; Stein et al., 2008). This result indicates that sediment/soil organic matter plays an important role for SDZ sorption. Electrostatic interaction was shown to explain strong sorption of some polar pharmaceuticals including sulfonamides to natural organic matter and sludge (Kahle and Stamm, 2007b).

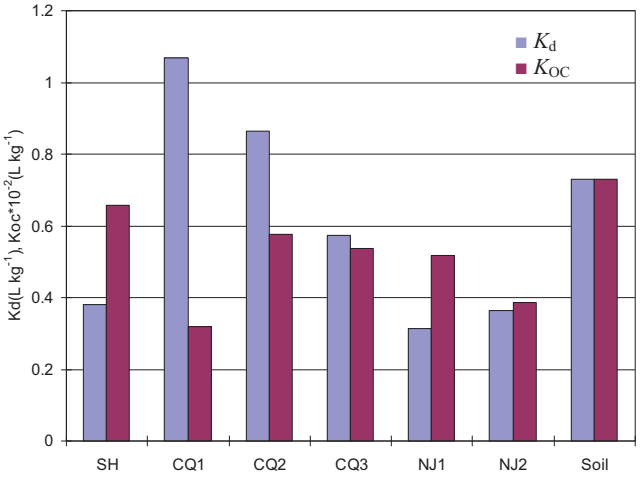

Figure 4.29 Comparison of K_d and K_{oc} values for SDZ sorption on different Yangtze sediments and Merzenhausen soil

The possible binding mechanisms can be assumed as surface complexation, van der Waals forces, cation bridging and anion exchange, depending on the sorbents. Indeed, the contribution of different factors like pH value, content of inorganic components, surface area, porosity of the sorbents and also organic matter content can not be quantified because sediments are very heterogeneous and complex sorbents.

4.3.3 Desorption isotherms

To avoid transformation/degradation as discussed in Chapter 4.1, the contact time of ad/desorption experiments were chosen as 2 days. Desorption isotherms of SDZ on Yangtze sediments and Merzenhausen soil are shown in Figure 4.30.

Sorption of SDZ on SH is partly reversible with desorption points slightly above the sorption isotherm. All the other sorbents reveal clearly hysteretic desorption of SDZ. Most of these systems show pronounced concentration independent hysteresis.

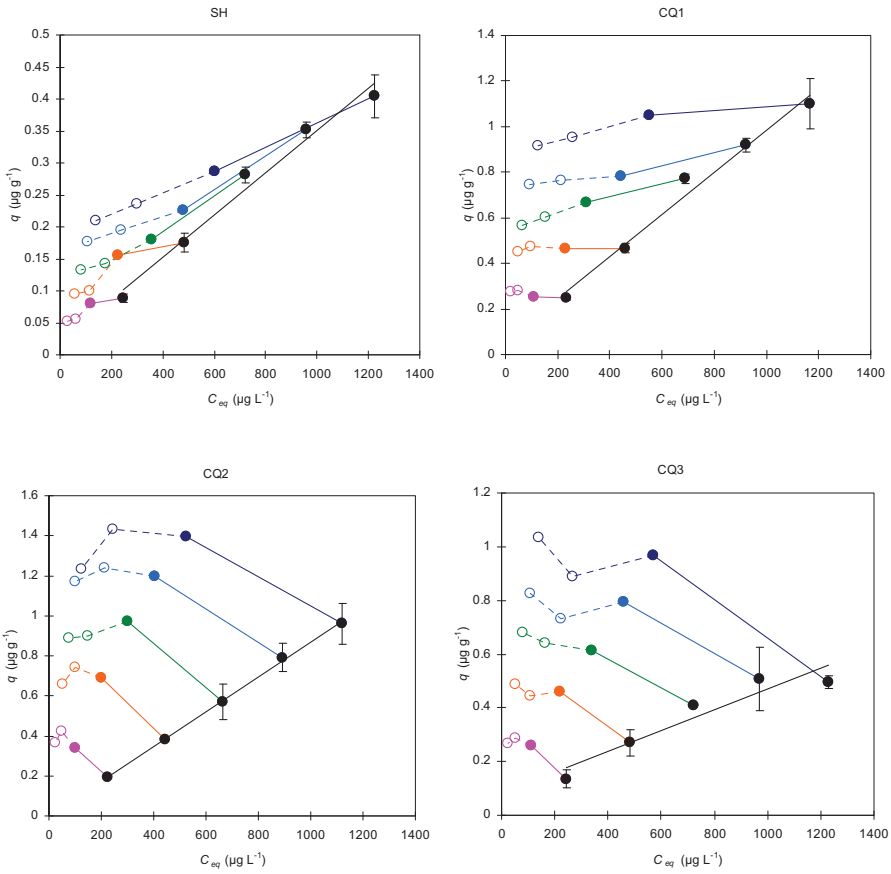

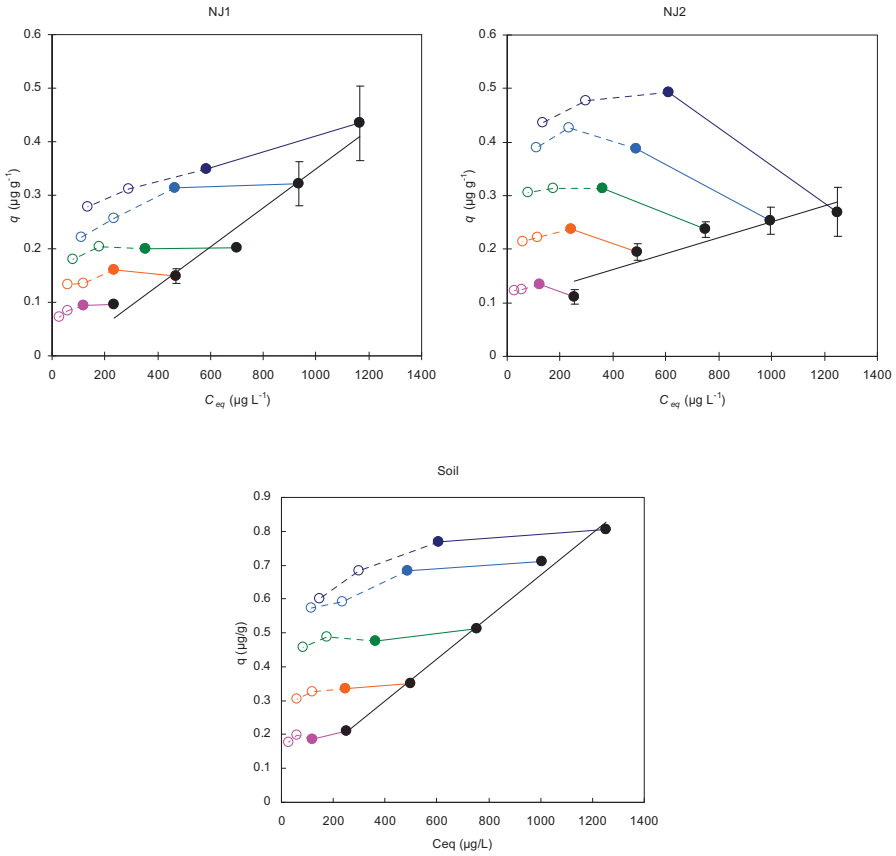

Figure 4.30 Desorption isotherms of ^{14}C-SDZ on Yangtze sediments and Merzenhausen soil – data obtained by oxidizer method (● – adsorption, black solid line – fitted adsorption isotherm, colored point – first desorption step, colored open points – second and third desorption steps)

For CQ2 and CQ3, the first points in desorption isotherms show higher adsorbed amount than the corresponding points of the adsorption isotherms. This result could be interpreted by sorption kinetics (see Figure 4.27). The sorption equilibrium time for these sediments is more than 2 days. When the first desorption step starts after 2 days adsorption, the system is still not at equilibrium and the adsorption process is continuing. So the sorption rate is a decisive factor for these desorption results. A similar type of desorption isotherm could also be observed for NJ2.

For CQ1 and NJ1, common hysteresis effect was observed. Sorption kinetics of these two sorbents (Figure 4.27) show that the equilibrium time is less than 2 days. The calculated

sorption rate constants k_1 for both are 2.00 d^{-1} and 4.75 d^{-1}, respectively, which are obviously higher than all the other sorbents (Table 4.7). This result reveals a fast adsorption but slow desorption kinetics for both two sediments. The similar desorption isotherm was also observed for Merzenhausen soil, but the kinetic result shows a slow sorption on soil (more than 2 days). Thus desorption hysteresis could be caused by both sorption nonequilibrium and slow desorption kinetics.

In contrast to the pure minerals, except goethite, hysteresis occurs more or less on all sediments and soil. Hysteresis is due to the irreversible sorption of a fraction of the sorptive and thus truly thermodynamic. Nevertheless, hysteresis can take place due to experimental artifacts. It is known that a number of experimental artifacts may contribute to the hysteresis (Celis and Koskinen, 1999). One possible cause of artificial hysteresis can be mass balance errors in the form of unaccounted mass loss of analyte that is falsely ascribed to the sorbent at the desorption point (Stein et al., 2008). But in our study this can be excluded because the adsorbed amount in the desorption process was directly determined from the solid residues with labeled SDZ by the oxidizer method. Another possible cause is nonattainment of diffusive equilibrium during the sorption and/or desorption direction (Stein et al., 2008). This can be the interpretation for the desorption isotherms of CQ2, CQ3 and NJ2 on the base of the sorption kinetic experiments which were discussed above.

However, it can not be ruled out that hysteresis was caused by slow desorption of the SDZ from the solids. Zhao et al. (2001) interpreted hysteresis of polycyclic aromatic hydrocarbons (PAH) sorption to soil by slow desorption mechanism. Wehrhan (2007) also proved the desorption of SDZ from soil is rate-limited and much slower than adsorption. In addition to the discussion above, it can also not be ruled out that part of observed hysteresis was true as mentioned by Stein et al. (2008). In this case, sorbate-induced irreversible structural deformation of the organic matter in the sorbent may have been causative (Sander et al., 2006).

As discussed in Chapter 4.2, desorption isotherms can be fitted by Freundlich model. Values of the Freundlich equilibrium constant (K_f) and the exponent ($1/n$) at different initial concentrations on sediment SH, CQ1, NJ1 and Merzenhausen soil were determined by nonlinear regression and are listed in Table 4.9. The Freundlich model can not fit the sorption data for all the initial concentrations due to the data scattering. For SH sediment, the higher value of the Freundlich exponent ($1/n$) than all the others proves the slight hysteresis, which is

consistent with the conclusions above. All the *1/n* values obtained from desorption isotherms are lower than that from adsorption isotherms suggesting strong sorption hysteresis. The calculations are failed for CQ2, CQ3 and NJ2 because of their unusual isotherm courses can not be described by Freundlich model. So these data were analyzed by "rate limited" and "stage-rate" models and they are discussed in the modeling part (Chapter 4.4).

Table 4.9 Freundlich isotherm parameter values for SDZ desorption on sediments / soil

adsorbent	C_i^* (mg L^{-1})	K_f^{**} ($\mu g^{1-1/n} L^{1/n} g^{-1}$)	$1/n^{**}$	r^2
SH	0.25	0.021 (±0.005)	0.26 (±0.05)	0.932
	0.50	0.025 (±0.010)	0.32 (±0.08)	0.907
	0.75	0.019 (±0.009)	0.41 (±0.09)	0.921
	1.00	0.029 (±0.016)	0.36 (±0.09)	0.889
	1.25	0.037 (±0.013)	0.33 (±0.06)	0.951
CQ1	0.25	-	-	-
	0.50	-	-	-
	0.75	0.31 (±0.03)	0.13 (±0.02)	0.965
	1.00	0.49 (±0.09)	0.090 (±0.03)	0.781
	1.25	0.60 (±0.04)	0.086 (±0.01)	0.973
NJ1	0.25	0.048 (±0.007)	0.13 (±0.03)	0.914
	0.50	0.098 (±0.025)	0.076 (±0.05)	0.553
	0.75	0.15 (±0.02)	0.044 (±0.027)	0.576
	1.00	0.099 (±0.024)	0.18 (±0.04)	0.914
	1.25	0.094 (±0.017)	0.21 (±0.03)	0.965
Soil	0.25	0.22 (±0.02)	0.06 (±0.04)	0.614
	0.50	0.37 (±0.01)	0.06 (±0.01)	0.967
	0.75	0.52 (±0.13)	0.05 (±0.02)	0.752
	1.00	0.72 (±0.02)	0.11 (±0.02)	0.929
	1.25	0.80 (±0.02)	0.13 (±0.02)	0.957

*C_i is initial concentration of solution

**value in parentheses is the 95% confidence interval

4.4 Sorption modeling with "Rate-limited sorption" and "Two-stage one-rate sorption" models

The sorption isotherms of SDZ on different sorbents especially on sediments and soil showed pronounced hysteresis. One possible cause is nonattainment of diffusive equilibrium during the sorption and/or desorption direction (Stein et al., 2008). There are increasing evidences that in many cases hysteresis is caused by slow sorption kinetics (Boesten and van der Pas, 1988; Pignatello, 1989; Miller and Pedit, 1992; Sabbah et al., 2005), implying that equilibrium may not be attained in many batch experiments.

As a possible solution for this problem and to estimate sorption parameters and predict sorption behavior, the sorption data were evaluated by the rate-limited sorption (RLS) and the two-stage one-rate sorption (2S1R) models. These models are able to provide an estimation of the equilibrium isotherm based on nonequilibrium data.

The 2S1R model is a widely used approach which assumes two different types of domains in sorbents, one with instantaneous sorption and one with rate-limited sorption (Brusseau et al., 1989; Streck et al., 1995; Altfelder et al., 2000). The RLS model is a simplified case of 2S1R which assumes only one sorption domain with rate-limited sorption. If the equilibrium distribution of a substance is not instantaneous, a rate-limited solute uptake by the sorbents needs to be considered (Chapter 2.5). Both models could be a solution to describe the sorption data.

4.4.1 Rate-limited sorption (RLS)

The rate limited uptake of solute is often considered when an equilibrium distribution of a substance is not instantaneously reached. From the kinetic study, the sorption equilibrium time for soil and some sediment samples are more than two days (see Figure 4.27). Because of the two days contact time in batch experiments, non-equilibrium sorption may be the principal cause of sorption hysteresis. The RLS model is also the simplest case assuming one sorption site and one rate, so all the data sets were calculated by the RLS model first (see equation 2.13 and 2.14 in Chapter 2.5.1).

Before starting the inverse parameter optimization with the program FitHyst, the initial parameter estimates must be chosen. For the RLS model, 3 parameters including α (the sorption rate coefficient), K_f (the Freundlich equilibrium constant) and m (the Freundlich exponent, $1/n$, Chapter 2.4) were estimated from the kinetics and batch sorption experiments and then used as initial input parameters for the modeling.

The sorption isotherms (see Figure 4.25 and Figure 4.30) were modeled with all data including 3 desorption steps. But the models fitted data well only for CQ2 and CQ3. The possible reason is the nonideal character of the desorption data. As discussed in Chapter 3.2.2 (mass balance), the experimental error leads to increasing uncertainty with increasing desorption steps. The reason is the increasing scattering of analytical data at the very low concentration level after desorption. To avoid this problem, the modeling was performed on the adsorption data and only one desorption step.

Figure 4.31 shows the results (2 days contact time = “quasi equilibrium” isotherm) of the RLS model for all the sorption data with one desorption step, except CQ2 and CQ3. The calculated parameters are listed in Table 4.10.

For the minerals, Al_2O_3 and illite, the desorption isotherms are nearly reversible in 2 days. The RLS model can fit the adsorption of Al_2O_3 very well, but underestimates desorption compared to the observations. For illite, it overestimates adsorption and predicts desorption better.

For sediments and Merzenhausen soil, the RLS model gives best fit to CQ1, CQ2, CQ3, NJ1 and NJ2, despite pronounced hysteresis observed. But for the SH and soil, the desorption process was overestimated by RLS.

The RLS model can also estimate the equilibrium adsorption isotherms according to the ad/desorption modeling of the two-day data. It is an efficient tool to predict sorption equilibrium and interpret the desorption hysteresis under nonequilibrium conditions. The estimated adsorption equilibrium isotherms from the RLS model of all the sorbents are also shown in Figure 4.31. These isotherms are higher than the “two-day adsorption isotherms” from the batch experiments indicating that the “two-day adsorption isotherms” are not at equilibrium. Both the kinetic results of batch experiments (Chapter 4.2.1 and Chapter 4.3.1)

and the calculated T_e values from the RLS model (Table 4.10) reveal that the sorption equilibrium time is more than 2 days for most adsorbents. These results could also be the explanation of the unusual desorption isotherms of CQ2 and CQ3 and the hysteresis effects for other adsorbents.

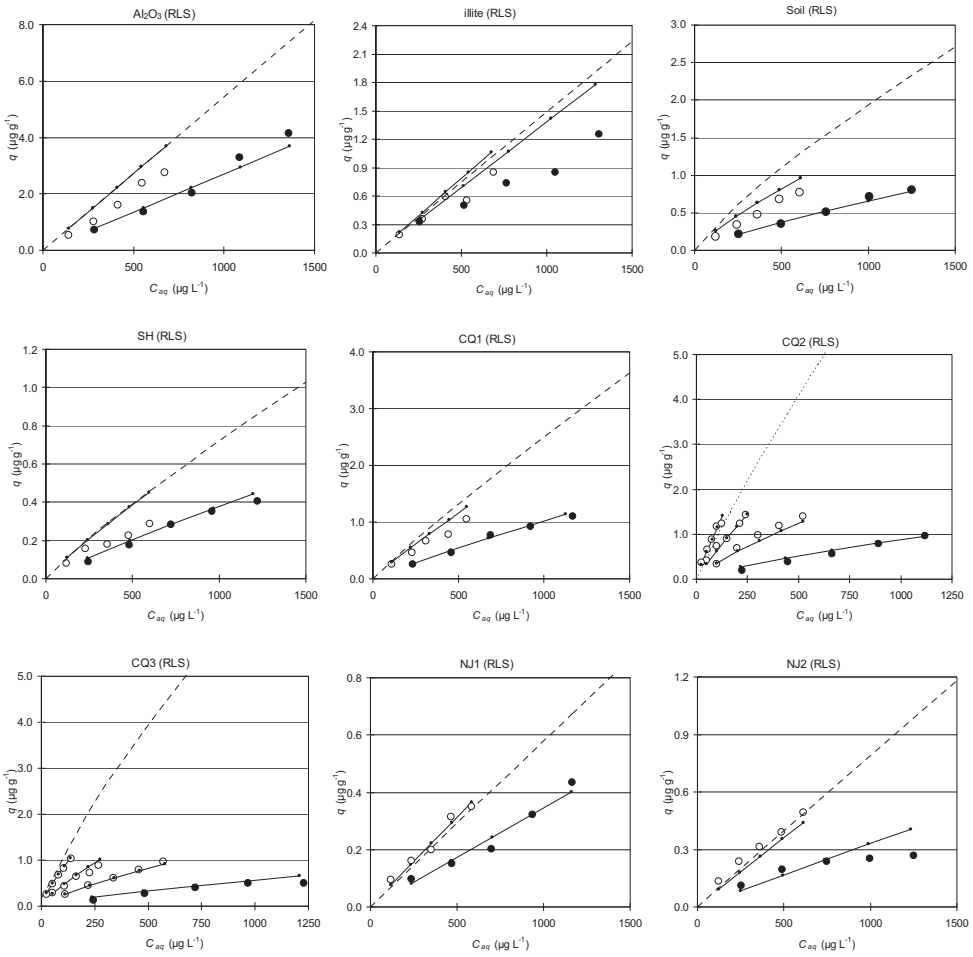

Figure 4.31 Adsorption and one desorption step modeling (three desorption steps for CQ2 and CQ3) of ^{14}C-SDZ on different sorbents by RLS model (● - adsorption experimental data, ○ - desorption experimental data, ─ modeled isotherms for 2 days contact time, --- estimated equilibrium isotherm)

The time scale for the kinetic process, T_e, can be calculated by the rate parameter α, which is defined as sorption rate coefficient and calculated from the modeling of the sorption data. One should distinguish between α and the rate parameter k which was obtained from the experimental kinetic curves by application first-order kinetics (see Chapter 4.3.1). This k

value serves as an initial input parameter for sorption modeling to obtain important parameters like K_f, m and α.

The results are listed in Table 4.10. The values of Freundlich exponent m reveal a good agreement with those *1/n* obtained from Freundlich model discussed in Chapter 4.3 (see Table 4.8). The T_e values amounts from 0.8 days for illite to 25 days for CQ3. These T_e values show the similar tendency with the kinetic experiments. Nevertheless, the experimental k values and the T_e values from the RLS model fit the power function $y = x^A$ with a correlation coefficient $r^2 = 0.55$. These results are helpful to interpret the strong hysteresis effects on CQ2 and CQ3, the slow desorption kinetics is the main reason of hysteresis.

Table 4.10 ^{14}C-SDZ ad / desorption on different sorbents: calculated parameters of the RLS model

	α (d^{-1})	SE_α	K_f ($mg^{1-m}L^m kg^{-1}$)	SE_{K_f}	m	SE_m	SSQ	T_e^* (d)
Al_2O_3	0.34	0.07	5.44	0.54	1.0**	-	$9.9 \cdot 10^{-5}$	2.94
Illite	1.25	0.44	1.49	0.19	1.0**	-	$5 \cdot 10^{-4}$	0.8
Soil	0.20	0.04	1.94	0.28	0.82	0.06	$1.2 \cdot 10^{-4}$	5.0
SH	0.36	0.29	0.72	0.42	0.88	0.39	$1 \cdot 10^{-3}$	2.78
CQ1	0.25	0.10	2.50	0.79	0.92	0.17	$1 \cdot 10^{-3}$	4.0
CQ2	0.06	0.01	7.67	1.53	0.91	0.07	$2.8 \cdot 10^{-3}$	16.7
CQ3	0.04	0.008	6.81	1.38	0.79	0.04	$8.7 \cdot 10^{-4}$	25
NJ1	0.44	0.08	0.58	0.08	0.99	0.11	$4.7 \cdot 10^{-5}$	2.27
NJ2	0.26	0.15	0.79	0.31	0.99	0.23	$2.8 \cdot 10^{-4}$	3.85

α is the sorption rate coefficient, K_f is the Freundlich equilibrium constant and m is the dimensionless Freundlich exponent. SE_α, SE_{K_f} and SE_m are the standard error of application relative to each of the parameters (α, K_f and m), SSQ is the sum of squares.

* characteristic time scale for the kinetic process calculated from α

** linear sorption model was used, thus the exponent m is 1.0

The RLS model calculates the Freundlich equilibrium constant K_f and exponent m in equilibrium from the two-day isotherm experimental data. As discussed in Chapter 4.2 and 4.3, the sorption data can also be described by the Freundlich model with the parameter K_f and *1/n* (the same definition as m in the RLS model). But the parameters obtained from experimental data and modeling can not be compared directly. Because the modeling was based on sorption data in the low SDZ concentration range (< 1.5 mg L^{-1}), the sorption isotherms are nearly linear in this range (see Chapter 4.2.2 and Chapter 4.3.2). The modeling results also support this conclusion, with Freundlich exponents close to 1, which indicates linear sorption. But this exponent obtained from the experimental data in the high concentration range is 0.62 for

Al_2O_3 and 0.56 for illite, which is indicative of a strong nonlinearity. On the other hand, the Freundlich equilibrium constant K_f from the experimental data is the value of the "two-day adsorption isotherm" but not the equilibrium value. The K_f value from the RLS model is the estimated equilibrium value. Thus these parameters obtained from different methods are not comparable.

4.4.2 Two-stage one-rate sorption (2S1R)

The ad/desorption isotherms show nearly reversible sorption of SDZ on Al_2O_3 and illite, respectively. The RLS model is developed and can be used for such kind of pure systems. But for sediments and soil, the sorbents can be modelled as particles with different sorption sites, at least two different sites, e.g. mineral and OM (Streck et al., 1995). The 2S1R model, which assumes two sorption sites for sorptives with different kinetic sorption rates, were used to get a better understanding of the sorption behavior of SDZ on different sediments (see equation 2.16 to 2.17 in Chapter 2.5.2).

Compared with the RLS model, 2S1R has one additional parameter, f_1, which is the dimensionless fraction of the total sorbent that exhibits equilibrium sorption. This parameter is quite sensitive and often leads to negative value or higher standard error or higher correlation with other parameters in this work. Sometimes f_1 should be fixed for multiple sites and rates models to make the program running (Wehrhan, 2007). In this study, if all the parameters were free during modeling with 2S1R model, the calculated results would always give extremely high standard error. So one of the input parameters had to be fixed to avoid this problem. Sometimes f_1 was tried to be fixed but this led to the total correlation between α and K_f (correlation coefficient is -1). Since the parameter f_1 can only be obtained from the modeling, it is better to let f_1 free and fix other parameters.

The results for all sorbents are shown in Figure 4.32 and additionally the 2S1R modeling parameters are listed in Table 4.11.

For Al_2O_3, K_f was fixed because of the high correlation with α. As shown in the Figure 4.32, the 2S1R model fit the adsorption isotherm quite well but this fitting is not sufficient for the desorption comparing with RLS model. The f_1 value (-0.05) is negative, which is meaningless from the definition (see Chapter 2.5.2). Considering the standard error (SE = 0.12), this value

is uncertain. So RLS model fitted the data better for Al_2O_3.

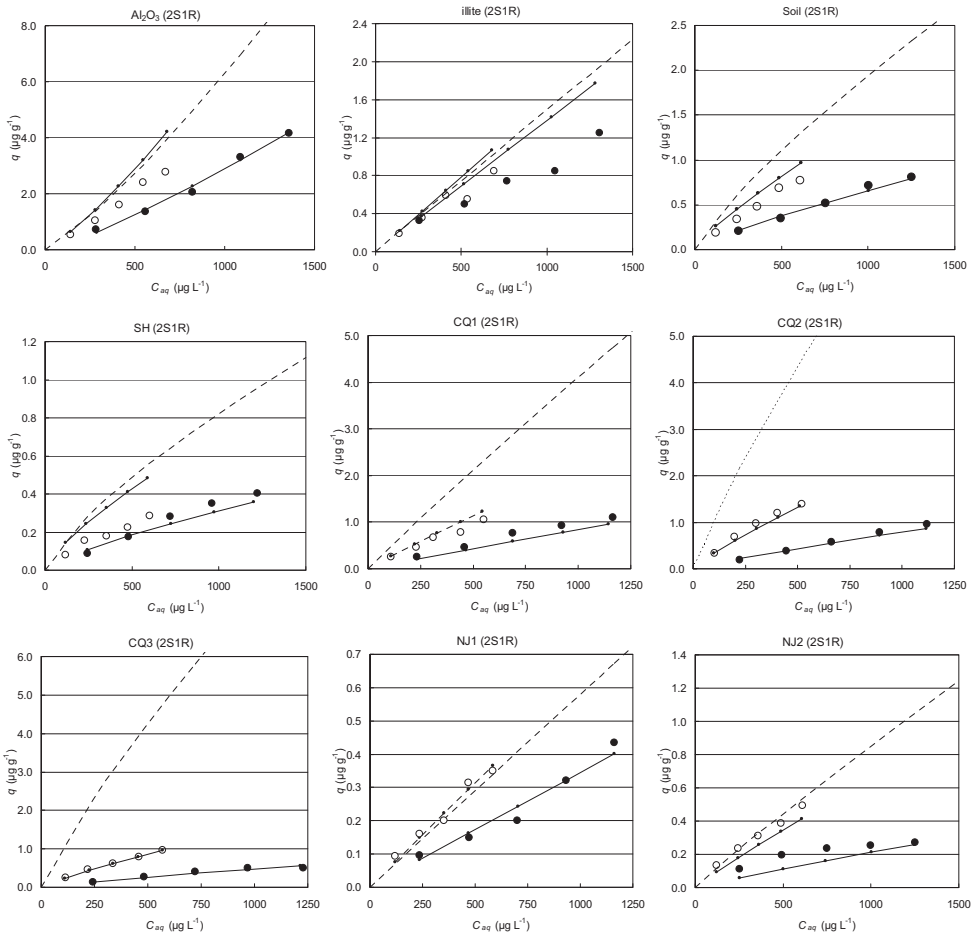

Figure 4.32 Adsorption and one desorption step modeling of ^{14}C-SDZ on different sorbents by 2S1R model (● - adsorption experimental data, ○ - desorption experimental data, ─ modeled isotherms for 2 days contact time, --- estimated equilibrium isotherm)

The modeling results for illite were nearly the same with RLS model. If K_f was fixed, α and f_1 would be totally negatively correlated. Thus α was fixed with the value from RLS model. On the contrary to Al_2O_3, the f_1 value is positive but quite low (0.001) with much higher standard error (SE = 0.28). Due to the obviously reversible sorption on illite, it's not necessary to use more sites and rates in the modeling.

For soil, also due to the high correlation of K_f and α (-0.92), the K_f value was fixed to 1.94

(the value calculated from RLS model). As shown in Table 4.11, the new parameter f_1, which represents the fraction of the total soil that undergoes equilibrium sorption, was negative and also considering the *SE* value (0.03), it is uncertain. The other parameters like K_f and m gave the same values from this model. Consequently this model nearly provides the same results compared with RLS model (see Figure 4.31). Thus, in this case, RLS model is sufficient to describe the sorption behavior.

There is nearly no difference between the RLS and 2S1R model (Figure 4.31 and Table 4.10) for sorption on CQ1, CQ2 and CQ3. The positive f_1 value for CQ1 indicates the possibility that 2S1R model could give better fit for the data but this value is quite low and uncertain comparing with *SE* value (0.048). For CQ2 and CQ3, the 2S1R model always gives a negative f_1 value and no better fit for the data comparing with RLS model.

Table 4.11 ^{14}C-SDZ ad/desorption on different sorbents: calculated parameters of 2S1R model

	α_2 (d^{-1})	SE_α	f_1	SE_{f1}	K_f ($mg^{1-m}L^m kg^{-1}$)	SE_{Kf}	m	SE_m	SSQ	T_e^{**}(d)
Al_2O_3	0.34	0.11	-0.05	0.12	6.31*	-	1.21	0.13	$3.6\cdot10^{-5}$	2.94
illite	1.25*	-	0.001	0.28	1.49	0.21	1.0***	-	$5\cdot10^{-4}$	0.8
Soil	0.20	0.03	-0.00076	0.03	1.94*	-	0.82	0.06	$1\cdot10^{-4}$	5.0
SH	0.36	0.35	-0.168	0.38	0.82*	-	0.76	0.27	$6.9\cdot10^{-4}$	2.78
CQ1	0.11	0.03	0.001	0.048	4.10*	-	0.95	0.16	$1.1\cdot10^{-3}$	9.09
CQ2	0.06	0.005	-0.018	0.008	7.67*	-	0.87	0.05	$2.1\cdot10^{-4}$	16.7
CQ3	0.046	0.004	-0.02	0.01	6.81*	-	0.86	0.07	$1.9\cdot10^{-4}$	21.7
NJ1	0.46	0.36	-0.015	0.34	0.58*	-	0.99	0.12	$4.8\cdot10^{-5}$	2.17
NJ2	0.30	0.08	-0.22	0.01	0.79*	-	0.94	0.12	$8.1\cdot10^{-5}$	3.33

α_2 is the sorption rate coefficient, f_1 is the dimensionless fraction of the total sorbent that exhibits equilibrium sorption, K_f is the Freundlich equilibrium constant and m is the dimensionless Freundlich exponent. $SE_{\alpha 2}$, SE_{f1}, SE_{Kf} and SE_m are the standard error of application relative to each of the parameters (α_2, f_1, K_f and m), SSQ is the sum of squares.

* input data were fixed

** characteristic time scale for the kinetic process calculated from α_2

*** linear sorption model was used, thus the exponent m is 1.0

For the sorption on NJ1 and NJ2, the 2S1R model always gives a negative f_1 value if it is not fixed. So as before, the K_f value was fixed and the other calculated parameters are shown in

Table 4.11. As shown in Figure 4.32, the 2S1R model gives no obvious difference from RLS model. For both sediments, the f_1 values are negative and have no considerable influence on modeling indicating that the sorption on NJ1 and NJ2 is only rate dependent.

As with RLS model, the estimated equilibrium adsorption isotherms from 2S1R model are also shown in Figure 4.32. The similar Freundlich equilibrium constant K_f and exponent m from both models give comparable equilibrium isotherms.

Theoretically, the models with more parameters are expected to give a better fit for the data. But comparing the modeling results of RLS and 2S1R models, the 2S1R model nearly gives no difference with RLS model. The additional parameter f_1 is negligible in all the cases. In the work of Wehrhan (2007), Cho (2007) and Unold et al. (2009), the sorption data of SDZ on soils were modeled by RLS, 2S1R and even more sites and rates models. The f_1 values were also very low and sometimes had to be fixed. Thus there is no need to try more complicate models like two-sites two-rates (2S2R) or three-sites two-rates (3S2R). The RLS model can describe most cases in this study. The sorption rate is the dominant factor for sorption of SDZ on different minerals, sediments and Merzenhausen soil.

4.5 Transport of SDZ in sediment columns

Proper determination of sorption equilibrium parameters of SDZ such as distribution coefficients is essential for making accurate predictions on the fate and transport of SDZ in water/sediments. Batch or column techniques were most commonly used to determine the distribution coefficients in the laboratory. Although both methods characterize the sorption behavior of SDZ, sediment columns are the more realistic experimental setups which have the advantage of being conducted under conditions approximating those observed in the field. The compatibility of two techniques is of a great interest to be investigated.

Many researchers have attempted to compare the sorption parameters from batch and column studies, but the findings have been inconsistent. For example, good agreement between the results of two techniques has been reported for sorption of hydrophobic organic chemicals such as naphthalene (NAP) (Nkedi-Kizza et al., 1987; MacIntyre et al., 1991; Bayard et al., 1998), for fenuro and monuron (Spurlock et al., 1995) and for 1,2,4-trichlorobenzene and tetrachloroethene (Young et al., 1998). In contrast, many studies reported that the batch study consistently overestimated retardation coefficients compared with the results from column study (e.g. MacIntyre and Stauffer, 1988; Celorie et al., 1989; Maraqa et al., 1998). The discrepancies were attributed to different causes such as loss of sorbents from the column (Lion et al., 1990), immobile water regions in the column (MacIntyre et al., 1991; Maraqa et al., 1997; Plassard et al., 2000), reduction in soil particle spacing in the column compared with batch systems (Celorie et al., 1989), different solid/liquid ratio (Wang et al., 2009), failure to account for sorption nonlinearity (Brusseau, 1995), nonsingularity (van Genuchtern et al., 1977), or nonequilibrium (e.g. Brusseau et al., 1991; Maraqa et al., 1998; Altfelder et al., 2001) etc. It was well documented that the transport is a function of pore water velocity (e.g. Bouchard et al., 1988; Brusseau, 1992; Kelsey and Alexander, 1995; Langner et al., 1998; Maraqa et al., 1999). In this study, column technique was conducted to investigate the fate of SDZ in Yangtze river sediments and compared with batch experimental results.

From the results of batch experiments, the low K_d values (< 1.0 L kg^{-1}, see Table 4.8) indicate high mobility of SDZ in sediments and soil. To simulate and investigate the fate of SDZ in sediment, column experiments under saturated conditions in 10^{-2} M NaCl electrolyte were performed with sediment/quartz mixtures (to test the stability of hydrodynamic conditions) and with pure sediments. To evaluate the effect of input concentration and flow rate on the

transport, three experiments with different input scenarios were performed with sediment SH and named as SH-a, SH-b and SH-c. SH-a and SH-b were applied with same flow rate (0.2 ml min^{-1}) and pulse duration (500 min) but with different input concentration (SH-a: 775 μg L^{-1}, SH-b: 50 μg L^{-1}). Lower flow rate (0.05 ml min^{-1}) was applied in experiment SH-c with same input concentration as SH-b to compare the effect of flow rate. All the parameters in these three scenarios were listed in Table 3.8 (Chapter 3.2.3).

Water flow and solute transport in sediment columns were treated as one-dimensional transport problems in the mathematical solutions. The convection-dispersion equation (CDE) is commonly used to describe the transport of solutes with linear sorption. In this study, the input concentrations of SDZ for the column experiments were in the range of 40-800 μg L^{-1}. In this concentration range sorption was linear in batch experiments (Chapter 4.3). Thus all the column experimental data were modeled by program Stanmod.

The experimental data can be expressed by breakthrough curves (BTCs) which together with the modeling give the information of transport behavior of a reactive solute in the column. The BTCs in this study were described with the modified equation 2.22, 2.25 and 2.26 (see Chapter 2.6):

A) Equilibrium CDE (see Chapter 2.6.1)

$$R\frac{\partial C}{\partial t} = D\frac{\partial^2 C}{\partial x^2} - v\frac{\partial C}{\partial x} - \mu C$$

and

B) Nonequilibrium CDE (see Chapter 2.6.2)

$$\beta R\frac{\partial C_1}{\partial T} = \frac{1}{P}\frac{\partial^2 C_1}{\partial Z^2} - \frac{\partial C_1}{\partial Z} - \omega(C_1 - C_2) - \mu_1 C_1$$

$$(1-\beta)R\frac{\partial C_2}{\partial T} = \omega(C_1 - C_2) - \mu_2 C_2$$

and calculated by Stanmod software with CXTFIT 2.0 code (see Chapter 2.6).

For equilibrium CDE model, the program was used to estimate the pore-water velocity (v), the

dispersion coefficient (D) and the retardation factor (R). For nonequilibrium CDE model, the coefficient of partitioning between the equilibrium and nonequilibrium phases (β) and the mass transfer coefficient (ω) for transfer between the two phases could also be fitted. The most interesting parameter, R (retardation factor) is related to the sorption distribution coefficient K_d, by equation [2.23] (see Chapter 2.6.1). So the K_d obtained from batch experiments can be used to predict R and compared with the value from column experiments (Chapter 2.6).

4.5.1 Transport of the inert tracer nitrate

The nitrate BTCs were used to estimate the parameters v and D by a non-linear parameter estimation procedure based on the Levenberg-Marquardt algorithm. The CXTFIT code (Toride et al., 1999) was used to analytically solve the CDE for the appropriate boundary conditions, i.e. a flux-type upper boundary condition and a zero gradient at the lower boundary. The estimated transport parameters and the experimentally determined Darcian flow velocity, q, the volumetric water content, $\theta = q/v$, and the dispersivity, $\lambda = D/v$, were used to fix the water flow for the transport simulations of SDZ.

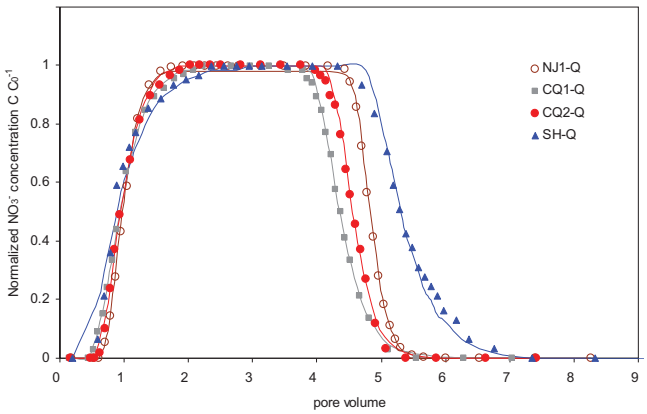

Figure 4.33 Breakthrough curves of nitrate for the 4 different sediments (mixed with quartz, ratio of sediments:quartz is 1:2). Experimental data - colored points, fitted curves by equilibrium CDE - colored lines. (experimental conditions see Table 3.8 in Chapter 3.2.3)

The measured BTCs of nitrate and the model fits with the equilibrium CDE are shown in Figure 4.33 (sediments with quartz) and Figure 4.34 (pure sediment SH). The estimated transport parameters are listed in Table 4.12.

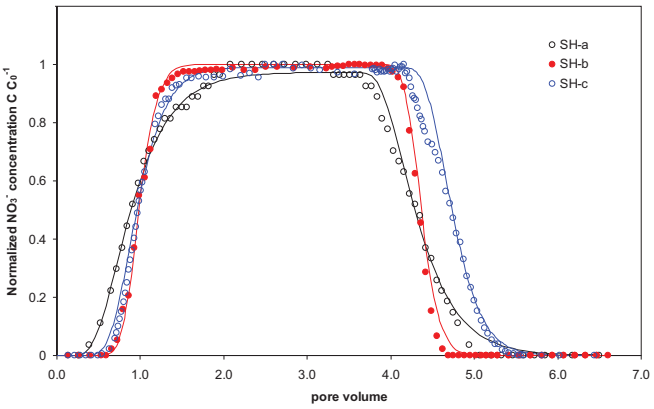

Figure 4.34 Breakthrough curves of nitrate for the SH sediment at different conditions. Experimental data - colored points, fitted curves by equilibrium CDE - colored lines (flow velocity: SH-a, 0.2 ml min^{-1}; SH-b, 0.2 ml min^{-1}; SH-c, 0.05 ml min^{-1})

Table 4.12 Transport parameters for the conservative tracer nitrate in sediments (Equilibrium CDE)

	v (cm min^{-1})	D (cm^2 min^{-1})	r^2	q (cm min^{-1})	θ (cm^3 cm^{-3})	λ (cm)	ρ (g cm^{-3})
NJ1-Q	0.087 (±0.001)*	0.021 (±0.001)	0.996	0.028	0.32	0.24	1.58
CQ1-Q	0.074 (±0.001	0.047 (±0.003)	0.999	0.028	0.38	0.64	1.32
CQ2-Q	0.078 (±0.001)	0.033 (±0.003)	0.998	0.028	0.36	0.42	1.37
SH-Q	0.098 (±0.004)	0.12 (±0.03)	0.986	0.028	0.29	1.22	1.53
NJ1	0.058 (±0.0001)	0.0029 (±0.0001)	0.999	0.028	0.48	0.05	1.43
SH-a	0.065 (±0.001)	0.067 (±0.007)	0.995	0.028	0.43	1.03	1.37
SH-b	0.066 (±0.001)	0.01 (±0.001)	0.998	0.028	0.42	0.15	1.43
SH-c	0.014 (±0.0002)	0.0058 (±0.0008)	0.983	0.0068	0.49	0.41	1.35

v is pore water velocity, D is dispersion coefficient, the r^2 value is a measure of the relative magnitude of the total sum of squares associated with the fitted equation, q is the experimentally determined Darcian flux density, θ is water content, λ is dispersivity and ρ is the bulk density.

* values between brackets indicate 95% confidence interval.

The equilibrium CDE was able to describe all BTCs (Figure 4.33 and Figure 4.34). So it can be concluded that no non-equilibrium processes affected the nitrate transport and that all water participated in the convective flow.

4.5.2 Transport of SDZ

From the batch experiments and modeling results, the equilibrium time of SDZ sorption to sediments was more than 2 days. Thus it can be assumed that the sorption in the column is also under non-equilibrium condition. For nonequilibrium CDE model, the input parameters v and D could be obtained from the modeling of the tracer NO_3^-. Based on the definition of ω in Table 2.3, it can be estimated from the known parameters, such as α (sorption rate), θ (water content) and L (column length). So the retardation factor R and the partitioning coefficient β (coefficient of partitioning between the equilibrium and nonequilibrium phases) could be calculated by the program.

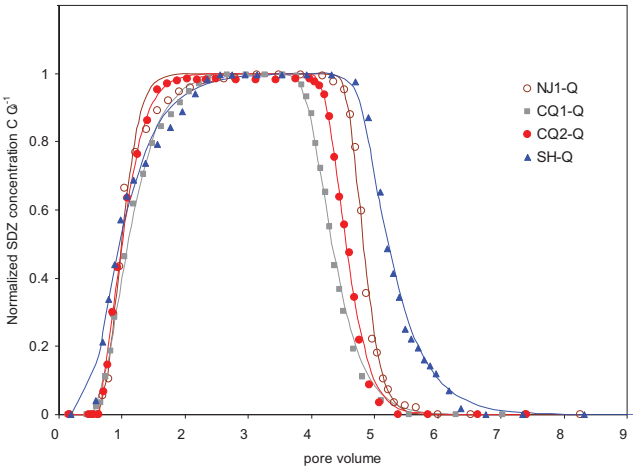

Figure 4.35 Breakthrough curves of SDZ in the 4 different sediments (mixed with quartz, ratio of sediment:quartz is 1:2). Experimental data: colored point. Fitted curves by equilibrium CDE: colored lines. (experimental conditions see Table 3.8 in Chapter 3.2.3)

The modeling results for all the transport data with nonequilibrium CDE showed larger standard errors and confidence interval of β and ω. In case of fixing ω, the value of β is nearly equal to 1 which indicates the equilibrium sorption. The Stanmod program gave a hint that the sorption equilibrium is reached and the equilibrium CDE should be used. Thus all the data

sets were calculated again with equilibrium CDE model. The experimental and modeling results are shown in Figure 4.35 (sediments with quartz) and Figure 4.36 (pure sediment SH). The predicted retardation coefficients R_p were also calculated from the distribution coefficient of adsorption isotherm and are listed together with transport parameters in Table 4.13.

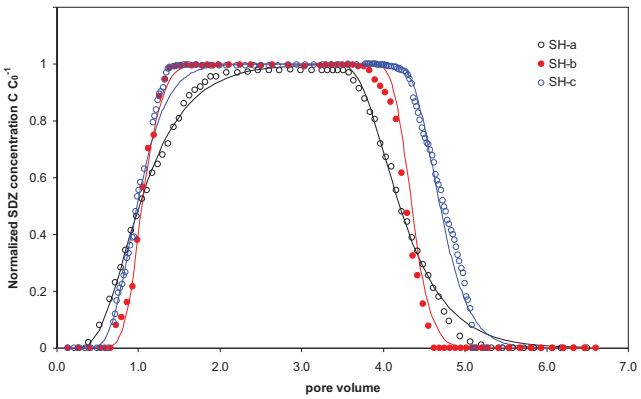

Figure 4.36 Breakthrough curves of SDZ in SH sediments at different conditions. Experimental data: colored point. Fitted curves by equilibrium CDE: colored lines (flow velocity: SH-a, 0.2 ml min^{-1}; SH-b, 0.2 ml min^{-1}; SH-c, 0.05 ml min^{-1}; input concentration: SH-a, 775 µg L^{-1}; SH-b, 50 µg L^{-1}; SH-c, 40 µg L^{-1})

Table 4.13 Transport parameters for SDZ in sediments (equilibrium CDE)

	C_{in} (µg L^{-1})	Δt (min)	ρ (g cm^{-3})	θ (cm^3 cm^{-3})	R	R_p*	K_d (cm^3 g^{-1})	r^2
NJ1-Q	100	500	1.58	0.32	1.02±0.02	-	0.004	0.991
CQ1-Q	100	500	1.32	0.38	1.16±0.02	-	0.046	0.997
CQ2-Q	100	500	1.37	0.36	1.05±0.016	-	0.013	0.997
SH-Q	100	500	1.53	0.29	1.08±0.03	-	0.015	0.992
NJ1	50	500	1.43	0.48	1.08±0.01	1.92	0.027	0.997
SH-a	775	500	1.37	0.43	1.11±0.007	2.21	0.034	0.996
SH-b	50	500	1.43	0.42	1.02±0.008	2.29	0.0059	0.996
SH-c	40	2000	1.34	0.49	1.009±0.01	2.04	0.0033	0.983

*predicted retardation coefficient from batch experiment K_d

From the BTCs of SDZ and comparing with tracer NO_3^-, there is only weak retardation of SDZ, which indicates very low sorption during the column experiments. This conclusion is not in contradiction to sorption batch experiments, because of the very low sorbed SDZ amounts (<10%) on sediments. Nevertheless, the low sorbed SDZ amounts reveal slow desorption kinetics. The calculated parameters (Table 4.13) also proved this result.

To evaluate the modeling results, the experimental data against modeling data of the transport experiments SH-a and SH-b were plotted in Figure 4.37. The slopes of both figures are nearly equal to 1 with a high correlation coefficient $r > 0.995$. This result exhibits an excellent agreement between the model estimates and experimental data.

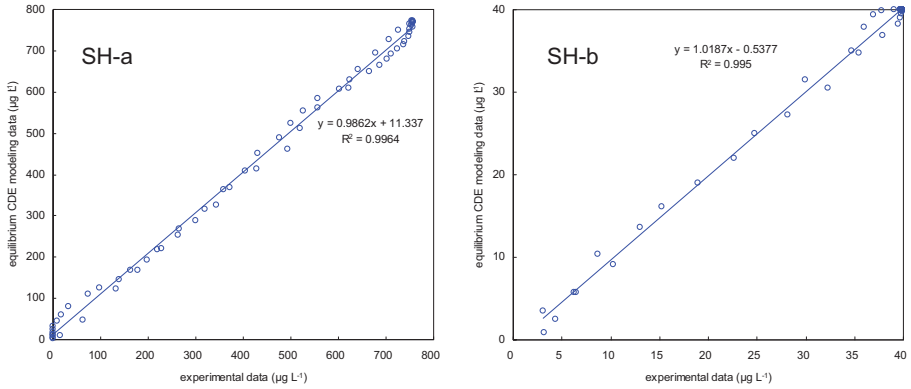

Figure 4.37 Correlation between experimental data and predicted data of SDZ concentration in the effluent from the breakthrough experiment with SH-sediment

The values of retardation coefficient R are about 50% smaller than that predicted ones from batch experiments (R_p, Table 4.13). In the column experiments of this study, a continuous release of mineral and organic colloids during the conditioning procedure of the column was observed. This can cause falsified analytical results due to interferences between DOM and SDZ in UV-detection and can lead to a further decrease of sorption capacity. To confirm this, later a batch experiment was performed by using the sediment after conditioning of the column. The result is presented in Figure 4.38-A. After conditioning, the sorption capacity decreased markedly with K_d values about 3 times lower than before. The possible reason is the loss of active sorption sites like soluble organic matter and mineral colloids due to the conditioning ("washout"). The same experiment was also performed with soil. As shown in Figure 4.38-B, conditioning of the column has no significant effect on soil sorption capacity. This result reveals that sediment contains more removable components with active sites for SDZ sorption.

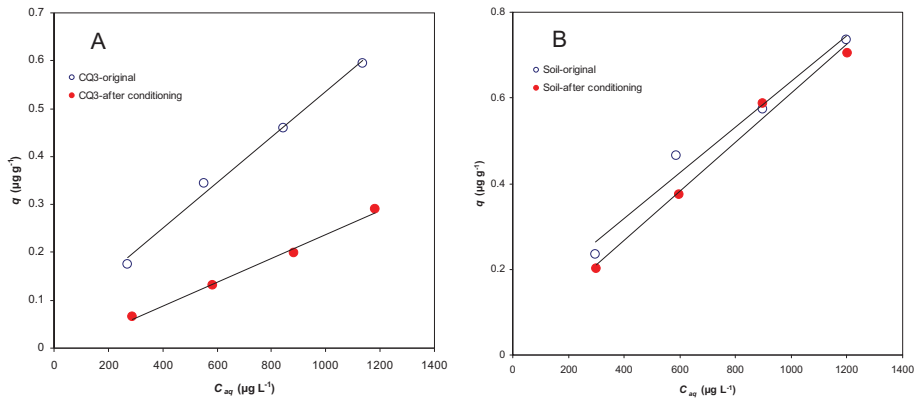

Figure 4.38 Adsorption comparison before and after conditioning (A: sediment CQ3; B: soil)

Another reason can be applying an equilibrium model to the data although the sorption equilibrium was not reached within the time scale of the batch or column experiments. As discussed in Chapter 4.3 and 4.4 about the sorption kinetics, both batch and column experiments were performed under nonequilibrium condition. If sorption equilibrium is assumed erroneously, incorrect equilibrium constants that are lower than the true equilibrium values will be estimated (Brusseau, 1991). Maraqa et al. (1998) investigated data from both batch and column experiments for the sorption of dimethylphthalate (DMP) and found that *R* value was also 50% smaller than predicted from batch experiments and the retardation factor decreased with increasing pore-water velocity. In another paper from them (Maraqa et al., 1999), they pointed out that sorption nonequilibrium appeared to be of a diffusive nature rather than due to a slow chemical reaction. Sorption mass-transfer coefficients varied proportionally with pore-water velocity. The same results were presented by Kim et al. (2006). They found that with increasing flow rate, decreased retardation of aqueous benzene was observed due to less reaction time. But in our study, the retardation factor of SH sediment was nearly identical at the pore-water velocities 0.84 cm h^{-1} and 3.9 cm h^{-1}, respectively. The reason could be the difference of pore-water velocity was not distinguishable comparing with 0.62-36.5 cm h^{-1} (Maraqa et al., 1999). The other possibility could be that SDZ is hydrophilic compounds with higher mobility in column comparing with hydrophobic organic chemicals like benzene.

Additionally, Altfelder et al. (2001) interpreted the result of Maraqa et al. (1998) as the inadequately data fitting and experimental difficulties in detecting the tailing of

nonequilibrium breakthrough curves. They demonstrated that information on tailing may be crucial when nonequilibrium sorption parameters are to be estimated by fitting a transport model to bereakthrough curves of organic compounds. Thus the lack of tail data could also be the cause for underestimated *R* values in this work due to the detected limit of HPLC.

Chapter 5

Summary

This study investigated the transformation, sorption and transport behavior of the pharmaceutical antibiotic sulfadiazine (SDZ) in the Yangtze sediment/water system under laboratory conditions. Selected Yangtze sediments (and a soil for comparison) and their components including metal oxides, clay minerals and humic substance were chosen as sorbents. Both radioactively labeled SDZ (^{14}C-SDZ) and unlabeled SDZ were used as target compounds for batch and column experiments. ^{14}C-SDZ concentrations in solution and solid phase were detected by radio-HPLC, a liquid scintillation counter (LSC) and the oxidizer method. Unlabeled SDZ was determined by HPLC-UV. The structure of transformation products was identified by LC-MS-MS and high-resolution mass spectroscopy (FT-ICR-MS, Q-Tof MS). Different sorption and transport models were conducted to fit the experimental data.

The photodegradation and biodegradation of SDZ was ruled out in this study. Transformation products were only detected in the SDZ-goethite system. The concentration of transformation products increased with increasing goethite concentration and contact time. In contrast, the presence/absence of oxygen had no effect on transformation under the experimental conditions used. The solubility of goethite increased with increasing SDZ concentration, which is indicative of the formation of the Fe^{III}-SDZ complex. All these results show that the transformation of SDZ is a chemical reaction on the goethite surface. A significant amount of a new, unknown transformation product (M1) was observed. The structure of further transformation products was identified as 4-(2-iminopyrimidin-1(2H)-yl)aniline (M2) and p-(pyrimidin-2-yl)aminoaniline (M3). All the main transformation products were found to be the extrusion of SO_2 from SDZ. M2 and M3 were produced in low concentrations and could be identified by LC-MS-MS in comparison with the photolysis products of SDZ and from the literature data. M1 was assumed to have a very similar structure to that of M2, but the actual structure is still unclear. The binding mechanism of SDZ on goethite was assumed to be surface complexation, which occurs by the replacement of OH group from goethite by SDZ^- ligands (“ligand exchange mechanism”). The possible transformation pathway was proposed

on the basis of monodentate inner-sphere complexation and intramolecular S_N reaction, but spectroscopic evidence would be required to prove this hypothesis.

Sorption kinetics of SDZ on minerals exhibit an equilibrium time within 2 days, but slow sorption behavior on humic acid, most sediments and soil was observed, which is in accordance with other studies. Nevertheless, to avoid any possible degradation of SDZ, batch experiments with 2 days contact time were performed to investigate the adsorption/desorption behavior of SDZ on Yangtze sediments and components (Al_2O_3, illite, goethite). Sorption kinetic data were fitted well by first order kinetics. Most of the adsorption isotherms determined in this study were significantly non-linear and could be best described by the Freundlich sorption isotherm. The amounts of SDZ adsorbed on illite and goethite decreased with increasing pH value, which indicates that surface charge is dominant in SDZ sorption. Besides pH, surface area is another key factor for SDZ sorption on minerals. The amount adsorbed on humic acid is much higher than on minerals. This result indicates that the sediment/soil organic matter plays an important role in SDZ sorption. This conclusion could also be drawn by comparing the sorption coefficients K_d and K_{OC} of sediments.

Sorption hysteresis occurred on all sediments except SH. It was assumed that desorption started before adsorption was complete (non-equilibrium conditions). Sorption models including rate-limited sorption (RLS) and two-stage one-rate sorption (2S1R) were conducted to estimate the equilibrium isotherm based on non-equilibrium data and to obtain the best fit parameters for describing the sorption hysteresis. Both models fitted all the data well with one desorption step. In fact, the RLS model could describe most cases in this study with the least number of parameters. The modeling results suggested that the sorption rate is the dominant factor for hysteresis of SDZ on different minerals, sediments and soil. In general, this experimental procedure combined with the modeling presented here can be applied in adsorption/desorption studies of unstable chemicals. The fitted parameters were used to predict the transport behavior of SDZ.

Transport behavior of SDZ in Yangtze sediments was investigated by column experiments. Experimental conditions including flow rate, input concentration and pulse duration were varied to obtain the optimal parameters for describing the transport behavior. The equilibrium convective dispersion equation (CDE) fitted the data better than the non-equilibrium CDE. The retardation factor R obtained from this model was about 50% lower than that predicted

from the K_d values of batch experimental data. The possible reason is the loss of active sorption sites such as soluble organic matter and mineral colloids due to the conditioning of the sediment column. Indeed, after conditioning, the sorption capacity of sediments decreased markedly with K_d values about 3 times lower than before. In contrast, for soil, the conditioning had no significant effect on sorption capacity. Based on this experimental experience, an improved experimental procedure for column studies with sediment can be suggested.

This study was the first attempt to investigate the behavior of SDZ in Yangtze sediments. The investigation of transformation product structure, sorption and transport behavior as well as data modeling provided fundamental information on SDZ behavior in the river/sediment system for further research. The fate of SDZ in the environment especially in river/sediments requires detailed knowledge of sorption and transformation processes. The main transformation product M1 of SDZ on goethite and other possible products from sediments and/or components need to be identified. In fact, the sorption binding mechanism and transformation pathways require more spectroscopic evidence. Following transformation and transport, the transformation products are released into the environment and become potential secondary pollutants. The risk assessment of these new substances in the environment may be a new topic for future studies.

References

Aharoni C. and Sparks D.L., (1991), Kinetics of soil chemical-reactions - A theoretical treatment, Rates of Soil Chemical Processes, Volume: 27, Pages: 1-18

Ajibade P.A., Kolawole G.A., O'Brien P., Helliwell M. and Raftery J., (2006), Cobalt(II) complexes of the antibiotic sulfadiazine, the X-ray single crystal structure of [Co(C10H9N4O2S)2(CH3OH)2], Inorganica Chimica Acta 359, 3111-3116

Alder A.C. et al., (2000), Determination of antibiotics in Swiss wastewater, Antibiotics in the Environment, Cranfield, UK

Alder A.C. et al., (2001), Occurrence and fate of fluoroquinolone, marcolide, and sulfonamide antibiotics during wastewater treatment and in ambient waters in Switzerland, Pharmaceuticals and Personal Care Products in the Environment: Scientific and Regulatory Issues: 56-69

Altfelder S., Streck T. and Richter J., (2000), Nonsingular sorption of organic compounds in soil: The role of slow kinetics. J. Environ. Qual.29:917-925.

Altfelder S., Streck T., Maraqa M.A. et al., (2001), Nonequilibrium sorption of dimethylphthalate - Compatibility of batch and column techniques, Soil Society of America Journal, Volume: 65, Issue: 1, Pages: 102-111

Bajpai A.K. et al., (2000), Static and Kinetic Studies on the Adsorption Behavior of Sulfadiazene, Adsorption 6: 349-357

Barriuso E., Laird D.A., Koskinen W.C. et al., (1994), Atrazine desorption from smectites, Soil Society of America Journal, Volume: 58, Issue: 6, Pages: 1632-1638

Bayard R., Barna L., Mahjoub B. and Gourdon R., (1998), Investigation of naphthalene sorption in soils and soil fractions using batch and column assays, Envrion. Toxicol. Chem. 17: 2383-2390

Ben W., Qiang Z., Adams C., Zhang H. and Chen L., (2008), Simultaneous determination of sulfonamides, tetracyclines and tiamulin in swine wastewater by solid-phase extraction and liquid chromatography–mass spectrometry, Journal of Chromatography A Volume 1202, Issue 2, 22 August 2008, Pages 173-180

Bialk H.M. and Pedersen J.A., (2008), ^{15}N NMR investigation of enzymatic coupling of sulfonamide antimicrobials with humic substances. Environ. Sci. Technol. 42: 106-112

Bialk H.M., Hedman C., Castillo A. and Pedersen J.A., (2007), Laccase-mediated Michael addition of ^{15}N-sulfapyridine to a model humic constituent. Environ. Sci. Technol. 41: 3593-3600

Bialk H.M., Simpson A.J. and Pedersen J.A., (2005), Cross-coupling of sulfonamide antimicrobial agents with model humic constituents. Environ. Sci. Technol. 39: 4463-4473

Boesten JJTI., van der Pas LJT., (1988), Modeling adsorption desorption-kinetics of pesticides in a soil suspension, Soil Science, Volume: 146, Issue: 4, Pages: 221-231

Boily J.F., Lützenkirchen J., Balmes O., Beattie and Sjöberg, (2001), Modelling proton binding at the goethite-water interface. Coll. & Surf. A 179, 11-27

Boreen, A.L., Arnold, W.A., and McNeill, K., (2005), Triplet-sensitized photodegradation of sulfa drugs containing six-membered heterocyclic groups: Identification of an SO2 extrusion photoproduct, Environ. Sci. Technol. 39 (10), pp. 3630-3638

Bouchard D.C., Wood A.L., Campell M.L., Nkedi-Kizza P. and Rao P.S.C., (1988), Sorption nonequilibrium during solute transport, J. Contam. Hydrol. 2: 209-223

Boxall A.B.A. et al., (2002), The sorption and transport of a sulphonamide antibiotic in soil systems, Toxicology Letters 131: 19-28

Boxall A.B.A. et al., (2004), Veterinary medicines in the environment, Rev Environ Contam Toxicol 180: 1-91

Brown C.J., Cook D.S. and Sengier L., (1985), Bis[N1-(2-(pyrimidinyl)sulphanilamido] zinc-Ammonia(1/2), *[Zn(C10H9N4O2S)2].2NH3, Acta Cryst. C41, 718-720

Brownawell B.J., Chen H. and Collier J.M. et al., (1990), Adsorption of organic cations to natural materials,

Environ. Sci. Technol. Volume: 24, Issue: 8, Pages: 1234-1241

Brusseau M.L., (1991), Transport of organic-chemicals by gas advection in structured or heterogeneous porous-media-development of a model and application to column experiments, Water Resources Research, Volume: 27, Issue: 12, Pages: 3189-3199

Brusseau M.L., (1992), Nonequilibrium transport of organic chemicals: The impact of pore-water velocity, J. Contam. Hydrol. 9: 353-368

Brusseau M.L., (1995), The effect of nonlinear sorption on transformation of contaminants during transport in porous media, J. Contam. Hydrol. 17: 277-291

Brusseau M.L., Jessrup R. and Rao P., (1989), Modelling transport of solutes influenced by multiprocess nonequilibrium, Water Resource Research, 25, 1971-1988,

Celis R. and Koskinen W.C., (1999), Characterization of Pesticide Desorption from Soil by the Isotopic Exchange Technique Soil Science Society of America Journal 63:1659-1666

Celorie J.A., Woods S.L. and Vinson T.S., (1989), A comparison of sorption equilibrium distribution coefficients using batch and centrifugation methods, J. Enviorn Qual, Volume: 18, Issue: 3, Pages: 307-313

Chiou C.T. et al,. (2000), Sorption of selected organic compounds from water to a peat soil and its humic-acid and humin fractions: Potential sources of the sorption non-linearity. Environ. Sci. Technol. 34: 1254-1258

Chiou C.T., (1989), In reactions and movement of organic chemicals in soils, Soil Society of America: Madison, WI, 1989: 1-30

Cho M.M., (2007), Fate of Antibiotics in the Soil: Adsorption/Desorption and Transformation Studies of Sulfadiazine in Two Soils, Master dissertation

Chun C. Hozalski R.M. and Arnold W.A., (2005), Degradation of drinking water disinfection byproducts by synthetic goethite and magneitie, Environ. Sci. Technol. 2005, 39, 8525-8532

Cook D.S. and Turner M.F., (1975), Crystal and molecular structure of silver sulphadiazine (N1-pyrimidin-2-ylsulphanilamide), Journal of the Chemical Society-Perkin Transaction 2, Issue: 10, Pages: 1021-1025

Cornell R.M., Schwertmann U., (2003), The Iron Oxide - Structure, properties, reactions, occurrences and uses. WILEY-VCN Verlag GmbH & Co. KGaA, Weinheim

Dannenberg A. and Pehkonen S.O., (1998), Investigate of the heterogeneously catalyzed hydrolysis of organophosphorus pestsides, J. Agric. Food Chem. 1998, 46, 325-334

Drillia P., Stamatelatou K. and Lyberatos G., (2005), Fate and mobility of pharmaceuticals in solid matrices, Chemosphere, Volume 60, Issue 8, Pages 1034-1044

Evanko C.R. and Dzombak D.A., (1999), Surface complexation modeling of organic acid sorption to goethite, J. Colloid & Interface Science. Volume: 214, Issue: 2, Pages: 189-206

Filius J.D., Hiemstra T. and van Riemsdijk H., (1997), Adsorption of small weak organic acid on goethite: modeling of mechanisms, J. Colloid & Interface Science, 195, 368-380

Förster M., Laabs V., Lamshöft M., Groeneweg J., Zühlke S., Spiteller M., Krauss M., Kaupenjohann M. and Amelung W., (2009), Sequestration of manure-applied sulfadiazine residues in soils, Environ. Sci. Technol., 43 (6), 1824-1830.

Gao J. and Petersen J.A., (2010), Sorption of sulfonamide antimicrobial agents to humic acid-clay complexes, J. Environ. Qual, 39: 228-235

Gao J. et al., (2005), Adsorption of Sulfonamide Antimicrobial Agents to Clay Minerals, Environ. Sci. Technol. 39: 9509-9516

Geelhoed J.S., Hiemstra T., and Van Riemsdijk W.H., (1997), Phosphate and sulfate adsorption on goethite: Single anion and competitive adsorption, Geochimica et Cosmochimica Acta, Volume: 61, Issue: 12, Pages: 2389-2396

Gelsomino A., Cacco G., Nannipieri P., (2000), Sorption of L-methionine-sulphoximine on humic acids and clay minerals, Biology and Fertility of Soils, Volume: 31, Issue: 3-4 Pages: 356-359

Gerstl Z, (1990), Estimation of organic chemical sorption by soils, J Contam Hydrol 6: 357-375

Giles C.H., Silva A.P.D. and Easton I.A., (1974), A general treatment and classification of the solute adsorption isotherm part. II. Experimental interpretation, J. Colloid & Interface Sci., 47, 766

Haller M.Y., Muller S.R., McArdell C.S., Alder A.C. and M.J.F. (2002), Quantification of veterinary antibiotics (sulfonamides and trimethoprim) in animal manure by liquid chromatography–mass spectrometrySuter, J. Chromatogr. A 952 (2002), p. 111

Hartig C., Storm T. and Jekel M., (1999), Detection and identification of sulphonamide drugs in municipal waste water by liquid chromatography coupled with electrospray ionization tandem mass spectrometry, Journal of Chromatography A 854, pp. 163–173.

Heise J., Höltge S., Schrader S., Kreuzig R., (2006), Chemical and biological characterization of non-extractable sulphonamide residues in soil, Chemosphere, 65 (11), 2352-2357

Hillel D., (1998), Environmental Soil Physics, Academic Press, San Diego

Hirsch et al., (1999) Occurrence of antibiotics in the aquatic environment, Sci Total Environ 225: 109-118

Hirsch R., Ternes T.A., Haberer K., Mehlich A., Ballwanz F. and Kratz K.L., (1998). Determination of antibiotics in different water compartments via liquid chromatography electrospray tandem mass spectrometry. J Chromatogr A 518 2, pp. 213–223

Holten Lützhøft H.C., Vaes W.H.J., Freidig A.P., Halling-Sørensen B. and Hermens J.L.M., (2000). 1-octanol/water distribution coefficient of oxolinic acid: influence of pH and its relation to the interaction with dissolved organic carbon. Chemosphere, 40, 711–714

Hong F. And Pehkonen S., (1998), Hydrolysis of phorate using simulated envrionmental conditions: rates, mechanisms, and product analysis, J. Agric. Food Chem. 1998, 46, 1192-1199

Höper et al., (2002), Eintrag und Verbleib von Tierarzneimittelwirkstoffen in Böden, Bodenschutz 4: 141-148

Huang W., Yu H., Weber W.J., Jr. (1998), Hysteresis in the sorption and desorption of hydrophobic organic contaminants by soils and sediments. 1. A comparative analysis of experimental protocols. J. Contam. Hydrol.31, 129-148

Ingerslev F. and Halling-Sørensen B., (2000), Biodegradability properties of sulfonamides in activated sludge, Environ. Toxicol. & Chem. Vol. 19, No. 10: 2467-2473

Jin S., (1997), Regulation, realities and recommendation on antimicrobial use in food animal production in China. In: The medical impact of the use of antimicrobials in food animals. WHO, Geneva (Section 2.3.4)

Jonsson C.M., Persson P., Sjoberg S. et al., (2008), Adsorption of Glyphosate on Goethite: Molecular Characterization of Surface Complexes, Environ. Sci. & Technol., 42 Issue: 7 Pages: 2464-2469

Jørgensen S.E. and Halling-Sørensen B., (2000), Drugs in the environment Chemosphere Volume 40, Issue 7, Pages 691-699

Kahle M. and Stamm C., (2007a), Time and pH-dependent sorption of the veterinary antimicrobial sulfathiazole to clay minerals and ferrihydrite, Chemosphere 68, 1224–1231

Kahle M. and Stamm C., (2007b), Sorption of the Veterinary Antimicrobial Sulfathiazole to Organic Materials of Different Origin Environ. Sci. Technol., 41 (1), pp 132–138

Kasteel R., Cho M.M., Unold M., Groeneweg J., Vanderbought J. and Vereecken H., (2010), Transformation and sorpiton of the veterinary antibiotics sulfadiazine in two soils: a short-term batch study, Environ. Sci. Technol. 44, 4651-4657

Kay P. and Boxall A.B., (2000), Environmental risk assessment of veterinary medicines in slurry, SSLRC Contract JF 611OZ, Cranfield Universityb

Kelsey J.W. and Alexander M., (1995), Effect of flow rate and path length of p-nitrophenol biodegradation during transport in soil, Soil. Sci. Am. J. 59: 113-117

Khalaf M, (2003), Effect of the fractionation and immobilization on the sorption properties of humic acid, Ph.D. theses

Kim S., Ha H., Choi N. and Kim D., (2006), Influence of flow rate and organic carbon content on benzene transport in a sandy soil, Hydrol. Process. 20, 4307-4316

Klagkou K., (2003), Fragmentation pathways of sulphonamides under electrospray tandem mass spectrometric conditions, Rapic Communications in Mass Spectrometry, Volume: 17 Issue: 21 Pages: 2373

Kolpin D.W. et al., (2002), Pharmaceuticals, hormones, and other organic wastewater contaminants in US streams, 1999-2000, A national reconnaissance. Environ. Sci. Technol. 36: 1202-1211

Kreuzig R. and Höltge S., (2005), Investigations on the fate of sulfadiazine in manured soil: Laboratory experiments and test plot studies, Environ. Toxicol & Chem. Vol. 24, No. 4: 771-776

Laird D.A., Yen P.Y., Koskinen W.C. et al., (1994) Sorption of atrazine on Soil Clay Components, Environ. Sci. & Technol., Volume: 28, Issue: 6, Pages: 1054-1061

Lamshöft M., Sukul P., Zühlke S. and Spiteller M., (2007), Metabolism of 14C-labelled and non-labelled sulfadiazine after administration to pigs, Anal Bioanal Chem (2007) 388: 1733-1745

Lan Y., Deng B., Kim C. and Thornton E.C., (2007), Influence of soil minerals on chromium(VI) reduction by sulfide under anoxic conditions, Geochemical Transactions 2007, 8:4 doi:10.1186/1467-4866-8-4

Lan Y., Deng B., Kim C. et al., (2007), Influence of soil minerals on chromium(VI) reduction by sulfide under anoxic conditions, Geochemical Transactions, Volume: 8, Pages: 1-10

Langhammer J-P, Büning-Pfaue H, (1989), Bewertung von Arzneistoff-Rückständen aus der Gülle im Boden. Lebensmittelchem Gerichtl Chem 43: 103-113

Langmuir I. (1916), The constitution and fundamental properties of solids and liquids. part i. solids. J. Am. Chem. Soc. 38, 2221-2295

Langner H.W., Inskeep W.P., Gaber H.M., Jones W.L., Das B.S. and Wraith J.M., (1998), Pore water velocity and residence time effects on the degradation of 2,4-D during transport, Environ. Sci. Technol. 32: 1308-1315

Lawrence M.A.M et al., (2000), Can adsorption isotherms predict sediment bioavailability? Chemosphere, 41: 1091-1100

Li J., Cai Y., Shi Y., Mou S. and Jiang G., (2007), Determination of sulfonamide compounds in sevage and river by mixed hemimicelles solid-phase extraction prior to liquid chromatography-spectrophotometry, Journal of Chromatography A, 1139 (2007), 178-184

Lindsey M.E., Meyer M. and Thurman E.M., (2001), Analysis of trace levels of sulfonamide and tetracycline antimicrobials in groundwater and surface water using solid phase extraction and liquid chromatography/mass spectrometry, Anal. Chem. 73 (2001), pp. 4640–4646

Lion L.W., Stauffer T.B. and MacIntyre W.G., (1990), Sorption of hydrophobic compounds on aquifer materials: analysis methods and the effect of organic carbon, J. Contam. Hydrol. 5: 215-234

Ma L., Southwick L.M., Willis G.H. and Selim H.M., (1993), Hysteretic characteristics of atrazine adsorption-desorption by a Sharkey soil, Weed Science, 41: 627 1993

MacIntyre W.G. and Stauffer T.B., (1988), Liguid chromatography applications to determination of sorption on aquifer materials, Chemosphere, 17: 2161-2173

MacIntyre W.G., Stauffer T.B. and Antworth C.P., (1991), A comparison of sorption coefficients determined by batch, column, and box methods on a low organic-carbon aquifer material, Ground Water, Volume: 29, Issue: 6, Pages: 908-913

Maraqa M.A., Wallace R.B. and Voice T.C., (1997), Effects of degree of water saturation on dispersivity and immobile water in sandy soil columns, J. Contam. Hydrol. 25: 199-218

Maraqa M.A., Wallace R.B. and Voice T.C., (1999), Effects of residence time and degree of water saturation on sorption nonequilibrium parameters. Journal of Contaminant Hydrology 36, 53-72

Maraqa M.A., Zhao X., Wallace R.B. and Voice T.C., (1998), Retardation coefficients of noionic organic compounds determined by batch and column techniques, Soil Sci. Soc. Am. J. 62: 142-152

Martínez-Carballo E., González-Barreiro C., Scharf S. And Gans O., (2007), Envrionmental monitoring study of selected veterinary antibiotics in animal manure and soils in Austria, Environmental Pollution 148 (2007), 570-579

McBride M.B., (1994), Environmental chemistry of soils, Oxford University press, New York Oxford

Menabue L. and Saladini M., (1993), Coordination behavior of sulfa-drugs: synthesis, structural, and spectroscopic investigation on M(II)(N1-pyrimidin-2YL-sulfanilamido)2·XH2O, Journal of Inorganic Biochemistry, 49, 201-207

Miao X.-S., Bishay F., Chen M. and Metcalfe C.D., (2004), Occurrence of antimicrobials in the final effluents of wastewater treatment plants in Canada, Environmental Science and Technology 38, pp. 3533–3541.

Miller C.T. and Pedit J.A., (1992), Use of a reactive surface-diffusion model to describe apparent sorption-

desorption hysteresis and abiotic degradation of lindane in a subsurface material, Environ. Sci. Technol., 1992, 26 (7), pp 1417–1427

Mueller S.R., Singer H., Stoob K., Burkhardt M. Hartmann N., Goetz C., Stamm C. And Waul C., (2003), Occurrence and fate of antibiotics in manure, soil and water. Mitt. Lebensm. Hyg. 2003, 9486), 574-578

Nelsen D.R., Vangenuchten M.T. and Biggar J.W., (1986), Water-flow and solute transport processes in the unsaturated zone, Water Resources Research, Volume: 22, Issue: 9, Pages: S89-S108

Nkedi-Kizza P., Biggar J.W., Selim H.M., et al., (1984), On the equivalence of two conceptual models for describing ion exchange during transport through an aggregated oxisol, Water Resource Research. 20, 1123-1130

Nkedi-Kizza P., Rao P.S.C. and Hornsby A.G., (1987), Influence of organic cosolvent on leaching of hydrophobic organic chemicals through soils, Environ. Sci. Technol. 21: 1107-1111

Nowack B. and Sigg L., (1996), Adsorption of EDTA and metal-EDTA complexes onto goethite, J. Colloid & Interface Science, Volume: 177, Issue: 1, Pages: 106-121

OECD. Adsorpion-Desorption Using a Batch Equilibrium Method; Technical Guideline 106; Organization for Economic Cooperation and Development: 2000

OECD. OECD guideline for the testing of chemicals-leaching in soil columns; Organization for Economic Cooperation and Development: 1999

Peak D., Ford R.G. and Sparks D.L., (1999), An in situ ATR-FTIR investigation of sulfate bonding mechanisms on goethite, J. Colloid & Interface Science, Volume: 218, Issue: 1, 289-299

Peng X., Tan J., Tang C., Yu Y. and Wang Z., (2008), Multiresidue determination of fluoroquinolone, sulfonamide, trimethoprim, and chloramphenicol antibiotics in urban waters in China, Environmental Toxicology and Chemistry Volume 27, Issue 1

Peng X., Wang Z., Kuang W., Tan J. and Li K., (2006), A preliminary study on the occurrence and behavior of sulfonamides, ofloxacin and chloramphenicol antimicrobials in wastewaters of two sewage treatment plants in Guangzhou, China, Science of The Total Environment, Volume 371, Issues 1-3, 1 December 2006, Pages 314-322

Pfeifer T., Tuerk J. and Fuchs R., (2005), Structural characterization of sulfadiazine metabolites using H/D exchange combined with various MS/MS experiments, Journal of the American Society for Mass Spectrometry 16, pp. 1687–1694.

Pfeifer T., Tuerk J., Bester K., and Spiteller M., (2002), Determination of selected sulfonamide antibiotics and trimethoprim in manure by electrospray and atmospheric pressure chemical ionization tandem mass spectrometry, Rapid Communications in Mass Spectrometry, Volume 16 Issue 7, Pages 663 - 669

Pignatello J.J. and Xing B., (1996), Mechanisms of slow sorption of organic chemicals to natural particles, Environ. Sci. Technol. 1996, Vol. 30, No. 1, 1-11

Pignatello J.J., (1989), Sorption Dynamics of Organic Compounds in Soils and Sediments. SSSA Special Publication No. 22. Soil Science Society of America, Inc., Madison, WI. 1989. p 45-80, 11 fig, 3 tab, 104 ref.

Pignatello J.J., (2000), The measurement and interpretation of sorption and desorption rates for organic compounds in soil media. Advances in Agronomy, 69, 1-73

Plassard F., Winiarski T. and Petit-Ramel M., (2000), Retention and distribution of three heavy metals in a carbonated soil: comparison between batch and unsaturated column studies, J. Contam. Hydrol. 42: 99-111

Pusino A., Pinna M.V. and Gessa C., (2004), Azimsulfuron sorption-desorption on soil, JOURNAL OF AGRICULTURAL AND FOOD CHEMISTRY, Volume: 52, Issue: 11, Pages: 3462-3466

Ramberg L. and Bäcklund B., (1940), Ark. Kemi. Mineral. Geol. 1940, 27, Band, 13A, 1 (Chem. Abstr., 1940, 34, 4725)

Rietra R.P.J.J., Hiemstra T. and van Riemsdijk W.H., (1999), Sulfate adsorption on goethite, J. Colloid & Interface Science, Volume: 218, Issue: 2, Pages: 511-521

Roger M.N., (1997), An Introduction to Surface Chemistry

Sabbah I., Ball W.P., Young D.F. and Bouwer E.J., (2005), Misinterpretations in the modeling of contaminant desorption from envrionmental solids when equilibrium conditions are not fully understood, Environmental

Engineering Science, 22, 350-366

Sakurai H. and Ishimitsu T., (1979), Microionization constants of sulphonamides, Talantu. Vol 27, pp 293-298

Salfity J.A., Regazzoni A.E. and Blesa M.A., (2000), Interfacial chemistry of dissolving metal oxide particles: Dissolution by organic acids. Chap. 14 p. 513-540. Interfacial dynamics (Ed. N. Kallay) Marcel Dekker N.Y.

Sander M., Lu Y. and Pignatello J.J., (2005), A thermodynamically based method to quantify true sorption hysteresis, Journal of Environmental Quality, Volume: 34, Issue: 3, Pages: 1063-1072

Sanders S.M., Srivastava P., Feng Y. And Dane J.H., (2008), Sorption of the veterinary antimicrobials sulfadimethoxine and ormetoprim in soil, J.of Environ. Quality, Vol 37, 1510-1518

Sarmah A.K., Meyer M. T. and Boxall A.B.A., (2006), A global perspective on the use, sales, exposure pathways, occurrence, fate and effects of veterinary antibiotics (Vas) in the environment, Chemosphere 65 (2006), 725-759

Schmidt B., Ebert J., Lamshöft M., Thiede B., Schumacher-Buffel R., Rong J., Corvini P. and Schäffer A.J., (2008), Fate in soil of 14C-sulfadiazine residues contained in the manure of young pigs treated with a veterinary antibiotic, Environ Sci Health B 43:8–20

Schwarzenbach R.P., Gschwend P.M., Imboden D.M., (2003), Environmental organic chemistry (2nd edition), John Wiley and Sons, New York

Schwarzenbach, RP et al., (1993), Environmental organic chemistry, J Wiley, New York, p 681

Sheals J., Granstrom M., Sjoberg S. et al., (2003), Coadsorption of Cu(II) and glyphosate at the water-goethite (alpha-FeOOH) interface: molecular structures from FTIR and EXAFS measurements, J. Colloid & Interface Science, Volume: 262,Issue: 1, Pages: 38-47

Sheals J., Sjoberg S. and Persson P., (2002), Adsorption of glyphosate on goethite: Molecular characterization of surface complexes, Environ. Sci. & Technol., 36, Issue: 14, 3090-3095

Simunek J., van Genuchten M.Th., Sejna M., Toride N. and Leij F.J., (1999), The STANMOD computer software for evaluating solute transport in porous media using analytical solutions of convection-dispersion equation, Version 1.0 and 2.0

Spurlock F.C., Haung K. and van Genuchten M.T., (1995), Isotherm nonlinearity and nonequilibrium sorption effects on transport of fenuron and monuron in soil columns, Envrion. Sci. Technol. 29:1000-1007

Stein K., Ramil M., Fink G., Sander M. and Ternes T.A., (2008), Analysis and sorption of psychoactive drugs onto sediment, Environ. Sci. Technol. 2008, 42, 6415-6423

Stoob K., Singer H.P., Stettler S., Hartmann N., Mueller S.R., Stamm C.H., (2006), Exhaustive extraction of sulfonamide antibiotics from aged agricultural soils using pressurized liquid extraction, J Chromatogra A, 1128 (1-2), 1-9

Stoob K., Singer HP., Mueller S.R., et al., (2007), Dissipation and Transport of Veterinary Sulfonamide Antibiotics after Manure Application to Grassland in a Small Catchment, Environ. Sci. & Technol. 41: 7349-7355

Streck T., Poletika N.N., Jury W.A. and Farmer W.J., (1995), Description of simazine transport with rate-limited, two-stage, linear and nonlinear sorption. Water Resour. Res. 31: 811-822

Stumm W. (1992), Chemistry of the solid/water interface. Wiley, New York

Stumm W. and Furrer G. (1987), The dissolution of oxides and aluminum silicates: Examples of surface-coordination-controlled kinetics. In: Stumm, W. (ed.) Aquatic surface chemistry. J. Wiley & Sons, New York, 197-219

Sukul P. and Spiteller M. (2006), Sulfonamides in the environment as veterinary drugs, Rev. Environ. Contam. Toxicol. 187, 67-101

Sukul P.; Lamshoft M.; Zuhlke S. and Spiteller M., (2008a), Photolysis of C-14-sulfadiazine in water and manure. Chemosphere 71: 717 – 725.

Sukul P.; Lamshoft M.; Zuhlke S. and Spiteller M., (2008b), Sorption and desorption of sulfadiazine in soil and soil-manure systems, Chemosphere Volume 73, Issue 8, November 2008, Pages 1344-1350

Swanson R.A. and Dutt G.R., (1973), Chemical and physical processes that affect atrazine and distribution in soil systems, Soil Science Society of America Journal, Volume: 37, Issue: 6, Pages: 872-879

Tejedor-Tejedor M.I., Yost E.C., Anderson M.A., (1990), Characterization of benzoic and phenolic complexes at the goethite/aqueous solution interface using cylindrical internal reflection Fourier transform infrared spectroscopy. Part 1. Methodology, Langmuir, Volume 6, Issue 5, 979–987

Ter Laak T.L., Gebbink W.A. and Tolls J., (2006a), Estimation of soil sorption coefficients of veterinary pharmaceuticals from soil properties, Environmental Toxicology and Chemistry, Vol. 25, No. 4, pp. 933-941

Ter Laak T.L., Gebbink W.A. and Tolls J., (2006b), The effect of pH and ionic strength on the sorption of sulfachloropyridazine, tylosin, and oxytetracycline to soil, Environmental Toxicology and Chemistry, Vol. 25, No. 4, pp. 904-911

Thiele-Bruhn S. and Aust M.-O., (2004), Effects of Pig Slurry on the Sorption of Sulfonamide Antibiotics in Soil, Arch. Environ. Contam. Toxicol. 47: 31-39

Thiele-Bruhn S. et al., (2004), Sorption of Sulfonamide Pharmaceutical Antibiotics on Whole Soils and Particle-Size Fractions, J. Environ. Qual. 33: 1331-1342

Thiele-Bruhn S., (2000), Adsorption of the antibiotic pharmaceutical compound sulfapyridine by a long-term differently fertilized loess Chernozem, J. Plant Nutr. Soil. Sci. 163: 589-594

Thiele-Bruhn S., (2003), Pharmaceutical antibiotic compounds in soils – a review, J. Plant Nutr Soil Sci. 166: 145-167

Thiele-Bruhn S., Seibicke T. and Leinweber P. (2002), Sorption of sulfonamide antibiotic pharmaceuticals in soil particle size fractions, SETAC Europe 12th annual meeting, 12-16 May, 2002, Vienna

Tiehm A. Technologiezentrum Wasser, Germany

Tolls J., (2001), Sorption of Veterinary Pharmaceuticals in Soils: A Review, Environ. Sci. Tech. Vol. 35, No. 17: 3397-3406

Tombácz E. and Szekeres, (2001), Effects of impurity and solid-phase dissolution on surface charge titration of aluminum oxide, Progr Colloid Polym Sci 117: 18-26

Toride N., Leij F.J. and van Genuchten M.Th., (1995), The CXTFIT code for estimation transport parameters from laboratory or field tracer experiments, Version 2.0, Research report No. 137, U.S. Salinity Laboratory

Torrents A. and Stone A.T., (1991), Hydrolysis of phenyl picolinate at the mineral/water interface, Environ. Sci. Technol. 1991, 25, 143-149

Unold M., Kasteel R., Groeneweg J. and Vereecken H., (2009), Transport and transformation of sulfadiazine in soil columns packed with a silty loam and a loamy sand, Journal of Contaminant Hydrology Volume 103, Issues 1-2, 7 Pages 38-47

van Genuchten M.T. and Wagenet R.J., (1989), Two-site/two-region models for pesticide transport and degradation: theoretical development and analytical solutions, Soil Sci. Soc. Am. J., 53, 1303-1310

van Genuchten M.T., Wierenga P.J. and O'Connor G.A., (1977), Mass transfer studies in sorbing porous media: III. Experimental evaluation with 2,4,5-T, Soil Sci. Soc. Am. J. 41: 278-284

Villalobos M. and Leckie J.O., (2001), Surface complexation modeling and FTIR study of carbonate adsorption to goethite, J. Colloid & Interface Science, Volume: 235, Issue: 1, Pages: 15-32

Vree T.B. et al., (1995), Isolation, identification and determination of sulfadiazine and its hydorxy metabolies and conjugates from man and Rhesus monkey by high-performance liquid chromatography, Journal of Chromatography B, 670: 111-123

Wang G., Sorption/Desorption Reversibility of Polycyclic Aromatic Hydrocarbons (PAHs) in Soils and Carbonaceous Materials, Ph.D dissertation, 2008

Wang T., Li M. and Teng S., (2009), Bridging the gap between batch and column experiments: A case study of Cs adsorption on granite, Journal of Hazardous Materials, Volume: 161, Issue: 1, Pages: 409-415

Wehrhan A., (2007), Fate of veterinary pharmaceuticals in soil: An experimental and numerical study on the mobility, sorption and transformation of sulfadiazine, PhD thesis

Wijnja H. and Schulthess C.P., (2000), Vibrational spectroscopy study of selenate and sulfate adsorption mechanisms on Fe and Al (hydr)oxide surfaces, J. Colloid & Interface Science, Volume: 229, Issue: 1, Pages: 286-297

Wolters A. and Steffens M., (2005), Photodegradation of antibiotics on soil surfaces: Laboratory studies on

sulfadiazine in an ozone-controlled environment, Environ. Sci. Technol.2005, 39, 6071-6078

Xing B. and Pignatello J.J., (1997), Dual-mode sorption of low-polarity compounds in glassy poly(vinyl chloride) and soil organic matter, Environ. Sci. & Tech. Volume: 31, Issue: 3, Pages: 792-799

Xu W., Zhang G., Li X., Zou S., Li P., Hu Z. and Li J., (2007), Occurrence and elimination of antibiotics at four sewage treatment plants in the Pearl River Delta (PRD), South China. Water Research, Volume 41, Issue 19, November 2007, Pages 4526-4534

Xu W., Zhang G., Zou S., Li X. and Liu Y., (2008), Determination of selected antibiotics in the Victoria Harbour and the Pearl River, South China using high-performance liquid chromatography-electrospray ionization tandem mass spectrometry, Environmental Pollution, Volume 145, Issue 3, February 2007, Pages 672-679

Yang S., Cha J. and Carlson K., (2004), Quantitative determination of trace concentrations of tetracycline and sulfonamide antibiotics in surface water using solid-phase extraction and liquid chromatography/ion trap tandem mass spectrometry. Rapid Commun. Mass Spectrom. 2004, 18(18), 2131-2145

Yost E.C., Tejedor-Tejedor M.I. and Anderson M.A., (1990), In situ CIR-FTIR characterization of salicylate complexes at the goethite/aqueous solution interface, Environ. Sci. & Technol., 24, Issue: 6, 822-828

Young D.F. and Ball W.P., (1998), Estimating diffusion coefficients in low-permeability porous media using a macropore column. Environ. Sci. Technol. 32: 2578-2584

Yu L., Fink G., Wintgens T. et al., (2009), Sorption behavior of potential organic wastewater indicators with soils, WATER RESEARCH, Volume: 43, Issue: 4, Pages: 951-960

Zhao D., Pignatello J.J., White J.C. et al., (2001), Dual-mode modeling of competitive and concentration-dependent sorption and desorption kinetics of polycyclic aromatic hydrocarbons in soils, Water Resources Research, Volume: 37, Issue: 8, Pages: 2205-2212

Acknowledgements

1. **Einsatz von multispektralen Satellitenbilddaten in der Wasserhaushalts- und Stoffstrommodellierung – dargestellt am Beispiel des Rureinzugsgebietes**
   von C. Montzka (2008), XX, 238 Seiten
   ISBN: 978-3-89336-508-1

2. **Ozone Production in the Atmosphere Simulation Chamber SAPHIR**
   by C. A. Richter (2008), XIV, 147 pages
   ISBN: 978-3-89336-513-5

3. **Entwicklung neuer Schutz- und Kontaktierungsschichten für Hochtemperatur-Brennstoffzellen**
   von T. Kiefer (2008), 138 Seiten
   ISBN: 978-3-89336-514-2

4. **Optimierung der Reflektivität keramischer Wärmedämmschichten aus Yttrium-teilstabilisiertem Zirkoniumdioxid für den Einsatz auf metallischen Komponenten in Gasturbinen**
   von A. Stuke (2008), X, 201 Seiten
   ISBN: 978-3-89336-515-9

5. **Lichtstreuende Oberflächen, Schichten und Schichtsysteme zur Verbesserung der Lichteinkopplung in Silizium-Dünnschichtsolarzellen**
   von M. Berginski (2008), XV, 171 Seiten
   ISBN: 978-3-89336-516-6

6. **Politikszenarien für den Klimaschutz IV – Szenarien bis 2030**
   hrsg.von P. Markewitz, F. Chr. Matthes (2008), 376 Seiten
   ISBN 978-3-89336-518-0

7. **Untersuchungen zum Verschmutzungsverhalten rheinischer Braunkohlen in Kohledampferzeugern**
   von A. Schlüter (2008), 164 Seiten
   ISBN 978-3-89336-524-1

8. **Inorganic Microporous Membranes for Gas Separation in Fossil Fuel Power Plants**
   by G. van der Donk (2008), VI, 120 pages
   ISBN: 978-3-89336-525-8

9. **Sinterung von Zirkoniumdioxid-Elektrolyten im Mehrlagenverbund der oxidkeramischen Brennstoffzelle (SOFC)**
   von R. Mücke (2008), VI, 165 Seiten
   ISBN: 978-3-89336-529-6

10. **Safety Considerations on Liquid Hydrogen**
    by K. Verfondern (2008), VIII, 167 pages
    ISBN: 978-3-89336-530-2

11. **Kerosinreformierung für Luftfahrtanwendungen**
von R. C. Samsun (2008), VII, 218 Seiten
ISBN: 978-3-89336-531-9

12. **Der 4. Deutsche Wasserstoff Congress 2008 – Tagungsband**
hrsg. von D. Stolten, B. Emonts, Th. Grube (2008), 269 Seiten
ISBN: 978-3-89336-533-3

13. **Organic matter in Late Devonian sediments as an indicator for environmental changes**
by M. Kloppisch (2008), XII, 188 pages
ISBN: 978-3-89336-534-0

14. **Entschwefelung von Mitteldestillaten für die Anwendung in mobilen Brennstoffzellen-Systemen**
von J. Latz (2008), XII, 215 Seiten
ISBN: 978-3-89336-535-7

15. **RED-IMPACT**
Impact of Partitioning, Transmutation and Waste Reduction Technologies on the Final Nuclear Waste Disposal
SYNTHESIS REPORT
ed. by W. von Lensa, R. Nabbi, M. Rossbach (2008), 178 pages
ISBN 978-3-89336-538-8

16. **Ferritic Steel Interconnectors and their Interactions with Ni Base Anodes in Solid Oxide Fuel Cells (SOFC)**
by J. H. Froitzheim (2008), 169 pages
ISBN: 978-3-89336-540-1

17. **Integrated Modelling of Nutrients in Selected River Basins of Turkey**
Results of a bilateral German-Turkish Research Project
project coord. M. Karpuzcu, F. Wendland (2008), XVI, 183 pages
ISBN: 978-3-89336-541-8

18. **Isotopengeochemische Studien zur klimatischen Ausprägung der Jüngeren Dryas in terrestrischen Archiven Eurasiens**
von J. Parplies (2008), XI, 155 Seiten, Anh.
ISBN: 978-3-89336-542-5

19. **Untersuchungen zur Klimavariabilität auf dem Tibetischen Plateau - Ein Beitrag auf der Basis stabiler Kohlenstoff- und Sauerstoffisotope in Jahrringen von Bäumen waldgrenznaher Standorte**
von J. Griessinger (2008), XIII, 172 Seiten
ISBN: 978-3-89336-544-9

20. **Neutron-Irradiation + Helium Hardening & Embrittlement Modeling of 9%Cr-Steels in an Engineering Perspective (HELENA)**
by R. Chaouadi (2008), VIII, 139 pages
ISBN: 978-3-89336-545-6

21. **in Bearbeitung**

22. **Verbundvorhaben APAWAGS (AOEV und Wassergenerierung) – Teilprojekt: Brennstoffreformierung – Schlussbericht**
von R. Peters, R. C. Samsun, J. Pasel, Z. Porš, D. Stolten (2008), VI, 106 Seiten
ISBN: 978-3-89336-547-0

23. **FREEVAL**
Evaluation of a Fire Radiative Power Product derived from Meteosat 8/9 and Identification of Operational User Needs
Final Report
project coord. M. Schultz, M. Wooster (2008), 139 pages
ISBN: 978-3-89336-549-4

24. **Untersuchungen zum Alkaliverhalten unter Oxycoal-Bedingungen**
von C. Weber (2008), VII, 143, XII Seiten
ISBN: 978-3-89336-551-7

25. **Grundlegende Untersuchungen zur Freisetzung von Spurstoffen, Heißgaschemie, Korrosionsbeständigkeit keramischer Werkstoffe und Alkalirückhaltung in der Druckkohlenstaubfeuerung**
von M. Müller (2008), 207 Seiten
ISBN: 978-3-89336-552-4

26. **Analytik von ozoninduzierten phenolischen Sekundärmetaboliten in *Nicotiana tabacum* L. cv Bel W3 mittels LC-MS**
von I. Koch (2008), III, V, 153 Seiten
ISBN 978-3-89336-553-1

27. **IEF-3 Report 2009. Grundlagenforschung für die Anwendung**
(2009), ca. 230 Seiten
ISBN: 978-3-89336-554-8

28. **Influence of Composition and Processing in the Oxidation Behavior of MCrAlY-Coatings for TBC Applications**
by J. Toscano (2009), 168 pages
ISBN: 978-3-89336-556-2

29. **Modellgestützte Analyse signifikanter Phosphorbelastungen in hessischen Oberflächengewässern aus diffusen und punktuellen Quellen**
von B. Tetzlaff (2009), 149 Seiten
ISBN: 978-3-89336-557-9

30. **Nickelreaktivlot / Oxidkeramik – Fügungen als elektrisch isolierende Dichtungskonzepte für Hochtemperatur-Brennstoffzellen-Stacks**
von S. Zügner (2009), 136 Seiten
ISBN: 978-3-89336-558-6

31. **Langzeitbeobachtung der Dosisbelastung der Bevölkerung in radioaktiv kontaminierten Gebieten Weißrusslands – Korma-Studie**
von H. Dederichs, J. Pillath, B. Heuel-Fabianek, P. Hill, R. Lennartz (2009), Getr. Pag.
ISBN: 978-3-89336-532-3

32. **Herstellung von Hochtemperatur-Brennstoffzellen über physikalische Gasphasenabscheidung**
von N. Jordán Escalona (2009), 148 Seiten
ISBN: 978-3-89336-532-3

33. **Real-time Digital Control of Plasma Position and Shape on the TEXTOR Tokamak**
by M. Mitri (2009), IV, 128 pages
ISBN: 978-3-89336-567-8

34. **Freisetzung und Einbindung von Alkalimetallverbindungen in kohlebefeuerten Kombikraftwerken**
von M. Müller (2009), 155 Seiten
ISBN: 978-3-89336-568-5

35. **Kosten von Brennstoffzellensystemen auf Massenbasis in Abhängigkeit von der Absatzmenge**
von J. Werhahn (2009), 242 Seiten
ISBN: 978-3-89336-569-2

36. **Einfluss von Reoxidationszyklen auf die Betriebsfestigkeit von anodengestützten Festoxid-Brennstoffzellen**
von M. Ettler (2009), 138 Seiten
ISBN: 978-3-89336-570-8

37. **Großflächige Plasmaabscheidung von mikrokristallinem Silizium für mikromorphe Dünnschichtsolarmodule**
von T. Kilper (2009), XVII, 154 Seiten
ISBN: 978-3-89336-572-2

38. **Generalized detailed balance theory of solar cells**
by T. Kirchartz (2009), IV, 198 pages
ISBN: 978-3-89336-573-9

39. **The Influence of the Dynamic Ergodic Divertor on the Radial Electric Field at the Tokamak TEXTOR**
von J. W. Coenen (2009), xii, 122, XXVI pages
ISBN: 978-3-89336-574-6

40. **Sicherheitstechnik im Wandel Nuklearer Systeme**
von K. Nünighoff (2009), viii, 215 Seiten
ISBN: 978-3-89336-578-4

41. **Pulvermetallurgie hochporöser NiTi-Legierungen für Implanat- und Dämpfungsanwendungen**
von M. Köhl (2009), XVII, 199 Seiten
ISBN: 978-3-89336-580-7

42. **Einfluss der Bondcoatzusammensetzung und Herstellungsparameter auf die Lebensdauer von Wärmedämmschichten bei zyklischer Temperaturbelastung**
von M. Subanovic (2009), 188, VI Seiten
ISBN: 978-3-89336-582-1

43. **Oxygen Permeation and Thermo-Chemical Stability of Oxygen Permeation Membrane Materials for the Oxyfuel Process**
by A. J. Ellett (2009), 176 pages
ISBN: 978-3-89336-581-4

44. **Korrosion von polykristallinem Aluminiumoxid (PCA) durch Metalljodidschmelzen sowie deren Benetzungseigenschaften**
von S. C. Fischer (2009), 148 Seiten
ISBN: 978-3-89336-584-5

45. **IEF-3 Report 2009. Basic Research for Applications**
(2009), 217 Seiten
ISBN: 978-3-89336-585-2

46. **Verbundvorhaben ELBASYS (Elektrische Basissysteme in einem CFK-Rumpf) - Teilprojekt: Brennstoffzellenabgase zur Tankinertisierung - Schlussbericht**
von R. Peters, J. Latz, J. Pasel, R. C. Samsun, D. Stolten
(2009), xi, 202 Seiten
ISBN: 978-3-89336-587-6

47. **Aging of ^{14}C-labeled Atrazine Residues in Soil: Location, Characterization and Biological Accessibility**
by N. D. Jablonowski (2009), IX, 104 pages
ISBN: 978-3-89336-588-3

48. **Entwicklung eines energetischen Sanierungsmodells für den europäischen Wohngebäudesektor unter dem Aspekt der Erstellung von Szenarien für Energie- und CO_2 - Einsparpotenziale bis 2030**
von P. Hansen (2009), XXII, 281 Seiten
ISBN: 978-3-89336-590-6

49. **Reduktion der Chromfreisetzung aus metallischen Interkonnektoren für Hochtemperaturbrennstofzellen durch Schutzschichtsysteme**
von R. Trebbels (2009), iii, 135 Seiten
ISBN: 978-3-89336-591-3

50. **Bruchmechanische Untersuchung von Metall / Keramik-Verbundsystemen für die Anwendung in der Hochtemperaturbrennstoffzelle**
von B. Kuhn (2009), 118 Seiten
ISBN: 978-3-89336-592-0

51. **Wasserstoff-Emissionen und ihre Auswirkungen auf den arktischen Ozonverlust**
Risikoanalyse einer globalen Wasserstoffwirtschaft
von T. Feck (2009), 180 Seiten
ISBN: 978-3-89336-593-7

52. **Development of a new Online Method for Compound Specific Measurements of Organic Aerosols**
by T. Hohaus (2009), 156 pages
ISBN: 978-3-89336-596-8

53. **Entwicklung einer FPGA basierten Ansteuerungselektronik für Justageeinheiten im Michelson Interferometer**
von H. Nöldgen (2009), 121 Seiten
ISBN: 978-3-89336-599-9

54. **Observation – and model – based study of the extratropical UT/LS**
by A. Kunz (2010), xii, 120, xii pages
ISBN: 978-3-89336-603-3

55. **Herstellung polykristalliner Szintillatoren für die Positronen-Emissions-Tomographie (PET)**
von S. K. Karim (2010), VIII, 154 Seiten
ISBN: 978-3-89336-610-1

56. **Kombination eines Gebäudekondensators mit H2-Rekombinatorelementen in Leichwasserreaktoren**
von S. Kelm (2010), vii, 119 Seiten
ISBN: 978-3-89336-611-8

57. **Plant Leaf Motion Estimation Using A 5D Affine Optical Flow Model**
by T. Schuchert (2010), X, 143 pages
ISBN: 978-3-89336-613-2

58. **Tracer-tracer relations as a tool for research on polar ozone loss**
by R. Müller (2010), 116 pages
ISBN: 978-3-89336-614-9

59. **Sorption of polycyclic aromatic hydrocarbon (PAH) to Yangtze River sediments and their components**
by J. Zhang (2010), X, 109 pages
ISBN: 978-3-89336-616-3

60. **Weltweite Innovationen bei der Entwicklung von CCS-Technologien und Möglichkeiten der Nutzung und des Recyclings von CO_2**
Studie im Auftrag des BMWi
von W. Kuckshinrichs et al. (2010), X, 139 Seiten
ISBN: 978-3-89336-617-0

61. **Herstellung und Charakterisierung von sauerstoffionenleitenden Dünnschichtmembranstrukturen**
von M. Betz (2010), XII, 112 Seiten
ISBN: 978-3-89336-618-7

62. **Politikszenarien für den Klimaschutz V – auf dem Weg zum Strukturwandel, Treibhausgas-Emissionsszenarien bis zum Jahr 2030**
hrsg. von P. Hansen, F. Chr. Matthes (2010), 276 Seiten
ISBN: 978-3-89336-619-4

63. **Charakterisierung Biogener Sekundärer Organischer Aerosole mit Statistischen Methoden**
von C. Spindler (2010), iv, 163 Seiten
ISBN: 978-3-89336-622-4

64. **Stabile Algorithmen für die Magnetotomographie an Brennstoffzellen**
von M. Wannert (2010), ix, 119 Seiten
ISBN: 978-3-89336-623-1

65. **Sauerstofftransport und Degradationsverhalten von Hochtemperaturmembranen für CO2-freie Kraftwerke**
von D. Schlehuber (2010), VII, 139 Seiten
ISBN: 978-3-89336-630-9

66. **Entwicklung und Herstellung von foliengegossenen, anodengestützten Festoxidbrennstoffzellen**
von W. Schafbauer (2010), VI, 164 Seiten
ISBN: 978-3-89336-631-6

67. **Disposal strategy of proton irradiated mercury from high power spallation sources**
by S. Chiriki (2010), xiv, 124 pages
ISBN: 978-3-89336-632-3

68. **Oxides with polyatomic anions considered as new electrolyte materials for solid oxide fuel cells (SOFCs)**
by O. H. Bin Hassan (2010), vii, 121 pages
ISBN: 978-3-89336-633-0

69. **Von der Komponente zum Stack: Entwicklung und Auslegung von HT-PEFC-Stacks der 5 kW-Klasse**
von A. Bendzulla (2010), IX, 203 Seiten
ISBN: 978-3-89336-634-7

70. **Satellitengestützte Schwerewellenmessungen in der Atmosphäre und Perspektiven einer zukünftigen ESA Mission (PREMIER)**
von S. Höfer (2010), 81 Seiten
ISBN: 978-3-89336-637-8

71. **Untersuchungen der Verhältnisse stabiler Kohlenstoffisotope in atmosphärisch relevanten VOC in Simulations- und Feldexperimenten**
von H. Spahn (2010), IV, 210 Seiten
ISBN: 978-3-89336-638-5

72. **Entwicklung und Charakterisierung eines metallischen Substrats für nanostrukturierte keramische Gastrennmembranen**
von K. Brands (2010), vii, 137 Seiten
ISBN: 978-3-89336-640-8

73. **Hybridisierung und Regelung eines mobilen Direktmethanol-Brennstoffzellen-Systems**
von J. Chr. Wilhelm (2010), 220 Seiten
ISBN: 978-3-89336-642-2

74. **Charakterisierung perowskitischer Hochtemperaturmembranen zur Sauerstoffbereitstellung für fossil gefeuerte Kraftwerksprozesse**
von S.A. Möbius (2010) III, 208 Seiten
ISBN: 978-3-89336-643-9

75. **Characterization of natural porous media by NMR and MRI techniques: High and low magnetic field studies for estimation of hydraulic properties**
by L.-R. Stingaciu (2010), 96 pages
ISBN: 978-3-89336-645-3

76. **Hydrological Characterization of a Forest Soil Using Electrical Resistivity Tomography**
by Chr. Oberdörster (2010), XXI, 151 pages
ISBN: 978-3-89336-647-7

77. **Ableitung von atomarem Sauerstoff und Wasserstoff aus Satellitendaten und deren Abhängigkeit vom solaren Zyklus**
von C. Lehmann (2010), 127 Seiten
ISBN: 978-3-89336-649-1

78. **18th World Hydrogen Energy Conference 2010 – WHEC2010 Proceedings**
Speeches and Plenary Talks
ed. by D. Stolten, B. Emonts (2010)
ISBN: 978-3-89336-658-3

78-1. **18th World Hydrogen Energy Conference 2010 – WHEC2010 Proceedings**
Parallel Sessions Book 1:
Fuel Cell Basics / Fuel Infrastructures
ed. by D. Stolten, T. Grube (2010), ca. 460 pages
ISBN: 978-3-89336-651-4

78-2. **18th World Hydrogen Energy Conference 2010 – WHEC2010 Proceedings**
Parallel Sessions Book 2:
Hydrogen Production Technologies – Part 1
ed. by D. Stolten, T. Grube (2010), ca. 400 pages
ISBN: 978-3-89336-652-1

78-3. **18th World Hydrogen Energy Conference 2010 – WHEC2010 Proceedings**
Parallel Sessions Book 3:
Hydrogen Production Technologies – Part 2
ed. by D. Stolten, T. Grube (2010), ca. 640 pages
ISBN: 978-3-89336-653-8

78-4. **18th World Hydrogen Energy Conference 2010 – WHEC2010 Proceedings**
Parallel Sessions Book 4:
Storage Systems / Policy Perspectives, Initiatives and Cooperations
ed. by D. Stolten, T. Grube (2010), ca. 500 pages
ISBN: 978-3-89336-654-5

78-5. **18th World Hydrogen Energy Conference 2010 – WHEC2010 Proceedings**
Parallel Sessions Book 5:
Stategic Analysis / Safety Issues / Existing and Emerging Markets
ed. by D. Stolten, T. Grube (2010), ca. 530 pages
ISBN: 978-3-89336-655-2

78-6. **18th World Hydrogen Energy Conference 2010 – WHEC2010 Proceedings**
Parallel Sessions Book 6:
Stationary Applications / Transportation Applications
ed. by D. Stolten, T. Grube (2010), ca. 330 pages
ISBN: 978-3-89336-656-9

78 Set (complete book series)

18th World Hydrogen Energy Conference 2010 – WHEC2010 Proceedings
ed. by D. Stolten, T. Grube, B. Emonts (2010)
ISBN: 978-3-89336-657-6

79. **Ultrafast voltex core dynamics investigated by finite-element micromagnetic simulations**
by S. Gliga (2010), vi, 144 pages
ISBN: 978-3-89336-660-6

80. **Herstellung und Charakterisierung von keramik- und metallgestützten Membranschichten für die CO_2-Abtrennung in fossilen Kraftwerken**
von F. Hauler (2010), XVIII, 178 Seiten
ISBN: 978-3-89336-662-0

81. **Experiments and numerical studies on transport of sulfadiazine in soil columns**
by M. Unold (2010), xvi, 115 pages
ISBN: 978-3-89336-663-7

82. **Prompt-Gamma-Neutronen-Aktivierungs-Analyse zur zerstörungsfreien Charakterisierung radioaktiver Abfälle**
von J.P.H. Kettler (2010), iv, 205 Seiten
ISBN: 978-3-89336-665-1

83. **Transportparameter dünner geträgerter Kathodenschichten der oxidkeramischen Brennstoffzelle**
von C. Wedershoven (2010), vi, 137 Seiten
ISBN: 978-3-89336-666-8

84. **Charakterisierung der Quellverteilung von Feinstaub und Stickoxiden in ländlichem und städtischem Gebiet**
von S. Urban (2010), vi, 211 Seiten
ISBN: 978-3-89336-669-9

85. **Optics of Nanostructured Thin-Film Silicon Solar Cells**
by C. Haase (2010), 150 pages
ISBN: 978-3-89336-671-2

86. **Entwicklung einer Isolationsschicht für einen Leichtbau-SOFC-Stack**
von R. Berhane (2010), X, 162 Seiten
ISBN: 978-3-89336-672-9

87. **Hydrogen recycling and transport in the helical divertor of TEXTOR**
by M. Clever (2010), x, 172 pages
ISBN: 978-3-89336-673-6

88. **Räumlich differenzierte Quantifizierung der N- und P-Einträge in Grundwasser und Oberflächengewässer in Nordrhein-Westfalen unter besonderer Berücksichtigung diffuser landwirtschaftlicher Quellen**
von F. Wendland et. al. (2010), xii, 216 Seiten
ISBN: 978-3-89336-674-3

89. **Oxidationskinetik innovativer Kohlenstoffmaterialien hinsichtlich schwerer Lufteinbruchstörfälle in HTR´s und Graphitentsorgung oder Aufarbeitung**
von B. Schlögl (2010), ix, 117 Seiten
ISBN: 978-3-89336-676-7

90. **Chemische Heißgasreinigung bei Biomassenvergasungsprozessen**
von M. Stemmler (2010), xv, 196 Seiten
ISBN: 978-3-89336-678-1

91. **Untersuchung und Optimierung der Serienverschaltung von Silizium-Dünnschicht-Solarmodulen**
von S. Haas (2010), ii, 202 Seiten
ISBN: 978-3-89336-680-4

92. **Non-invasive monitoring of water and solute fluxes in a cropped soil**
by S. Garré (2010), xxiv, 133 pages
ISBN: 978-3-89336-681-1

93. **Improved hydrogen sorption kinetics in wet ball milled Mg hydrides**
by L. Meng (2011), II, 119 pages
ISBN: 978-3-89336-687-3

94. **Materials for Advanced Power Engineering 2010**
ed. by J. Lecomte-Beckers, Q. Contrepois, T. Beck and B. Kuhn
(2010), 1327 pages
ISBN: 978-3-89336-685-9

95. **2D cross-hole MMR – Survey design and sensitivity analysis for cross-hole applications of the magnetometric resistivity**
by D. Fielitz (2011), xvi, 123 pages
ISBN: 978-3-89336-689-7

96. **Untersuchungen zur Oberflächenspannung von Kohleschlacken unter Vergasungsbedingungen**
von T. Melchior (2011), xvii, 270 Seiten
ISBN: 978-3-89336-690-3

97. **Secondary Organic Aerosols: Chemical Aging, Hygroscopicity, and Cloud Droplet Activation**
by A. Buchholz (2011), xiv, 134 pages
ISBN: 978-3-89336-691-0

98. **Chrom-bezogene Degradation von Festoxid-Brennstoffzellen**
von A. Neumann (2011), xvi, 218 Seiten
ISBN: 978-3-89336-692-7

99. **Amorphous and microcrystalline silicon applied in very thin tandem solar cells**
by S. Schicho (2011), XII, 190 pages
ISBN: 978-3-89336-693-4

100. **Sol-gel and nano-suspension electrolyte layers for high performance solid oxide fuel cells**
by F. Han (2011), iv, 131 pages
ISBN: 978-3-89336-694-1

101. **Impact of different vertical transport representations on simulating processes in the tropical tropopause layer (TTL)**
by F. Plöger (2011), vi, 104 pages
ISBN: 978-3-89336-695-8

102. **Untersuchung optischer Nanostrukturen für die Photovoltaik mit Nahfeldmikroskopie**
von T. Beckers (2011), xiii, 128 Seiten
ISBN: 978-3-89336-696-5

103. **Impact of contamination on hydrogenated amorphous silicon thin films & solar cells**
by J. Wördenweber (2011), XIV, 138 pages
ISBN: 978-3-89336-697-2

104. **Water and Organic Nitrate Detection in an AMS: Laboratory Characterization and Application to Ambient Measurements**
by A. Mensah (2011), XI, 111 pages
ISBN: 978-3-89336-698-9

105. **Entwicklung eines neuen Konzepts zur Steuerung der thermischen Ausdehnung von glaskeramischen Verbundwerkstoffen mit angepasster Fließfähigkeit am Beispiel der Hochtemperatur-Brennstoffzelle**
von E. Wanko (2011), xi, 134 Seiten
ISBN: 978-3-89336-705-4

106. **Tomographic reconstruction of atmospheric volumes from infrared limb-imager measurements**
by J. Ungermann (2011), xiv, 153 pages
ISBN: 978-3-89336-708-5

107. **Synthese und Identifizierung von substituierten Mg-Al-Cl Doppelhydroxidverbindungen mit Schwerpunkt IR-Spektroskopie**
von B. Hansen (2011), XII, 121 Seiten
ISBN: 978-3-89336-709-2

108. **Analysis of spatial soil moisture dynamics using wireless sensor networks**
by U. Rosenbaum (2011), xxii, 120 pages
ISBN: 978-3-89336-710-8

109. **Optimierung von APS-ZrO2-Wärmedämmschichten durch Variation der Kriechfestigkeit und der Grenzflächenrauhigkeit**
von M. E. Schweda (2011), 168 Seiten
ISBN: 978-3-89336-711-5

110. **Sorption of a branched nonylphenol isomer and perfluorooctanoic acid on geosorbents and carbon nanotubes**
by C. Li (2011), X, 102 pages
ISBN: 978-3-89336-716-0

111. **Electron Transport in the Plasma Edge with Rotating Resonant Magnetic Perturbations at the TEXTOR Tokamak**
by H. Stoschus (2011), iv, 113 pages
ISBN: 978-3-89336-718-4

112. **Diffusion and Flow Investigations in Natural Porous Media by Nuclear Magnetic Resonance**
by N. Spindler (2011), viii, 144 pages
ISBN: 978-3-89336-719-1

113. **Entwicklung und Erprobung des Hygrometer for Atmospheric Investigations**
von T. Klostermann (2011), IV, 118 Seiten
ISBN: 978-3-89336-723-8

114. **Application of functional gene arrays for monitoring influences of plant/seasons on bacterial functions and community structures in constructed wetlands (Bitterfeld, Germany)**
by J. Ning (2011), xiv, 157 pages
ISBN: 978-3-89336-724-5

115. **Wasseraustrag aus den Kathodenkanälen von Direkt-Methanol-Brennstoffzellen**
von A. Schröder (2011), VII, 228 Seiten
ISBN: 978-3-89336-727-6

116. **CITYZEN Climate Impact Studies**
ed. by M. Schultz (2011), 45 pages
ISBN: 978-3-89336-729-0

117. **Software Tools zum interoperablen Austausch und zur Visualisierung von Geodatensätzen über das Internet**
von M. Schultz, M. Decker, S. Lührs (2011), iv, 156 Seiten
ISBN: 978-3-89336-730-6

118. **Optimierung eines Leichtbaudesigns für ein SOFC-Brennstoffzellenstack**
von T. Nguyen-Xuan (2011), III, 154 Seiten
ISBN: 978-3-89336-732-0

119. **Institute of Energy and Climate Research IEK-6:**
Nuclear Waste Management & Reactor Safety Report 2009/2010
Material Science for Nuclear Waste Management
ed. by M. Klinkenberg, S. Neumeier, D. Bosbach (2011), 242 pages
ISBN: 978-3-89336-735-1

120. **Fate of the Antibiotic Sulfadiazine in Yangtze River Sediments: Transformation, Sorption and Transport**
by N. Meng (2011), XII, 111 pages
ISBN: 978-3-89336-736-8

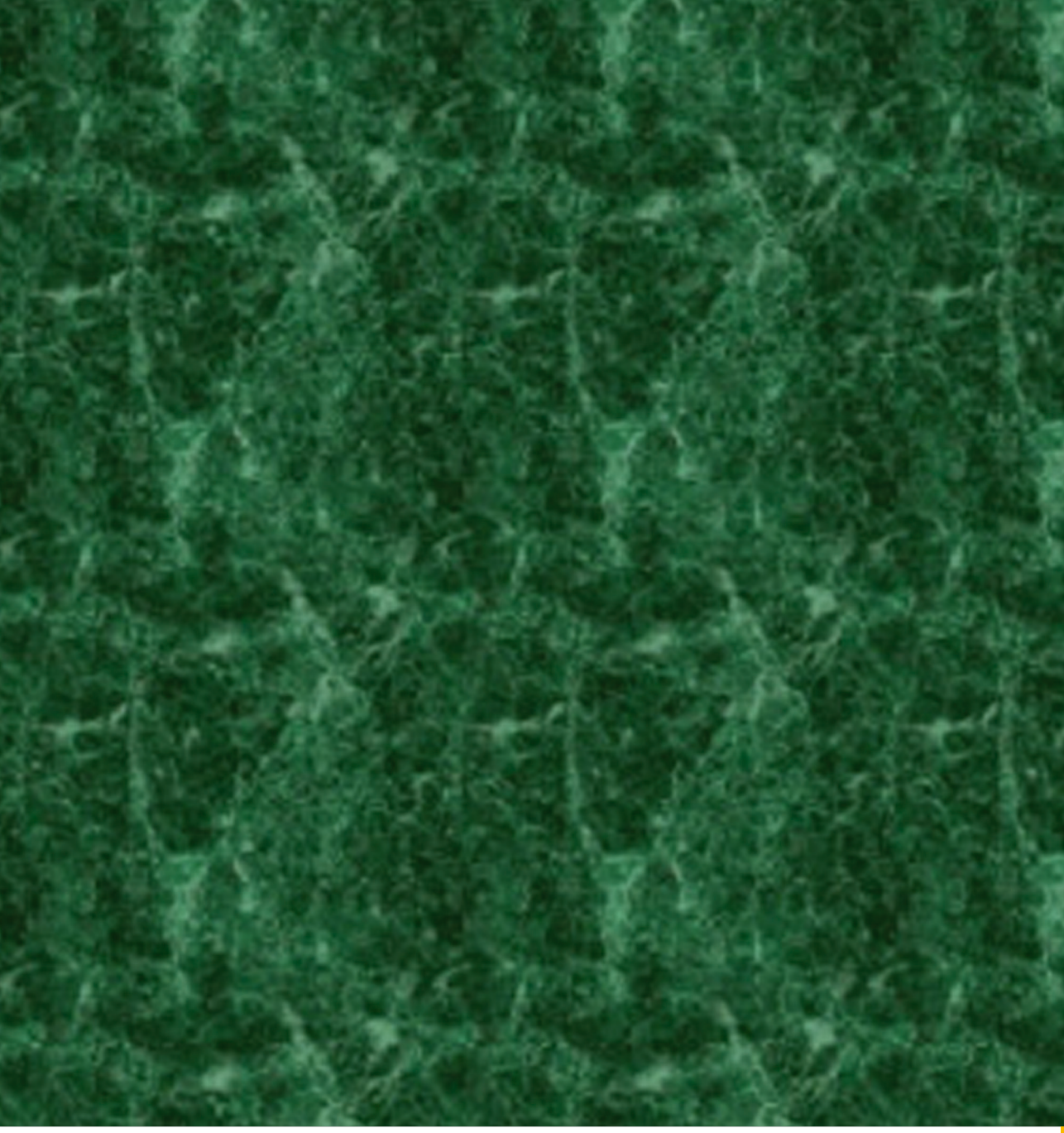

Energie & Umwelt / Energy & Environment
Band / Volume 120
ISBN 978-3-89336-736-8

JÜLICH
FORSCHUNGSZENTRUM